ESCUELA DE DOCTORADO
INTERNACIONAL DE LA USC

Daniel
Faílde Balea

Tesis doctoral

Topological Insulators: Advances in Thermoelectricity, Orbital Dynamics and Axion Electrodynamics

Santiago de Compostela, 2021

Programa de doctorado en Ciencia de Materiales

TESE DE DOUTORAMENTO

TOPOLOGICAL INSULATORS: ADVANCES IN THERMOELECTRICITY, ORBITAL DYNAMICS AND AXION ELECTRODYNAMICS

Daniel Failde Balea

ESCOLA DE DOUTORAMENTO INTERNACIONAL DA UNIVERSIDADE DE SANTIAGO DE COMPOSTELA

PROGRAMA DE DOUTORAMENTO EN CIENCIA DE MATERIAIS

SANTIAGO DE COMPOSTELA

2021

DECLARACIÓN DO AUTOR/A DA TESE

Topological Insulators: Advances in Thermoelectricity, Orbital Dynamics and Axion Electrodynamics

D./Dna. Daniel Faílde Balea

Presento a miña tese, seguindo o procedemento axeitado ao Regulamento, e declaro que:

1) A tese abarca os resultados da elaboración do meu traballo.
2) De selo caso, na tese faise referencia ás colaboracións que tivo este traballo.
3) A tese é a versión definitiva presentada para a súa defensa e coincide coa versión enviada en formato electrónico.
4) Confirmo que a tese non incorre en ningún tipo de plaxio doutros autores nin de traballos presentados por min para a obtención doutros títulos.

En Santiago de Compostela, 28 de decembro de 2021

Asdo.....

AUTORIZACIÓN DO DIRECTOR / TITOR DA TESE

Topological Insulators: Advances in Thermoelectricity, Orbital Dynamics and Axion Electrodynamics

D./Dna. Daniel Baldomir Fernández

INFORMA:

Que a presente tese, correspóndese co traballo realizado por D/Dna. Daniel Faílde Balea, baixo a miña dirección, e autorizo a súa presentación, considerando que reúne os requisitos esixidos no Regulamento de Estudos de Doutoramento da USC, e que como director desta non incorre nas causas de abstención establecidas na Lei 40/2015.

De acordo co indicado no Regulamento de Estudos de Doutoramento, declara tamén que a presente tese de doutoramento é idónea para ser defendida en base á modalidade de Monográfica con reproducción de publicaciones, nos que a participación do/a doutorando/a foi decisiva para a súa elaboración e as publicacións se axustan ao Plan de Investigación.

En Santiago de Compostela, 27 de Decembro de 2021.

Abstract

Topological Insulators: Advances in Thermoelectricity, Orbital Dynamics and Axion Electrodynamics

---

Daniel Failde Balea

Topological materials (TMs) are a special class of quantum materials which include Topological Insulators (TIs), Chern Insulators (CIs), Weyl Semimetals, Topological Superconductors and Magnetic Topological Insulators (MTIs). Their non-trivial topology, which differs from the trivial one of conventional systems, give these systems singular thermoelectric and magnetoelectric transport properties. These properties are not only rich from the physical point of view but they can be technologically beneficial for different applications being used as thermoelectrics, transistors, spintronic devices, superconductors, etc. Certainly, the origin of this thesis lies in the study of the thermoelectric properties of topological insulators, currently the best thermoelectric materials. Our perspective was theoretical from the beginning given the lack of a microscopic theory in the literature which answers why these systems have such an efficient thermoelectric response, represented by their well known experimental figure of merit. This leads us to explore other effects and interactions such as the electron-phonon coupling, thermal excitations, and other orbital magnetic effects and phenomena which are a consequence of their non-trivial topology and shall be developed in the following chapters of this thesis. We also give a new interpretation to the physics of these systems by introducing the figure of a topological intrinsic field which is derived from the Berry curvature defined in the non-trivial topological bands of these materials.

In Chapter 0 we examine the fundamental aspects of the Dirac Hamiltonian in relation to the topology and solid state physics. This preliminary chapter tries to give a pedagogical connection between the Berry phase effects and the Dirac Hamiltonian, which is the starting point to study the physics of topological insulators as well as other topological materials. Besides reviewing some of the basic properties of TIs in several space-time dimensions, introducing the effective Hamiltonian for 2D and 3D TIs and their associated effective actions, the concepts developed constitute the basis of this study of the thermoelectricity, orbital dynamics and axion electrodynamics in these materials. Recurring concepts along this thesis such as the Dirac Hamiltonian, the Berry curvature and its field interpretation, the helical nature of the edge states, time-reversal symmetry, the topological Chern-Simons action and the axion electrodynamics are addressed in this chapter.

In Chapter 1 we explore the physics of thermoelectricity in Topological Insulators. This study defined our first scientific article and provides a new quantum approach to the thermoelectric phenomenon in TMs, which gives a formula for the topological Seebeck coefficient and figure of merit quite close to the experimental value for Bi_2Te_3. First, we put this formalism into the proper mathematical context of these materials by making a direct identification between the different topological branches that can be defined from the Riemann-Hurwitz formula and the topological invariant Chern number. Degenerate energy levels have several states per a given eigenvalue and therefore the Berry connection and the Berry curvature become unitary non-Abelian matrix-valued. At room temperature, these are the most realistic quantum fundamental states that we have considered for those topological materials. Thus, within a Yang-Mills formalism, we calculated the gauge transformations of the Chern-Simons action and by using thermal quantum field

theory we reached an expression for the electric field E and potential V generated in TIs when a temperature gradient is applied. These expressions only employ the temperature T and the topological index μ among other natural constants, so they are easily translated to give an expression for the topological Seebeck coefficient. Remarkably, we identify two contributions to the thermoelectric phenomenon. One addressed directly to the diffusion when the electrons are within a topological band with topological index μ, which corresponds to a topological mass for the electromagnetic fields, and the other to the jump between topological branches when the temperature is enough to excite them. The topological sectors might be tunnelled assuming that we have instanton solutions, sharing in a natural form the Euclidean spacetime of the Thermofield Dynamics. This key coincidence allows us to find a relationship among the electric potential V, the topological mass μ and the temperature T through a gauge transformation. Therefore, we see how in these materials the thermodynamic and electromagnetism cannot be independent. In this scenario, one contribution can be addressed to the creation of electron-hole Schwinger pairs given that the critical electric E_c and magnetic B_c fields become experimentally accessible due to the low Fermi velocity (in relation to the light velocity) which determine the relativistic dispersion in these systems. Finally, we apply the obtained results in the surface of a topological insulator, where conducting states are placed, to give a value to their potential figure of merit. Neglecting contributions from the creation of Schwinger's pairs, we find that our Seebeck coefficient can be derived from the entropy `S` using the Berry phase appearing in the electron's wave function. Thus, considering the well-known quantum conductance of the edge states $G = ne^2/h$ with n the first Chern number and calculating the electronic thermal conductivity we give a general formula for the dimensionless figure of merit ZT in TIs in absence of lattice thermal conductivity. The obtained formula not only explains why these systems are so good thermoelectrics, it gives a value of around 2.7 for the lowest topological numbers, but it fits quite well the experimental result of 2.4 employing Bi_2Te_3/Sb_2Te_3 superlattices. Currently, this is the highest value ever observed and is obtained precisely using topological insulators in an experimental setup which reduces the contribution of the lattice thermal conductivity as we considered in our model. This study constituted our first approach to the problem and defined the route to analyze new interactions and effects in TIs.

Our next step focuses on the introduction of mechanical oscillations in the electron dynamics in TMs. This study is developed in Chapter 2 and responds to the aim of including the role of phonons in topological thermoelectricity. Our idea was that in a strongly coupled spin-orbit system as these materials are, the nucleus oscillation should induce an effective magnetic field in the surrounding electrons. But additionally, we need to know how these oscillations are going to affect the topological properties, such as the Berry curvature, and which consequences have this for the transport. To reach such a goal we translated the topological information contained in the Abelian Berry curvature into an effective topological intrinsic field b. It is well-known that the Berry curvature can be interpreted as a kind of magnetic monopole in the momentum space, one magnetic field with opposite sign for each band defined in a Dirac Hamiltonian. Taking into account

that this magnitude is well localized around a singularity, describing a narrow single peak Gaussian-like function in the momentum space, it is possible to translate it into a nearly constant magnetic field in the real space. This laborious task is done through Heisenberg's uncertainty principle to determine the effective area of the topological electrons. Therefore, the estimation of b is completed by considering a quantum flux associated to these electrons which we suppose orbiting around the singularity due to this non-trivial Berry curvature. We were conscious that most of these concepts are original from this study and must be tested, as we develop in Chapter 2 and also in Chapter 3. In the same way, the reader could find surprising when noticing that b corresponds with the quantum-material version of the Schwinger's critical magnetic field. Nevertheless, all the elements obtained are demonstrated to be part of an intuitive model that enlarge our study of the thermoelectricity in TIs and describes a new path to transform heat from the lattice or external fields into electricity.

To be more specific, we need to know that b is calculated from the Abelian Berry curvature defined in the bands of a gapped 2x2 Dirac Hamiltonian. This system, which has broken time-reversal symmetry, constitutes the simplest model of a Chern insulator. In contrast, a TI has time-reversal symmetry, although in two-dimensions (2D) or for 3DTI in thin-film conditions its 4x4 Dirac Hamiltonian can be decoupled into two time-reversal counterpart copies of a 2x2 Dirac Hamiltonian. That is, in presence of time-reversal symmetry the two Chern species of the TI contribute with an opposite b which takes a net value zero for the full Hamiltonian. In other words, to test b we need to introduce an opposite magnetic field B into each Chern species turning the Dirac Hamiltonian into a Dirac oscillator. Making a perturbative calculation two important consequences are deduced. First, if we apply an external magnetic field B with the same magnitude of b but with opposite sign, the Berry curvature falls to zero. That is, our vision of the topological intrinsic field is correct and well estimated. But what's more, we also demonstrate how certain oscillations can take part in the electron dynamics in a TI. Of course, these vibration modes are particular given that they need to have a linear/relativistic dispersion law with an effective velocity that can be compared with the Fermi velocity of the electrons and that must not break the time-reversal symmetry of the system. Polar optical phonon modes in Bi_2Te_3 and Bi_2Se_3 are proposed to fulfil these conditions based on recent studies although it might be general for other modes based on the fact that the spin-orbit coupling of these systems could not imply the necessity of having two counter-propagating phonon modes.

These results are also tested within the special axion electrodynamics of these systems. The last check of our model associates directly the temperature into the oscillation frequency. In this way, we found the same result as that the one obtained by using the Chern-Simons action (Chapter 1). Both formalisms need to be equivalent as one could imagine. But the consequences and motivation are very different. In the first case, we calculate directly the topological Seebeck coefficient from the Chern-Simons action using thermal field theory. Now, we associated directly the temperature with the frequency using the topological intrinsic field to demonstrate how the lattice oscillations caused

by the temperature contribute to the thermoelectric effect. The conclusion is that for some vibration modes in a wide range of frequencies the Seebeck coefficient of the system remains unalterable while the velocity of the electrons can increase or decrease if their coupling is coherent or decoherent. So, in summary, we have transformed energy from the lattice to the electrons which can be technologically favourable for the thermoelectricity in TIs where the topological states have definite conductivities and Seebeck coefficients through the topological invariants.

In Chapter 3 we explore with more detail the previous model to analyze the intrinsic orbital magnetism of TMs. This was motivated by the concept of orbit proposed before for the topological electrons, which induces us to demonstrate explicitly how a magnetic field modifies the different transport magnitudes in a non-zero Berry curvature system. The problem of a charged particle in a magnetic field is well-known in physics but in these quantum systems described by a Dirac Hamiltonian, we have a new ingredient which is the Berry curvature that experiments a coupling with the external magnetic field. This led us to read thoroughly several references in the literature to see how this problem was treated before. The introduction of a magnetic field in these systems has been analyzed using a semiclassical Lagrangian formalism and non-relativistic quantum mechanics. However, a relativistic formalism that starts directly from the Dirac Hamiltonian and gives analytical expressions for all the magnitudes involved had not been provided. In addition, we observe that the role of second-order corrections in the magnetic field becomes important at relatively low magnetic fields due to the small gaps which characterize the TMs in contrast to what occurs in other physical systems in condensed matter. In the first approach to the problem, we take the mass of the particle as constant. That is, we considered a gapped Dirac dispersion and calculated the correction to the system eigenstates in presence of a perpendicular magnetic field. This implies dealing with spinors, in contrast to what happens with other non-relativistic formalism, and with gauge dependent corrections derived from the degrees of freedom that we have when working with SU(N) unitary groups. Once determined the corrections to the system eigenstates we calculate after some tedious algebra the different transport magnitudes. Specifically, besides showing how the Berry curvature is modulated by the external magnetic field we see mathematically and numerically how the Chern number of the system remains unalterable. Thus, we quantify how a positive Berry curvature is enhanced by a positive magnetic field or reduced if we take the magnetic field negative as we postulated through the topological intrinsic field. In a schematic framework, we can imagine the relativistic electrons orbiting due to the non-zero Berry curvature, so by applying an external magnetic field we will have a redefinition of the velocity of the particles, radius, orbital magnetic moment, energy and density of states associated with the change of the effective field felt by these electrons. All these elements are calculated analytically up to second-order reaching general expressions which can be applied to a wide variety of compounds by containing no more ingredients than the band gap of the system, particle's velocity and magnitude of the magnetic field. Finally, these magnitudes are used to obtain the free energy of the system and hence the orbital magnetization and susceptibility in CIs and TIs which are predicted to feature a

dependence with the external magnetic field. The present study constitutes a method to study magnetoelectric and thermoelectric transport properties in 2D topological materials which allows taking into account other interactions in the system in a simple way.

One surprising result that is also found in the literature, is that the zero-field orbital susceptibility has the same expression for a non-zero Berry curvature system independently of whether its topology is trivial or non-trivial. This fact is remarkable given the differences between the Berry curvature of both regimes. This will be clear in Chapter 3 when we show how the magnetization depends directly on this quantity through the energy and the density of states. The key point is that we also need to consider the momentum dependence on the mass term arising from the parabolic behaviour of the energy spectrum at large momenta. As it is known, this term allows making a topological distinction which is not possible when considering a pure linear dispersion. Examples that need this term to define properly the topological invariant Chern number obtained from the Berry curvature as an integer can be found in the literature. However, this term is ignored given that most of the studies in the literature focus on graphene-like systems, which has a linear dispersion. The scenario which arises after introducing it into our formalism shows clear discrepancies between the orbital magnetic response of a trivial insulator and a non-trivial one. Thus, while a trivial insulator is predicted to have a limited response on this parameter, its non-trivial counterpart shows an additional term in the orbital magnetic susceptibility that can be written in terms of the square of the quantum magnetic flux. These results are postulated again to connect with the concept of orbit in TMs and with the effective field b. From the practical point of view, we find a new route to increase the intrinsic orbital magnetism of TIs and CIs by enhancing the parabolic dependence of their spectra. Subsequent studies can be done to extrapolate similar implications in other thermoelectric and magnetoelectric properties.

In Chapter 4 we carry our research to a different perspective by examining the axion electrodynamics which TIs need to explain their magnetoelectric properties. The axion electrodynamics sources as a generalization of the usual electrodynamics including the interaction of a kind of particles, named axions, with the electromagnetic field through a scalar field $\theta(r, t)$. In physics, this electrodynamics is proposed to be part of dark matter physics and was originally presented to study the charge-conjugation parity problem in quantum chromodynamics. However, these particles have been not yet measured and currently are considered virtual.

In this work, we move away from the usual application of axion electrodynamics oriented towards magnetoelectricity to analyze a more fundamental perspective. If axions are involved in the particular physics of TIs, then, besides producing special electric polarization and magnetizations when interacting with electric and magnetic fields they must then give rise to internal fields and pressures that are suitable to be measured. There is an analogy with another renowned effect in physics, which is the Casimir effect. The Casimir effect is originated from the quantum fluctuation of the vacuum when two parallel conductor plates are placed at a short distance. Briefly explained, it appears an attractive force between the plates associated with the negative energy region created in their inner

part when the plates cut the photons with lower wavelength. However, in the TIs given that all surfaces are metallic no photons are expected to penetrate inside them acting like a Faraday's cage, and the axions are the unique particles that can give the internal energy. By applying boundary conditions to the scalar field $\theta(r,t)$ we find a pressure for the TIs which is equivalent to the one of Casimir but with a very different origin and magnitude. Its origin lies in axions instead of photons while the smaller magnitude of this pressure is due mainly to the Fermi velocity which determines the relativistic framework in TMs. The theoretical calculations presented can lead to a direct verification of the axions besides implying a technological advantage when making thin-film based devices.

Overall, the work presented in this thesis aspires to collect a wide variety of original results for the topological materials which can have important implications into the experimental field besides going further in the singular physics of these materials. Specifically, we have developed a microscopic formalism for the mechanism of thermoelectricity in TIs taking into account directly the topological background of these systems and determining its contribution to the figure of merit. We have introduced the role of phonons into the relativistic context of these materials describing an original high efficient route for heat-electricity transformation. We have got an effective interpretation of the Berry curvature by means of the field b. Additionally, we have carried out a relativistic formalism that addresses the orbital magnetic response of 2D non-zero Berry curvature systems. We have demonstrated how the Berry curvature can be modulated by an external magnetic field introducing it as a dynamical magnitude. In this sense, we have determined the differences in the orbital magnetic response between topologically trivial and non-trivial insulators. Finally, we have treated the axion field $\theta(r,t)$ in the context of TIs giving an expression for the pressure associated with the axions and determining the ingredients needed for the experimental detection of these particles in TIs. Therefore, these theoretical advances have a direct application into different phenomena and properties and are sensible to be generalized to include other interactions and effects.

Resumo

Illantes Topolóxicos: Avances en Termoelectricidade, Dinámica Orbital e Electrodinámica Axiónica

Daniel Failde Balea

Os Materiais Topolóxicos (TMs) son unha clase especial de materiais cuánticos que inclúen os Illantes Topolóxicos (TIs), Illantes Chern (CIs), Semimetais de Weyl, Superconductores Topolóxicos e Illantes Topolóxicos Magnéticos. A súa topoloxía non trivial, que difire da trivial dun sistema convencional, outorga a estes sistemas propiedades de transporte termoeléctricas y magnetoeléctricas singulares. Estas propiedades non son soamente ricas dende o punto de vista físico senón que poden resultar tecnolóxicamente beneficiosas para diferentes aplicacións sendo usados como termoeléctricos, transistores, dispositivos para a espintrónica, superconductores, etc. Certamente, a orixe desta tese reside no estudo das propiedades termoeléctricas dos illantes topolóxicos, actualmente os mellores materiais termoeléctricos. A nosa perspectiva foi teórica dende o principio motivada pola ausencia na literatura dunha teoría microscópica que respondese por qué estos sistemas teñen unha resposta termoeléctrica tan eficiente. Esto levounos a explorar outros efectos e interaccións como o acoplamiento electrón-fonón, excitacións térmicas e outros efectos magnéticos orbitais e fenómenos que son consecuencia da súa topoloxía non trivial e que serán desenvoltos ó longo dos seguintes capítulos desta tese. Ademáis, tamén daremos unha nova interpretación á física destes sistemas introducindo a figura dun campo topolóxico intrínseco derivado da curvatura de Berry definida nas bandas topolóxicas non triviais destes materiais.

No Capítulo 0 examinamos os aspectos fundamentais do Hamiltoniano de Dirac en relación coa topoloxía e a física do estado sólido. Este capítulo preliminar tenta dar unha conexión pedagóxica entre os efectos da fase Berry e o Hamiltoniano de Dirac, que é o punto de partida para estudar a física dos illantes topolóxicos así como doutros materiais topolóxicos. Ademais de revisar algunhas das propiedades básicas dos TIs en varias dimensións espazo-temporais, introducindo o Hamiltoniano efectivo para TIs en 2D e 3D e as súas accións efectivas asociadas, os conceptos desenvoltos neste capítulo constitúen a base deste estudo da termoelectricidade, dinámica orbital e electrodinámica axiónica nestes materiais. Conceptos recorrentes ao longo desta tese como o Hamiltoniano de Dirac, a curvatura de Berry e a súa interpretación de campo, a natureza helicoidal dos estados de borde, a simetría de inversión temporal, a acción topolóxica de Chern-Simons e a electrodinámica axiónica abordaranse neste capítulo.

No Capítulo 1 exploramos a física da termoelectricidade nos illantes topolóxicos. Este estudo definiu o noso primeiro artigo científico e ofrece un novo enfoque cuántico ao fenómeno termoeléctrico en TMs, dando unha fórmula para o coeficiente Seebeck topolóxico e para a figura de mérito que toma un valor bastante próximo ao valor experimental para o Bi_2Te_3. En primeiro lugar, poñeremos este formalismo no contexto matemático axeitado destes materiais facendo unha identificación directa entre as distintas ramas topolóxicas que se poden definir a partir da fórmula de Riemann-Hurwitz e o número de Chern. Os niveis de enerxía dexenerados teñen varios estados para un autovalor dado e, polo tanto, a conexión de Berry e a curvatura de Berry convértense nunha matriz unitaria non Abeliana. A temperatura ambiente estes son os estados fundamentais cuánticos máis realistas que consideramos para eses materiais topolóxicos. Así, dentro dun formalismo de Yang-Mills calculamos as transformacións gauge da acción Chern-Simons e mediante o uso da

teoría cuántica de campos térmica acadamos unha expresión para o campo eléctrico E e o potencial V xerados nun TI cando se aplica un gradiente de temperatura. Estas expresións só empregan a temperatura T e o índice topolóxico μ entre outras constantes naturais, polo que son facilmente traducidas para dar unha expresión para o coeficiente Seebeck topolóxico. Salientablemente, identificamos dúas contribucións ao fenómeno termoeléctrico. Unha asociada directamente á difusión dos electróns dentro dunha banda topolóxica con índice topolóxico μ, que corresponde a unha masa topolóxica para os campos electromagnéticos, e outra ó salto entre ramas topolóxicas cando a temperatura é suficiente para excitalos. O sectores topolóxicos poderían ser *tunelizados* asumindo que temos solucións instantáneas, compartindo de forma natural o espazo-tempo Euclídeo da Dinámica de Termocampos. Esta coincidencia clave permite atopar unha relación entre o potencial eléctrico V, a masa topolóxica μ e a temperatura T mediante unha transformación gauge. Polo tanto, vemos como nestes materiais a termodinámica e o electromagnetismo non poden ser independentes. Neste escenario, unha das contribucións pódese asociar á creación do pares electrón-oco de Schwinger dado que os campos eléctricos críticos E_c e magnéticos B_c resultan experimentalmente accesibles debido á baixa velocidade de Fermi (respecto á velocidade da luz) que determina a dispersión relativista nestes sistemas. Finalmente, aplicamos os resultados obtidos na superficie dun illante topolóxico, onde se sitúan os estados condutores, para darlle valor á súa potencial figura de mérito. Rexeitando a contribución asociada á creación dos pares de Schwinger, atopamos que o noso coeficiente Seebeck pódese derivar da entropía $\mathtt{S}$ usando a fase de Berry presente na función de onda do electrón. Así, tendo en conta a coñecida condutancia cuantizada dos estados de bordo $G = ne^2/h$, con n o primeiro número Chern, e calculando a condutividade térmica electrónica, dámoslle unha fórmula xeral para a figura de mérito adimensional ZT en TIs en ausencia da condutividade térmica de red. A fórmula obtida non só explica por qué estes sistemas son tan bos termoeléctricos, dá un valor ao redor de 2.7 para os números topolóxicos máis baixos, senón que se axusta bastante ben cos resultados experimentais de 2.4 empregando superredes de Bi_2Te_3/Sb_2Te_3. Actualmente, este é o valor máis alto xamais observado e obtense precisamente usando illantes topolóxicos nunha configuración experimental que reduce a contribución da condutividade térmica da rede como consideramos no noso modelo. Este estudo constituíu a nosa primeira aproximación ao problema e definiu a vía para analizar novas interaccións e efectos en TIs.

O noso seguinte paso céntrase na introdución das oscilacións mecánicas na dinámica electrónica en TMs. Este estudo desenvólvese no Capítulo 2 e responde o obxectivo de incluir o papel dos fonóns na termoelectricidade topolóxica. A nosa idea era que nun sistema fortemente acoplado cun espín-orbital como son estos materiais, as oscilacións dos núcleos deberían inducir un campo magnético efectivo sobre os electróns circundantes. Pero ademais, tamén necesitamos saber cómo estas oscilacións van afectar ás propiedades topolóxicas, como é a curvatura de Berry, e que consecuencias ten isto para o transporte. Para alcanzar tal obxectivo, traducimos á información topolóxica contida dentro da curvatura de Berry Abeliana nun campo topolóxico intrínseco b. É ben sabido que a curvatura de Berry pode ser interpretada como unha clase de monopolo magnético no espazo de

momentos, un campo magnético con signo oposto para cada banda definida nun Hamiltoniano de Dirac. Tendo en conta que esta magnitude está ben localizada ao redor dunha singularidade, describindo unha función moi estreita de tipo similar á Gausiana cun solo pico, é posible traducila nun campo magnético prácticamente constante no espazo real. Esta laboriosa tarefa é realizada a través do principio de incertidumbre de Heisenberg para determinar a área efectiva dos electróns topolóxicos. Deste xeito, a estimación de b complétase considerando un fluxo magnético cuantizado asociado a estes electróns que imaxinamos orbitando ao redor da singularidade definida nesta curvatura de Berry non trivial. Somos conscientes que moitos destes conceptos son orixinais deste estudo e que deben ser postos a proba, como faremos nos Capítulos 2 e 3. Do mesmo xeito, o lector pode atopar sorprendente que b se corresponda coa versión para materiais cuánticos do campo magnético crítico de Schwinger. Sen embargo, todos os elementos obtidos demostraranse pezas dun modelo intuitivo que incrementará o estudo da termoelectricidade en TIs e que describirá unha nova ruta para a transformación de calor da rede ou campos externos en electricidade.

Sendo máis específicos, necesitamos saber que b se calcula a partir da curvatura de Berry Abeliana definida polas bandas dun Hamiltoniano de Dirac 2x2. Este sistema, que non presenta simetría de inversión temporal, constitúe o modelo máis simple dun Illante Chern. En contraste, un TI ten simetría de inversión temporal, aínda que en dúas dimensións (2D) ou para películas finas dun 3DTI, o seu Hamiltoniano de Dirac 4x4 pódese desacoplar en dúas copias dun Hamiltoniano 2x2 relacionadas pola inversión temporal. É dicir, en presenza de simetría de inversión temporal as dúas especies Chern do TI contribuirán cun b oposto tomando un valor neto de cero para o Hamiltoniano completo. Noutras palabras, para comprobar b necesitamos introducir un campo magnético B oposto en cada especie Chern convertindo o Hamiltoniano de Dirac no Hamiltoniano dun oscilador de Dirac. Facendo un cálculo perturbativo dedúcense dúas consecuencias importantes. Primeiro, si aplicamos un campo magnético B cóa misma magnitude que b pero con signo oposto, a curvatura de Berry cae a cero. É dicir, a nosa visión do campo topolóxico intrínseco e correcta e ben estimada. Pero ademais, tamén demonstramos como certas oscilacións poden tomar parte da dinámica electrónica nun TI. Por suposto, estos modos de vibración son particulares dado que precisan ter unha lei de dispersión lineal/relativista cunha velocidade efectiva que se poda comparar coa velocidade de Fermi dos electróns e que non rompa a simetría de inversión temporal do sistema. Os modos ópticos polares presentes en Bi_2Te_3 e Bi_2Se_3 son propostos a cumplir estas condicións basándose en estudos recentes, aínda que podería ser xeral para outros modos basándonos no feito de que o acoplamiento espín-órbita destes sistemas poderían non implicar a necesidade de dispoñer de dous modos fonónicos que se propágan en oposición.

Estes resultados tamén son postos a proba dentro da electrodinámica axiónica destes sistemas. A última comprobación do noso modelo asocia directamente a temperatura dentro da frecuencia de oscilación. Desta maneira, atopamos o mesmo resultado que aquel obtido usando a acción Chern-Simons (Capítulo 1). Ambos formalismos necesitan ser equivalentes como un mesmo podría pensar. Pero as consecuencias e a motivación son moi

diferentes. No primeiro caso, calculamos directamente o coeficiente Seebeck topolóxico a partir da acción de Chern-Simons utilizando teoría térmica de campos. Agora, asociamos directamente a temperatura coa frecuencia por medio do campo intrínseco topolóxico para demostrar como as oscilacións da rede causadas pola temperatura contribúen o efecto termoeléctrico. A conclusión é que para algúns modos de vibración nunha ampla gama de frecuencias, o coeficiente Seebeck do sistema permanece inalterable mentres que a velocidade dos electróns pode aumentar ou diminuír dependendo de se o seu acoplamento é favorable ou desfavorable. En resumo, transformamos enerxía do rede aos electróns a través dun mecanismo que pode ser tecnolóxicamente favorable para a termoelectricidade nos TIs, onde os estados topolóxicos teñen condutividades e coeficientes de Seebeck definidos a través dos invariantes topolóxicos.

No capítulo 3 exploramos con máis detalle o modelo anterior para analizar o magnetismo orbital intrínseco dos TMs. Isto foi motivado polo concepto de órbita proposto antes para os electróns topolóxicos, que nos induciu a demostrar explícitamente como un campo magnético modifica as diferentes magnitudes de transporte nun sistema de curvatura Berry distinto de cero. O problema dunha partícula cargada nun campo magnético é ben coñecido en física pero nestes sistemas cuánticos descritos por un Hamiltoniano de Dirac temos un novo ingrediente que é a curvatura de Berry que experimenta un acoplamento co campo magnético externo. Isto levounos a ler a fondo varias referencias na literatura para ver como se tratou este problema anteriormente. A introdución dun campo magnético nestes sistemas analizouse usando un formalismo Lagrangiano semiclásico e unha mecánica cuántica non relativista. Non obstante, non existía un formalismo relativista que parta directamente do Hamiltoniano de Dirac e dé unha expresión analítica para todas as magnitudes implicadas. Ademáis, observamos que o papel das correccións de segunda orde no campo magnético se fai importante a campos magnéticos relativamente baixos debido aos pequenos *gaps* de enerxía que caracterizan ós TMs en contraste co que ocorre noutros sistemas físicos na materia condensada. Nunha primeira aproximación abordamos o problema tomando a masa da partícula constante. É dicir, consideramos unha dispersión de Dirac e calculamos a corrección aos autoestados do sistema en presenza dun campo magnético perpendicular. Isto implica tratar con espinores, en contraste co que ocorre con outros formalismos non relativistas, e con correccións dependentes do gauge derivadas dos grados de liberdade que temos á hora de traballar con grupos unitarios $SU(N)$. Unha vez determinadas as correccións dos autoestados do sistema calculamos, tras unha pouca de álxebra tediosa, as diferentes magnitudes de transporte. En concreto, ademais de mostrar como a curvatura de Berry é modulada polo campo magnético externo, vemos matemáticamente e numéricamente como o número Chern do sistema mantense inalterable. Así, cuantificamos como unha curvatura de Berry positiva é potenciada por un campo magnético positivo ou reducida se tomamos o campo magnético negativo, como postulamos a través do campo intrínseco topolóxico. De xeito esquemático, podemos imaxinar os electróns relativistas orbitando debido á curvatura de Berry non nula, polo que, mediante a aplicación dun campo magnético externo teremos a redefinición da velocidade das partículas, radio, momento magnético orbital, enerxía e densidade de estados asociados ao

cambio do campo efectivo que senten estes electróns. Todos estes elementos calcúlanse analíticamente ata segunda orde acadando expresións xerais que se poden aplicar a unha gran variedade de compostos ao non precisar máis ingredientes que o *gap* de enerxía, a velocidade das partículas e a magnitude do campo magnético. Finalmente, estas magnitudes usaranse para obter a enerxía libre do sistema e de xeito directo a magnetización e susceptibilidade orbital en CIs and TIs que incorporan unha dependencia co campo magnético externo. O presente estudo constitúe un método para analizar propiedades de transporte termoeléctricas e magnetoeléctricas en materiais topolóxicos 2D xa que permite ter en conta de xeito simple outras interaccións dentro do sistema.

Un resultado sorprendente que tamén se atopa na literatura, é que a susceptibilidade orbital a campo zero ten a mesma expresión para sistemas con curvatura de Berry distinta de cero independentemente de se a súa topoloxía é trivial ou non. Este feito é notable dadas as diferenzas entre a curvatura de Berry de ambos réximes. Isto quedará claro no capítulo 3 cando mostremos como a magnetización depende directamente sobre esta cantidade a través da enerxía e da densidade de estados. O punto clave é que tamén hai que considerar a dependencia do momento do termo de masa que surge do comportamento parabólico do espectro de enerxía a grandes momentos. Como é sabido, este termo permite facer unha distinción topolóxica que non é posible cando se considera unha dispersión lineal perfecta. Exemplos desto pódense atopar na literatura onde se demostra que a presenza deste termo é necesaria para definir axeitadamente o número de Chern obtido a partir da curvatura de Berry como un número enteiro. Non obstante, este termo é ignorado comúnmente na literatura dado que a maioría dos estudos neste campo particular céntranse en sistemas de tipo grafeno, que ten unha dispersión lineal. O escenario que xorde despois de introducilo no noso formalismo amosa claras discrepancias entre a resposta magnética orbital dun illante trivial e outro non trivial. Así, mentres que se prevé que un illante trivial teña unha resposta limitada a este parámetro, o seu homólogo non trivial mostra un termo adicional na susceptibilidade magnética orbital que se pode escribir en termos do cadrado do fluxo magnético elemental. Estes resultados postulanse novamente para conectar co concepto de órbita nos TMs e co campo efectivo b. Dende o punto de vista práctico, atopamos unha nova vía para aumentar o magnetismo orbital intrínseco dos TIs e CIs incrementando a dependencia parabólica dos seus espectros. Estudos posteriores pódense levar a cabo para extrapolar implicacións similares noutras propiedades termoeléctricas e magnetoeléctricas.

No capítulo 4 levamos a nosa investigación a unha perspectiva diferente examinando a electrodinámica axiónica que necesitan os TIs para explicar as súas propiedades magnetoeléctricas. A electrodinámica axiónica xorde como unha xeneralización da electrodinámica usual, incluíndo a interacción dunha especie de partículas, denominadas axións, co campo electromagnético a través dun campo escalar $\theta(r,t)$. En física, esta electrodinámica está proposta a formar parte da física da materia oscura e presentouse orixinalmente para estudar o problema da paridade da conxugación da carga na cromodinámica cuántica. Non obstante, estas partículas aínda non foron detectadas e actualmente considéranse como virtuais.

Neste traballo, afastámonos da aplicación habitual da electrodinámica axiónica orientada cara á magnetoelectricidade para analizar unha perspectiva máis fundamental. Se os axións están implicados na particular física dos TIs, entón, ademais de producir polarizacións electricas e magnetizacións singulares ao interactuar con campos eléctricos e magnéticos, a súa presenza tamén debe dar lugar a campos internos e presións que poden ser medibles. Existe unha analoxía con outro efecto coñecido en física, que é o efecto Casimir. O efecto Casimir orixínase a partir da flutuacións cuánticas do baleiro cando dúas placas conductoras paralelas colócanse a pouca distancia. Explicado brevemente, aparece unha forza atractiva entre as placas asociada á rexión de enerxía negativa que se crea entre elas cando as placas cortan os fotóns con menor lonxitude de onda. Porén, nos TI en 3D dado que todas as superficies son metálicas, non se espera que ningún fotón penetre no seu interior actuando como unha gaiola de Faraday e os axións son as únicas partículas que poden dar enerxía interna. Aplicando condicións de contorno ao campo escalar $\theta(r,t)$ atopamos unha presión para os TIs que é equivalente ao de Casimir pero con orixe e magnitude moi diferentes. A súa orixe reside nos axións en lugar dos fotóns, mentres que a menor magnitude desta presión débese principalmente á velocidade de Fermi que determina o marco relativista nos TMs. Os cálculos teóricos presentados poden levar a unha verificación directa dos axións ademais de implicar unha vantaxe tecnolóxica á hora de fabricar dispositivos basados en películas delgadas.

En conxunto, os traballos presentados nesta tese aspiran a recoller unha gran variedade de resultados orixinais para os materiais topolóxicos que poden ter importantes implicacións no campo experimental ademais de ir máis aló na física singular destes materiais. En concreto, desenvolvemos un formalismo microscópico para o mecanismo da termoelectricidade en TIs tendo en conta directamente a súa topoloxía e determinando a contribución desta a figura de mérito. Introducimos o papel dos fonóns no contexto relativista destes materiais describindo unha nova ruta de alta eficiencia para a transformación de calor en electricidade. Obtimos unha interpretacion efectiva da curvatura de Berry por medio do campo b. Ademais, acadamos un formalismo relativista que aborda a resposta magnética orbital dos sistemas 2D con curvatura de Berry distinta de cero. Demostramos como a curvatura de Berry pode ser modulada por un campo magnético externo, introducindoa como unha magnitude dinámica. Neste sentido, determinamos as diferenzas na resposta magnética orbital entre illantes topoloxicamente triviais e non triviais. Finalmente, tratamos o campo axiónico $\theta(r,t)$ no contexto dos TIs, dando unha presión asociada aos axións e determinando os ingredientes necesarios para a detección experimental destas partículas en TIs. Os avances teóricos presentados teñen unha aplicación directa en diferentes fenómenos e propiedades e son sensibles a ser xeneralizado para incluír outras interaccións e efectos.

Agradecimientos

En primer lugar, quiero agradecer a mi director de tesis, el Prof. Daniel Baldomir Fernández, por todos estos años de duro trabajo, conversaciones profundas y buenos momentos. Si hoy puedo considerarme un investigador es gracias a él. Nos embarcamos en una aventura difícil, abriendo una nueva línea de investigación en un tema complejo, pero no podía haber elegido mejor compañero para este propósito. Su entusiasmo, constancia y sobretodo su forma de ver la física todavía me sorprenden a día de hoy. Nunca olvidaré estos años.

También tengo mucho que agradecer al Dr. David Serantes, cuyo soporte ha sido muy importante para que pudiese seguir desarrollando esta tesis y con el que he aprendido mucho de otras ramas de la física. A mi amigo Vicente Domínguez Arca, que me ha acompañado siempre en esta etapa y con quien he disfrutado de muchas tardes de trabajo, cafés y discusiones científicas. A mis compañeros de grupo Adolfo, Jan y Cristina que han hecho de esta etapa mucho mas enriquecedora. Ha sido un placer trabajar con vosotros. Tambíen a los profesores del área de Electromagnetismo Javier y Victor, con los que uno siempre aprende; al profesor Francisco Rivadulla del CIQUS y a Juan, Marisol, Rafa y Tona del Instituto de Investigaciones Tecnológicas, que siempre me han ayudado con cualquier cosa que necesitase.

Desde lo mas profundo de mi corazón quiero agradecer a mi pareja, familia y amigos su presencia y paciencia a lo largo de estos años, que no siempre han sido fáciles. A Tais, sin duda la mejor compañera de vida que existe. Mi gran apoyo en los momentos difíciles y la razón de tantos buenos momentos. Gracias por todos estos años maravillosos juntos y por los que vienen. A mis padres, a los cuales no sé si alcanzaré a explicar con palabras todo lo que significan para mí. Papá, Mamá, si hoy estoy aquí es gracias a vosotros. Sois el mejor modelo a seguir en todos los aspectos de la vida y no podría sentirme más orgulloso por ser vuestro hijo, gracias por darlo todo siempre por nosotros. A mis hermanas Sara y María a las cuales admiro profundamente. A mis abuelas Pili y Conchita, a mis tíos Gonzalo, Susu, Juanjo, Valentín, Rafa y Mabel y a mi madrina Lourdes que siempre han cuidado de mí. A mis amigos de siempre Cristian y Jimmy con los que he vivido momentos inolvidables y que siempre están ahí, pase el tiempo que pase. A mi gran amigo Emilio, al que también aplico lo anterior y con el que he vivido años y momen-

tos increíbles compartiendo piso. A mis amigos de la infancia Jaime y Pablo. También a mis físicos y amigos Adán, Jose e Isidro que han formado parte de mi vida desde que puse un pié en la facultad. A todos vosotros, sé que siempre me quedaré corto en palabras.

Por último quiero recordar a los que ya no están, pero sin los cuales hoy no sería la persona que soy. A mi abuelo *Io*, una persona extraordinaria que ha sido como un segundo padre para mí. A mi hermano Juan y a mi abuelo Valentín. Sé que jamás os olvidaré.

Contents

Introduction and Objectives

> "El camino marca una dirección. Y una dirección es mucho más que un resultado."
>
> — Jorge Bucay

The study of the topological phases of matter encompasses different disciplines. So in this area, condensed matter physics, quantum mechanics, quantum field theory and algebraic topology become essential tools to carry out a research. Personally, this implied a first formative stage to get familiar with the different concepts, effects and bibliography belonging to the topological materials (TMs), that would subsequently be applied to the study of the thermoelectricity in topological insulators (TIs). To get started, I found an excellent basis on the book *Topological Insulators: Dirac Equation in Condensed Matter* [1], from which I share its vision about the Dirac equation as the key to the door of topological insulators. I consider this book, among others, necessary before taking the leap to more specific scientific studies in the field [2–5].

From the historical point of view, the development of the topological band theory was motivated in the 1980s by the discovery of the Integer (IQHE) and Fractional Quantum Hall Effects (FQHE) [6, 7]. The integer quantum Hall effect, which is the quantum version of the Hall effect [8], determined how the longitudinal conductance of a 2D system modelled by a free electron gas vanishes when applying a strong perpendicular magnetic field at the same time it appears a transverse quantized conductance $\sigma = \nu\, e^2/h$, being ν the filling factor associated to the Landau Levels of the orbital electrons [9]. For its part, the FQHE applies to interacting electrons systems in which a quantized conductance is also observed but where the filling factor ν takes fractional values associated with the effective charge that particles have in the condensate. Parallel to these effects, additional contributions were postulated as a generalization to quantum mechanics of the anomalous Hall effect and spin Hall effect. The anomalous Hall effect emerged as an extension of the Hall effect for systems with non-zero magnetization $\mathcal{M}$ [10]. Here, a transverse anomalous velocity is generated with the application of an external electric field E. The origin of this velocity lies in the coupling between the electron's spin and its orbital dynamics, resulting in a spin-dependent band configuration in which electrons with opposite spin move with

opposite transverse velocities with respect to E. However, later on, it was postulated that the presence of a finite magnetization actually was not necessary. Thus, even though the net electric current is zero, it is still possible to measure the effects and conductance associated with both spin-currents. This is what we know today as the spin Hall effect [11, 12]. Just as the IQHE and FQHE, these latter effects also have their respective quantum versions in the QAHE and QSHE that also feature quantized conductivities [13–15]

The topological band theory arose intending to explain these effects and lived a crucial moment with the introduction of a new dynamical phase into the quantum wave function under adiabatic conditions [16]. This phase, known as the Berry phase, gave rise to postulate theoretically through adiabatic changes in the Bloch wave function, the existence of a new class of quantum materials with singular properties derived from their non-trivial topological order which feature the previously mentioned effects. In this context, one of the first breakout models was done by Haldane through his proposal for the integer quantum Hall effect without magnetic fields [17]. Here, Haldane developed a spinless fermion model in two-dimensional (2D) honeycomb lattices with periodic magnetic flux density. The peculiarity was that this magnetic flux was set in such a way that its net value per unit cell was zero, obtaining two copies of a 2x2 Dirac Hamiltonian with broken time-reversal symmetry at the points K and K' of the Brillouin Zone (BZ). Performing the calculation of the conductivity, Haldane showed a quantized transverse conductivity $\sigma_{xy} = \nu e^2/h$, where $\nu = 1/2\ [sgn(\mathbb{m}_K) + sgn(\mathbb{m}_{K'})]$ satisfies this relation between the effective masses in both points. Nowadays, we know that ν is in fact a topological invariant, the Chern number C. Afterwards, the idea of Haldane was revisited for Kane and Mele introducing a spin-orbit coupling (SOC) in the graphene lattice which plays the role of the periodic magnetic field with zero net flux preserving time-reversal symmetry for the system [18, 19]. In this case, the model takes into account the spin of the electron leading to 4x4 Dirac Hamiltonian which can be decoupled, in absence of Rashba term, in two non-interacting copies of a 2x2 Dirac Hamiltonian with opposite chirality. Thus, the same quantized conductivity found by Haldane can be associated to a pair of spin currents in a Quantum Spin Hall configuration in which opposite spins move in opposite directions. Kane and Mele also showed how spin and charge are transported by edge states, that are robust against disorder, placed at the boundary of the system while its bulk remains gapped [20]. However, the other significant result behind these works is how the Dirac Hamiltonian emerged as one powerful tool to analyze topological phases and exotic effects in solids [21]. This is not only due because it made it possible to connect in a direct way the topological invariants with the particle wave functions and symmetries in a solid but it also allowed to import singular phenomena from quantum field theory (QFT) to the context of condensed matter physics. That is why rapidly, these works led to the definition of a new class of quantum materials which include topological insulators [22–25], Chern insulators [26], Weyl semimetals [27–29], topological superconductors [30, 31], and more recently magnetic topological insulators [32–34], as well as to study different effects such as the chiral anomaly [35, 36], Majorana states [37–39], thermal hall effect [40, 41], anomalous thermoelectric transport [42, 43], etc.

In this thesis, we focus on the topological insulators, although some of the results obtained can be applied to Weyl semimetals and Chern insulators (CIs). This former relationship is trivial in some cases, given that the physics of 2DTIs can be explained from two time-reversal related Chern species, as it happens in the Kane-Mele model. Precisely, that was the first model proposed for a topological insulator, which has as principal elements, robust metallic edge states, an insulating bulk and time-reversal symmetry [22]. Edge states are named topologically protected because their existence is linked to a topological invariant which tolerates local non-magnetic perturbations [44]. On the other hand, time-reversal symmetry is guaranteed due to having SOC, allowing the existence of both counterpropagating edge states, in pairs of spin-momentum locking channels, known as Kramers pairs [45]. So in essence, TIs were born as candidates for Quantum Spin Hall systems. However, in practice graphene has a limited spin-orbit interaction and hence it was not the most ideal system to measure these effects. Elements with a greater atomic number should be involved to obtain a significant SOC interaction [46]. It did not take long until Bernevig, Hughes and Zhang (2006) presented their model predicting a quantum spin Hall regime in HgTe/CdTe Quantum Wells (QWs) [23] and only a year later, the first experimental realization of a 2DTI that presents a quantum spin Hall effect came [47]. What was clear after these studies was that a band inversion induced by the spin-orbit interaction should precede the topological regime. This fact was crucial for the discovery of the first family of three-dimensional topological insulators (3DTIs) that includes Bi_2Se_3, Bi_2Te_3 and Sb_2Te_3 [24], and for the appearance of a wide variety of studies analyzing singular properties of these systems depending on their dimensionality, symmetries and topological invariants [48–57].

In this sense, the majority of the effects studied in TIs have a quantum-theoretical framework, being well-known the relation between their magnetoelectric properties such as electric conductivity, polarization and magnetization with the topological invariant and Berry phase physics [49, 58, 59]. However, attending to the thermoelectricity, there was a lack of a physical model in the literature that treats this phenomenon within that theoretical context. Obviously, this task is not easy because a link between thermal quantum field theory, topology and solid state physics is not a straightforward task. What was evident is that TIs feature an excellent thermoelectric performance which is measured through the figure of merit [51, 60, 61]

$$Z = \frac{1}{T}\frac{S^2\sigma}{\kappa_e + \kappa_{ph}}$$

or in its dimensionless form ZT, being S the Seebeck coefficient, σ the electric conductivity, κ_e the electronic thermal conductivity, κ_{ph} the lattice thermal conductivity and T the temperature. Bi_2Te_3 as well as other tetradymites and their alloys are within the most common thermoelectric devices [62]. But additionally, besides being excellent thermoelectrics, some are topological insulators. Concretely, for p-type Bi_2Te_3/Sb_2Te_3 superlattices, both TIs, it has been reported a $ZT \sim 2.4$, which consists of the highest value

ever observed experimentally at room temperature [63]. To address this phenomenology directly to the topology exits a simple interpretation. If the topological edge states are responsible for the transport in TIs, then, a semiclassical Boltzmann formalism using Landauer approximation is the first logical step [43, 64–68]. This method is accurate in predicting high figures of merit, Seebeck coefficients and power factors ($S^2\sigma$). However, it does not usually take explicitly any topological information beyond the existence of the edge states and their ballistic nature. In contrast, some important efforts have been done directly addressing quantities such as the entropy and conductivities to the Berry phase and curvature, although they are not enough to provide a microscopical picture of the topological thermoelectricity [41, 49, 69, 70].

This thesis project arises with the aim of providing this connection between the thermoelectric phenomenon and topology. Therefore, our first efforts treat this effect from a new perspective using thermal quantum field theory with the effective Chern-Simons action that TIs employ [71]. The results obtained are summarized in Chapter 1 where we reach an expression for the topological Seebeck coefficient in terms of the topological invariant. Here, we find an anomalous contribution associated with the creation-annihilation of Schwinger's pairs close to the transition between states with different topological indexes, as well as a contribution from the electronic diffusion in a topological band which is close to the lower limit defined in ref. [69]. These ingredients are enough to give an expression for the topological figure of merit that TIs feature in their surface considering only the electronic part, i.e., in absence of lattice thermal conductivity. Thus, for the most basic topological numbers, we find a value $ZT \sim 2.7$ which fits quite accurately with the ones obtained using Bi_2Te_3/Sb_2Te_3 in a superlattice structure used to decrease the lattice thermal conductivity [63].

However, while temperature has been introduced directly in the previous formalism, phonons/lattice oscillations are also present at finite temperatures and at least their coupling with the topological electrons must be considered. Note that a topological insulator has time-reversal symmetry $\hat{T}$ and therefore excitations in the electronic Hamiltonian should preserve entropy to maintain $\hat{T}$. This second study is addressed in Chapter 2 where we demonstrate by means of an effective topological intrinsic field b, deduced from the non-trivial Berry curvature of TIs, how oscillations can be introduced in the electron dynamics through the Dirac oscillator. Noteworthy, we demonstrate how in certain conditions the coupling between electrons and phonons leads to isentropic processes just as in the formalism derived in Chapter 1 for thermal excitations but under a new approach. Moreover, the field b, which has a successful verification through electrodynamics and perturbation theory, allows us to figure out the intrinsic forces and fields that TIs present. In this sense, given the magnetic field interpretation of the Berry curvature in the k-space, the next natural step is the analysis of the electron dynamics in presence of magnetic fields that leads us to the study of the orbital dynamics in 2D topological electron systems with non-zero Berry curvature.

In Chapter 3 we analyze this issue by performing an accurate perturbative calculation which allows a precise determination of the Chern number C. The relativistic formalism

developed differs from other approaches using Landau levels, semiclassical Lagrangian formalism and non-relativistic quantum mechanics to give an expression for the orbital magnetization, thermal/electrical conductivity, density of states, energy, susceptibility, Berry curvature, etcetera [42, 72–77]. Thus, besides complementing some results of the previous works, the theoretical formalism developed provides a schematic picture about how the Berry curvature couples with an externally applied magnetic field inducing a redefinition of the remaining quantities previously mentioned which are given through analytical expressions. The ingredients obtained are enough to give an expression for the density of free energy, orbital magnetization and susceptibility which include non-negligible corrections due to the magnetic field. However, as the current literature indicates, this does not involve any difference between the zero-field orbital susceptibility in both topological non-trivial and trivial regimes. This is quite surprising, given that the transport properties of both phases are very different just as their topology. Thus, in the latter part of Chapter 3, we include the natural parabolic dependence in the energy spectrum of a TI which is needed to distinguish topologically both regimes through the Chern number. In this way, we finally unveil the differences between both systems involving an anomalous response that will be analyzed in detail.

Finally, in Chapter 4 we carry out an analysis of the axion electrodynamics in TIs that culminates with an expression for the pressure that axions are predicted to exert on the metallic surfaces of a TI. The obtained force is similar to the one obtained by Casimir for photons but with a very different origin and magnitude. Given that photons are not expected to enter inside a TI since all surfaces are metallic, resulting in a kind of Faraday cage, an experimental verification of the axions in TIs is discussed after these results.

This thesis has been developed inside the Materials Science PhD program of the University of Santiago de Compostela. The works and methods described along this manuscript aspire to give a theoretical framework for different properties of topological materials which can serve as a guide for further scientific studies, technological devices and real-life applications.

0 Topological insulators: Basic concepts

In this chapter, we will give the basic elements needed to understand some of the main aspects behind the topological insulators. For a more detailed discussion about the concepts developed here, there are excellent books that the reader can turn to [1–5] as well as specific research articles that are provided throughout the text.

0.1 Berry phase

The Berry phase is one of the principal aspects to be studied although their origin does not lie precisely inside the context of condensed matter physics but in quantum mechanics. In 1984 M.V. Berry demonstrated how an emergent phase arises when studying adiabatic changes of the quantum wave function [16]. These concepts were later translated to J. Zak using the Bloch wave functions in a solid [78]. Concretely, Berry considered an arbitrary Hamiltonian $H(\boldsymbol{R})$ which is defined on a parameter space $\boldsymbol{R} = (R_1, R_2, ..)$ with coordinates $R_j(t)$ $(j = 1, 2, ...)$ having an adiabatic time dependence. That is, he fixed the constraint that the coordinates must vary slowly in comparison with the energy scale defined by the wave functions $|\Psi(t)\rangle$ of the system. Thus, introducing a generic dependence for $|\Psi(t)\rangle = e^{-i\theta(t)} |n(\boldsymbol{R}(t)\rangle$ in the Schrödinger equation

$$i\hbar \frac{\partial |\Psi(t)\rangle}{\partial t} = H(\boldsymbol{R}(t)) |\Psi(t)\rangle \tag{0.1}$$

where $|n(\boldsymbol{R})\rangle$ form the basis of eigenstates at a given time satisfying the eigenvalue equation

$$H(\boldsymbol{R}) |n(\boldsymbol{R})\rangle = \xi^n(\boldsymbol{R}) |n(\boldsymbol{R})\rangle \tag{0.2}$$

being $\xi^n(\boldsymbol{R})$ the energy of the eigenstate $|n(\boldsymbol{R})\rangle$, Berry observed that the phase $\theta(t)$ presented an additional factor beyond the well-known dynamical phase. That is, the wave function

$$|\Psi(t)\rangle = e^{-\frac{i}{\hbar}\int_0^t dt' \xi^n(t')} \, e^{i\gamma^n} \, |n(\boldsymbol{R}(t)\rangle \tag{0.3}$$

differs from its usual expression in quantum mechanics $|\Psi(t)\rangle = e^{-\frac{i}{\hbar}\int_0^t dt' \xi^n(t')} |n(\boldsymbol{R}(t)\rangle$ by a phase factor $e^{i\gamma^n}$ where

$$\gamma^n = i \int_0^t \langle n(\boldsymbol{R}(t')| \frac{d}{dt'} |n(\boldsymbol{R}(t')\rangle \, dt' \tag{0.4}$$

is the Berry phase. Then, considering that the system evolution takes place between a time $t = 0$ and $t = T$ in such a way that $\boldsymbol{R}(t = 0) = \boldsymbol{R}(T)$, i.e., in a closed curve $\mathcal{C}$, the integral can be written as follows

$$\begin{aligned} \gamma^n &= i \int_0^T \langle n(\boldsymbol{R}(t')| \frac{d}{dt'} |n(\boldsymbol{R}(t')\rangle \, dt' = i \int_{\mathcal{C}} \langle n(\boldsymbol{R})| \nabla_{\boldsymbol{R}} |n(\boldsymbol{R})\rangle \cdot d\boldsymbol{R} \\ &= \int_{\mathcal{C}} \boldsymbol{\mathcal{A}}^n(\boldsymbol{R}) \cdot d\boldsymbol{R} = \iint_{\mathcal{C}} \boldsymbol{\nabla} \times \mathcal{A}^n(\boldsymbol{R}) \cdot d\boldsymbol{S} \\ &= \iint_{\mathcal{C}} \boldsymbol{\Omega}^n(\boldsymbol{R}) \cdot d\boldsymbol{S} \end{aligned} \tag{0.5}$$

making use of Stocke's theorem and where $d\boldsymbol{S}$ denotes the area element in the parameter space. Here, $\mathcal{A}^n(\boldsymbol{R}) = i \langle n(\boldsymbol{R})| \nabla_{\boldsymbol{R}} |n(\boldsymbol{R})\rangle$ is named the Berry potential, in analogy with the electromagnetic field, and $\boldsymbol{\Omega}^n$ is the Berry curvature

$$\begin{aligned} \boldsymbol{\Omega}^n(\boldsymbol{R}) &= i \, \nabla_{\boldsymbol{R}} \times \langle n(\boldsymbol{R})| \nabla_{\boldsymbol{R}} |n(\boldsymbol{R})\rangle = i \, \langle \nabla_{\boldsymbol{R}} n(\boldsymbol{R})| \times |\nabla_{\boldsymbol{R}} \, n(\boldsymbol{R})\rangle \\ &= i \sum_{m \neq n} \langle \nabla_{\boldsymbol{R}} \, n(\boldsymbol{R}) | m(\boldsymbol{R})\rangle \times \langle m(\boldsymbol{R}) | \nabla_{\boldsymbol{R}} \, n(\boldsymbol{R})\rangle \\ &= i \sum_{m \neq n} \frac{\langle n(\boldsymbol{R})| \nabla_{\boldsymbol{R}} H \, |m(\boldsymbol{R})\rangle \times \langle m(\boldsymbol{R})| \nabla_{\boldsymbol{R}} H \, |n(\boldsymbol{R})\rangle}{(\xi^n - \xi^m)^2} \end{aligned} \tag{0.6}$$

where we have used

$$|n\rangle \langle n| = 1 - \sum_{m \neq n} |m\rangle \langle m| \tag{0.7}$$

and the identity

$$\langle m| (\nabla H) |n\rangle = \langle m| \nabla (H |n\rangle) - \langle m| H |\nabla n\rangle = (\xi^n - \xi^m) \langle m| \nabla n\rangle \tag{0.8}$$

being $|m\rangle$ and $|n\rangle$ orthogonal eigenstates forming the basis of the Hilbert space of H. From here on out, we are going to suppress the label $\boldsymbol{R}$ for simplicity remembering that the parameter space is general and in particular, can apply either to the momentum or

real space coordinates. In correspondence with the Berry potential, the curvature can be interpreted as a magnetic field in the momentum space. Thus, as it is logical, the curvature can be demonstrated to be a gauge-independent magnitude under rotations of the basis while the Berry potential is not. Considering that $|n\rangle \to e^{iU(\boldsymbol{R})}|n\rangle$, being $U(\boldsymbol{R})$ single-valued, it is straightforward to see that

$$\boldsymbol{\mathcal{A}}^n \to \boldsymbol{\mathcal{A}}^n - \boldsymbol{\nabla} U(\boldsymbol{R}) \tag{0.9}$$

and hence the Berry phase results

$$\gamma^n \to \gamma^n - U(R=T) + U(R=0) = \gamma^n - 2\nu\pi \tag{0.10}$$

being ν an integer which accounts the number of closed loops completed during T, and where the factor 2π satisfies the condition $e^{iU(R=0)}|n(R=0)\rangle = e^{iU(R=T)}|n(R=T)\rangle = e^{iU(R=T)}|n(R=0)\rangle$.

0.2 Magnetic monopole interpretation of the Berry curvature

One of the key concepts used to derive an expression of the effective topological field b in Chapter 2 is the magnetic field interpretation of the Berry curvature. This can be seen easily by considering a two-level system just like in ref. [3]

$$H = \boldsymbol{d}\cdot\boldsymbol{\sigma} = \begin{bmatrix} d_z & d_x - id_y \\ d_x + id_y & -d_z \end{bmatrix} \tag{0.11}$$

where σ_i are the Pauli matrices and $d = |d|(\sin\theta\cos\phi, \sin\theta\sin\phi, \cos\theta)$ is a 3-component vector defined on a parameter space $\boldsymbol{R} = (\phi, \theta)$. Calculating the eigenvalues of Eq. (0.11) $\xi^{\pm} = \pm|d|$ and their corresponding eigensates

$$|+\rangle = \begin{bmatrix} \cos\theta/2 \\ e^{i\phi}\sin\theta/2 \end{bmatrix} \qquad |-\rangle = \begin{bmatrix} \sin\theta/2 \\ -e^{i\phi}\cos\theta/2 \end{bmatrix} \tag{0.12}$$

we can calculate directly their associated Berry potentials

$$\boldsymbol{\mathcal{A}}^{+} = (-\sin^2(\theta/2), 0) \qquad \boldsymbol{\mathcal{A}}^{-} = (-\cos^2(\theta/2), 0) \tag{0.13}$$

and curvatures

$$\boldsymbol{\Omega}^{\pm} = \pm\frac{\sin\theta}{2}\hat{\boldsymbol{u}} \tag{0.14}$$

being $\hat{\boldsymbol{u}} = \hat{\boldsymbol{\phi}} \times \hat{\boldsymbol{\theta}}$ the perpendicular unitary vector. Thus, making a transformation from (θ, ϕ) to a general subspace $\boldsymbol{R} = (R_i, R_j)$ and subsequently considering the trivial case $d(\boldsymbol{R}) = \boldsymbol{R}$ it can be shown that the Berry curvature [3]

$$\boldsymbol{\Omega}^{\pm} = \pm \frac{1}{2} \frac{\boldsymbol{d}}{d^3} \tag{0.15}$$

has the same form of a magnetic monopole of strength 1/2 with opposite signs for both eigenstates. Integrating the Berry curvature over a sphere or over any closed curve on its surface will give a factor 2π. In general notation this result will be $2\pi C$, being C the number of monopoles enclosed in the sphere. This number is not other than the Chern number C defined in algebraic topology measuring the number of singularities in a compact surface [2, 5].

$$C = \frac{1}{2\pi} \iint_C \boldsymbol{\Omega}^n d\boldsymbol{S} \tag{0.16}$$

These ingredients will be determinant in the transport properties of the material, specially in two-dimensions where we will be focused several times along this thesis and where the Berry curvature allows a simple determination of the system's topology by means of the first Chern number C. In this context, we have to remark that in presence of time-reversal symmetry, Kramers pairs will have also opposite Berry curvatures leading to a net field zero. This will be demonstrated later. Nevertheless, a generalization to higher dimensional system will be explored also taking into account degeneracy in the eigenstates which implies dealing with non-Abelian Berry potential and curvatures.

0.3 Two-level Dirac Hamiltonian

As a first approach to the physics of topological materials, it is straightforward to note that the Hamiltonian defined in Eq. (0.11) has the same form of a 2x2 Dirac Hamiltonian used to describe the relativistic dynamics of half-integer spin massive particles [79].

$$H = \begin{bmatrix} mc^2 & \hbar c(k_x - ik_y) \\ \hbar c(k_x + ik_y) & -mc^2 \end{bmatrix} \tag{0.17}$$

Where c is the speed of light, m the mass of the particle and $\boldsymbol{k}$ the wavevector associated with the particle momentum $\boldsymbol{p} = \hbar \boldsymbol{k}$. Additionally, there also exists a direct correspondence with the case of a half-integer spin particle in a magnetic field, low-energy tight-binding Hamiltonians with complex hopping elements, spin-orbit coupled systems and more [19, 80, 81]. In this case, we can rewrite the previous eigenstates in the following form

$$|+\rangle = \frac{1}{\sqrt{2}} \begin{bmatrix} \sqrt{1+\frac{mc^2}{\xi}} \\ e^{i\phi}\sqrt{1-\frac{mc^2}{\xi}} \end{bmatrix} \qquad |-\rangle = \frac{1}{\sqrt{2}} \begin{bmatrix} \sqrt{1-\frac{mc^2}{\xi}} \\ -e^{i\phi}\sqrt{1+\frac{mc^2}{\xi}} \end{bmatrix} \tag{0.18}$$

where ξ is the energy of the positive energy solution $\xi^+ = -\xi^- = \xi = \sqrt{m^2c^4 + \hbar^2c^2k^2}$ and $\phi = \arctan(k_y/k_x)$. Therefore, proceeding as before we find the components of the Berry potential for both bands

$$\mathcal{A}^+_{k_x} = +\frac{k_y}{2k^2}\left(1 - \frac{mc^2}{\xi}\right) \qquad \mathcal{A}^-_{k_x} = -\frac{k_y}{2k^2}\left(1 - \frac{mc^2}{\xi}\right) \tag{0.19}$$

$$\mathcal{A}^+_{k_y} = -\frac{k_x}{2k^2}\left(1 - \frac{mc^2}{\xi}\right) \qquad \mathcal{A}^-_{k_y} = +\frac{k_x}{2k^2}\left(1 - \frac{mc^2}{\xi}\right) \tag{0.20}$$

where we have made use of the derivatives for the positive

$$|\partial_{k_x}+\rangle = \frac{1}{\sqrt{2}} \begin{bmatrix} \frac{\Gamma_{kx}}{2\sqrt{1+\frac{M}{\xi}}} \\ -\frac{ik_y}{k^2}e^{i\phi}\sqrt{1-\frac{M}{\xi}} - \frac{\Gamma_{kx}e^{i\phi}}{2\sqrt{1-\frac{M}{\xi}}} \end{bmatrix} \tag{0.21}$$

$$|\partial_{k_y}+\rangle = \frac{1}{\sqrt{2}} \begin{bmatrix} \frac{\Gamma_{ky}}{2\sqrt{1+\frac{M}{\xi}}} \\ \frac{ik_x}{k^2}e^{i\phi}\sqrt{1-\frac{M}{\xi}} - \frac{\Gamma_{ky}e^{i\phi}}{2\sqrt{1-\frac{M}{\xi}}} \end{bmatrix} \tag{0.22}$$

and negative eigenstates

$$|\partial_{k_x}-\rangle = \frac{1}{\sqrt{2}} \begin{bmatrix} -\frac{\Gamma_{kx}}{2\sqrt{1-\frac{M}{\xi}}} \\ \frac{ik_y}{k^2}e^{i\phi}\sqrt{1+\frac{M}{\xi}} - \frac{\Gamma_{kx}e^{i\phi}}{2\sqrt{1+\frac{M}{\xi}}} \end{bmatrix} \tag{0.23}$$

$$|\partial_{k_y}-\rangle = \frac{1}{\sqrt{2}} \begin{bmatrix} -\frac{\Gamma_{ky}}{2\sqrt{1-\frac{M}{\xi}}} \\ -\frac{ik_x}{k^2}e^{i\phi}\sqrt{1+\frac{M}{\xi}} - \frac{\Gamma_{ky}e^{i\phi}}{2\sqrt{1+\frac{M}{\xi}}} \end{bmatrix} \tag{0.24}$$

where $M = mc^2$ stands for the energy gap between the positive and negative solutions and

$$\Gamma_{k_i} = \frac{\partial}{\partial k_i}\left(\frac{M}{\xi}\right) = -\frac{\hbar^2c^2M}{\xi^3}k_i \tag{0.25}$$

In this way, considering for instance the positive energy solution it is straightforward to reach the previous relations

$$\mathcal{A}^{+}_{k_x} = i\,\langle +|\partial_{k_x}+\rangle = \frac{i}{2}\left[-i\frac{k_y}{k^2}\left(1-\frac{M}{\xi}\right) - \frac{\cancel{\Gamma_{k_x}}}{\cancel{2}} + \frac{\cancel{\Gamma_{k_x}}}{\cancel{2}}\right] \tag{0.26}$$

and check the gauge-dependent nature of the Berry potential. With this purpose, we can consider a rotation of the eigenstate $|\bar{+}\rangle = e^{-i\phi}\,|+\rangle$ and hence obtain

$$\begin{aligned}\bar{\mathcal{A}}^{+}_{k_x} = i\,\langle \bar{+}|\partial_{k_x}\bar{+}\rangle &= i\,\langle +|\partial_{k_x}+\rangle + i\left(\frac{ik_y}{k^2}\right)\langle +|+\rangle \\ &= \mathcal{A}^{+}_{k_x} - \frac{k_y}{k^2} = -\frac{k_y}{2k^2}\left(1+\frac{M}{\xi}\right)\end{aligned} \tag{0.27}$$

which clearly differs from Eq. (0.19). The same procedure will be employed to determine gauge-dependent corrections to the system's eigenstates in Chapter 3 that must be removed to define properly the physical observables. Complementary, we can define the Berry curvature by applying Eq. (0.6)

$$\begin{aligned}\Omega^{+}_{k_x,k_y} &= i\left[\left\langle\partial_{k_x}+\middle|\partial_{k_y}+\right\rangle - \left\langle\partial_{k_y}+\middle|\partial_{k_x}+\right\rangle\right] \\ &= -2\,\mathrm{Im}\left\{\left\langle\partial_{k_x}+\middle|\partial_{k_y}+\right\rangle\right\} \\ &= \frac{\Gamma_{k_x}k_x + \Gamma_{k_y}k_y}{2k^2} = -\frac{\hbar^2c^2M}{2\xi^3}\end{aligned} \tag{0.28}$$

and for the negative solution we can proceed equally

$$\Omega^{-}_{k_x,k_y} = -\frac{\Gamma_{k_x}k_x + \Gamma_{k_y}k_y}{2k^2} = +\frac{\hbar^2c^2M}{2\xi^3} \tag{0.29}$$

or applying the simple substitution $\xi \to -\xi$ given that the system's Hamiltonian is particle-hole symmetric. One of the key points arises when calculating the Chern number

$$C = \frac{1}{2\pi}\iint \Omega^{+}_{k_x,k_y}\,d\phi k dk = \frac{1}{2}\int_0^\infty \Omega^{+}_{k_x,k_y}\,dk^2 = \frac{1}{2}\frac{M}{\xi}\Big|_0^\infty = -\frac{1}{2}sgn(M) \tag{0.30}$$

which results a half-integer number instead of an integer. This issue is due to our functions are not well-defined at the boundary $k \to \infty$ in the continuum limit. However, in the context of solid state physics, this problem is addressed by considering the parabolic dependence of the energy spectra that can be deduced naturally from several insightful tight-binding models in the study of topological phases of matter [17, 19, 45, 81–83]. Obtaining the Dirac Hamiltonian from these models results immediate. Consider for instance a simplified tight-binding Hamiltonian for half-integer spin particles in two-dimensions [1]

$$H_t = \xi_v \sum_{\alpha,\beta}^{N} c^{\dagger}_{\alpha\beta}\sigma_z c_{\alpha\beta} + it\sum_{\alpha,\beta}^{N-1}\left(c^{\dagger}_{\alpha+1\beta}\sigma_x c_{\alpha\beta} - c^{\dagger}_{\alpha\beta}\sigma_x c_{\alpha+1\beta}\right) + it\sum_{\alpha,\beta}^{N-1}\left(c^{\dagger}_{\alpha\beta+1}\sigma_y c_{\alpha\beta} - c^{\dagger}_{\alpha\beta}\sigma_y c_{\alpha\beta+1}\right) \tag{0.31}$$

where the summation α (β) runs over all the lattice sites in the x (y) direction, N is the number of sites which we take equal in both directions for simplicity and $c^{\dagger}_{\alpha\beta} = (c^{\dagger}_{\alpha\beta,\uparrow}, c^{\dagger}_{\alpha\beta,\downarrow})$ being $c^{\dagger}_{\alpha\beta}$ ($c_{\alpha\beta}$) the fermionic creation (annihilation) operator at site (α,β). Here, ξ_v represents the on-site energy which plays the role of a Zeeman term and the second and third summations stand for a complex spin-dependent first-neighbour hopping term. Thus, considering a square lattice with lattice constant a and performing the Fourier transform to the creation/annihilation operators, it is found that in the momentum space

$$H(k) = \begin{bmatrix} \xi_v & 2t(\sin(k_x a) - i\sin(k_y a)) \\ 2t(\sin(k_x a) + i\sin(k_y a)) & -\xi_v \end{bmatrix} \tag{0.32}$$

which at low energy $k \to 0$ results in a 2x2 Dirac Hamiltonian [84]

$$H(k) = \begin{bmatrix} \xi_v & \hbar v_F(k_x - ik_y) \\ \hbar v_F(k_x + ik_y) & -\xi_v \end{bmatrix} \tag{0.33}$$

where $v_F = 2ta/\hbar$ is the Fermi velocity of the electrons in the solid. It seems clear, that in the context of topological materials v_F replaces the speed of light c given that the Dirac dispersion law of massless fermions works with v_F in these materials [23, 24, 85]. Equivalent models can be built employing diatomic lattices for spinless particles where first neighbours are different atoms labelled as A and B, as in the Haldane model, or even both cases just as in the Kane-Mele model among others (Fig.0.1). The differences between them are the dimensions of the resulting Dirac Hamiltonian and its intrinsic symmetries.

The previous illustrative model can be completed by introducing second-neighbour hopping elements which are of course non-zero in the context of solid state physics. Considering that these hopping elements are given by

$$-t_2 \sum_{\ll i,j \gg} c^{\dagger}_i \sigma_z c_j = -t_2 \sum_{\alpha,\beta}^{N} c^{\dagger}_{\alpha+1\beta+1}\sigma_z c_{\alpha\beta} + ... \tag{0.34}$$

where the symbol $\ll\gg$ stands for second-neighbours, therefore, the resulting low-energy Dirac Hamiltonian reads

$$H(k) = \begin{bmatrix} M - \mathcal{B}k^2 & \hbar v_F(k_x - ik_y) \\ \hbar v_F(k_x - ik_y) & -(M - \mathcal{B}k^2) \end{bmatrix} \tag{0.35}$$

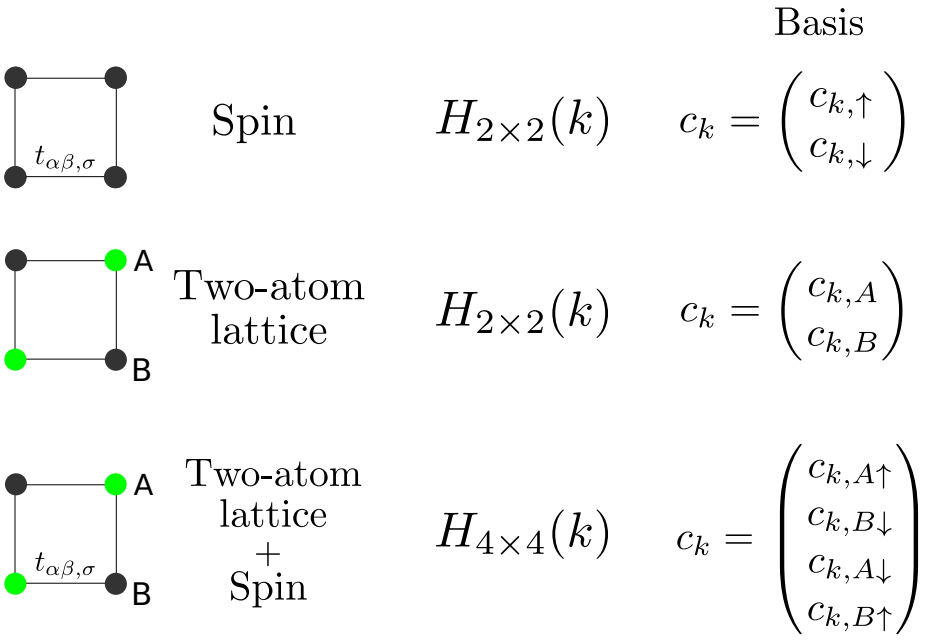

Figure 0.1: Examples of the different Dirac Hamiltonian that will be obtained taking into account spin and/or single/diatomic lattices. Square lattice is taken for simplicity and without loss of generality.

being $M = \xi_v - 4t_2$, $\mathcal{B} = -2t_2a^2$, $\xi = \pm\sqrt{(M - Bk^2)^2 + \hbar^2 v_F^2 k^2}$ the new energy spectra of both conduction and valence bands and $k^2 = k_x^2 + k_y^2$. In this situation, we have a k-dependent effective mass, due to $M(k) = M - \mathcal{B}k^2$, as usual in the context of materials science and an energy dispersion which is linear at low-energies and parabolic at large momenta. Strictly speaking, we have a Dirac hyperbola for each conduction and valence band. The calculation of the Berry potentials and curvatures on these bands still results direct, unlike now we have that

$$\Gamma_{k_i} = \frac{\partial}{\partial k_i}\left(\frac{M(k)}{\xi}\right) = -\frac{\hbar^2 v_F^2 (M + \mathcal{B}k^2)}{\xi^3} k_i \tag{0.36}$$

and therefore the Berry curvature

$$\Omega^{\pm}_{k_x,k_y} = \mp\frac{\hbar^2 v_F^2 (M + \mathcal{B}k^2)}{2\xi^3} \tag{0.37}$$

leaves the Chern number as an integer

$$C^+ = -\frac{1}{2}[sgn(\mathcal{B}) + sgn(M)] = \begin{cases} \pm 1 & M\mathcal{B} > 0 \\ 0 & M\mathcal{B} < 0 \end{cases} \tag{0.38}$$

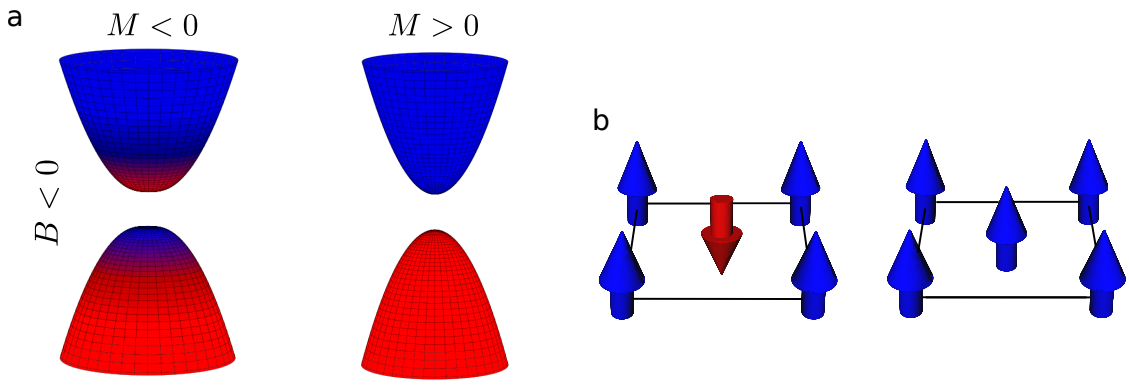

Figure 0.2: (**a**) Energy dispersion for the conduction and valence bands of Eq. (0.35) in non-trivial ($M\mathcal{B} > 0$) and trivial regimes ($M\mathcal{B} < 0$). Red and blue colors stand for the spin z-component. (**b**) Illustration of the k-dependent spin texture for the conduction band in both regimes where spin inversion takes places at the corners of the BZ of a non-trivial insulator.

for any non-zero value of $\mathcal{B}$. Notice that $\mathcal{B}$ will be defined as negative in the majority of cases since the energy tends to grow when increasing the particle momentum. So, we have a topologically non-trivial regime (Chern insulator) determined by a Chern number ± 1 for systems with negative M. This concept, which may seem counterintuitive in a first instance, simply stands for the band inversion that needs to precede the topological phase transition as it has been addressed in several cases [23, 24, 86–89]. Other quantities of interest could be the spin z-component of the electrons,

$$\langle + | \, \sigma_z \, | + \rangle = \frac{M - \mathcal{B}k^2}{\xi} \tag{0.39}$$

the electric conductivity and electric polarization as we will see shortly. In the first case, we can already appreciate some peculiarities that the topological regime features (Fig. 0.2). Finally, we have to remark that Eq. (0.35) is not the unique Dirac Hamiltonian describing topological phases of matter. This type of Hamiltonian can be found in the one derived by Bernevig, Hughes and Zhang for the HgTe/CdTe Quantum Wells which includes two copies of Eq. (0.35) to preserve time-reversal symmetry [23, 90, 91]. However, the resulting Hamiltonian and hence the topological constraint, extremely depend on the crystal structure of the system and its electronic interactions. In this way, the Dirac Hamiltonians derived by Haldane and Kane-Mele have a different relationship between the parameters M and $\mathcal{B}$ to determine the *boundaries* between the trivial and non-trivial regimes [17, 19, 92–94].

0.4 Quantized conductivity and electric polarization

One of the principal results that Haldane obtained in his low-energy model for the integer quantum Hall effects without magnetic fields, was the presence of quantized electrical conductivities directly associated with the Dirac Hamiltonian [17]. However, if this quantization wants to be addressed to the topology, its origin must be linked with the adiabatic theory. Of course, this is not the only possible route as we will see in Chapter 3 through the time-independent formalism developed to introduce magnetic fields into the relativistic dynamics of these systems or complementary, from the semiclassical equations of motion for systems with non-zero Berry curvature [73, 95, 96]. Both formalisms allow a simple determination of the Hall conductivity through the Středa formula [97]

$$\sigma_{xy} = -e\left(\frac{\partial n_e}{\partial B}\right)_{\mu} \tag{0.40}$$

where e is the elementary charge, n_e the electron density, B the magnetic field and μ the chemical potential. The other possibility goes through the introduction of an electric field which gives a vector potential

$$\boldsymbol{A}(t) = -\boldsymbol{E}\, t \tag{0.41}$$

given by Faraday's law, that is suitable to be introduced in the adiabatic corrections to the system eigenstates [1, 5, 58]

$$|n\rangle \to |n\rangle - i\hbar \sum_{m\neq n} \frac{\langle m|\partial_t n\rangle}{\xi^n - \xi^m}\,|m\rangle \tag{0.42}$$

provided that $\boldsymbol{E}$ is sufficiently small to carry out this evolution adiabatically. Supposing that $\boldsymbol{E}$ is a one-component vector, i.e., $\boldsymbol{E} = E\hat{\boldsymbol{x}}$ for instance, we can rewrite Eq. (0.42)

$$|n\rangle \to |n\rangle - i\hbar \sum_{m\neq n} \frac{\partial k_x}{\partial t}\frac{\langle m|\partial_{k_x} n\rangle}{\xi^n - \xi^m}\,|m\rangle = |n\rangle + ieE \sum_{m\neq n} \frac{\langle m|\partial_{k_x} n\rangle}{\xi^n - \xi^m}\,|m\rangle \tag{0.43}$$

where the latter identity uses the Peierls substitution $\boldsymbol{p} + e\boldsymbol{A}$ to address the temporal dependence of the wave vector $\boldsymbol{k}$. From here, it is straightforward to compute the longitudinal and transverse components of the velocity. In general notation, the average

velocity of a particle in a band n is

$$\begin{aligned}\langle n|\,\hat{v}_j\,|n\rangle \to \langle n|\,\hat{v}_j\,|n\rangle + ieE\sum_{m\neq n}\frac{\langle n|\,\hat{v}_j\,|m\rangle\,\langle m|\partial_{k_x}n\rangle}{\xi^n-\xi^m}\\ - ieE\sum_{m\neq n}\frac{\langle\partial_{k_x}n|m\rangle\,\langle m|\,\hat{v}_j\,|n\rangle}{\xi^n-\xi^m}\end{aligned} \tag{0.44}$$

where $\hat{v}_j=\frac{d}{dt}\hat{r}_j=\frac{i}{\hbar}[\hat{H},\hat{r}]=\frac{1}{\hbar}\partial_{k_j}H$ is the j-component of the velocity operator following Heisenberg notation and $\hat{r}$ is the position operator. It is easy to show that

$$\langle n|\,\hat{v}_j\,|n\rangle=\frac{1}{\hbar}\partial_{k_j}\xi^n \tag{0.45}$$

$$\begin{aligned}\langle n|\,\hat{v}_j\,|m\rangle=\frac{1}{\hbar}\langle n|\,(\partial_{k_j}H)\,|m\rangle)=\frac{1}{\hbar}(\xi^m-\xi^n)\,\langle n\big|\partial_{k_j}m\rangle\\ =\frac{1}{\hbar}(\xi^n-\xi^m)\,\langle\partial_{k_j}n\big|m\rangle\end{aligned} \tag{0.46}$$

which can be introduced in Eq. (0.44) to reach

$$\langle\Delta v_j^n\rangle=i\frac{eE}{\hbar}\left[\langle\partial_{k_j}n\big|\partial_{k_x}n\rangle-\langle\partial_{k_x}n\big|\partial_{k_j}n\rangle\right]=-\frac{eE}{\hbar}\,\Omega^n_{k_xk_j} \tag{0.47}$$

making use of Eq. (0.7). Therefore, while the change in the longitudinal component results clearly zero, the transverse velocity has a contribution proportional to the product of the electric field with the Berry curvature

$$v_y^n\equiv\langle v_y^n\rangle=\frac{1}{\hbar}\partial_{k_y}\xi^n-\frac{eE}{\hbar}\Omega^n \tag{0.48}$$

or in vector notation $\boldsymbol{v^n}=\frac{1}{\hbar}\boldsymbol{\nabla}\xi^n-\frac{e}{\hbar}\boldsymbol{E}\times\boldsymbol{\Omega^n}$ [98]. Physically, we are observing how a transverse velocity arises when applying adiabatically an electric field to a system with non-zero Berry curvature. But additionally, we can see intuitively, how the Berry curvature plays the role of a magnetic field for the electron dynamics inside a band n, justifying our interpretation through the field b in Chapter 2. Finally, obtaining the transverse conductivity from the previous formula is direct by taking the density of electric current

$$j_y^n=-\frac{e}{(2\pi)^2}\iint v_y^n f(k)\;d\phi kdk=\frac{e^2}{h}C\;E_x \tag{0.49}$$

where $f(k)$ is the Fermi-Dirac distribution function that is taken equal to the unity at zero temperature conditions and fully occupied bands. This fixes the Hall conductivity to be quantized in multiples of the Chern number C

$$\sigma_H \equiv \sigma_{xy}^n = \frac{e^2}{\hbar}\frac{1}{(2\pi)^2}\int \boldsymbol{\Omega}^n d\boldsymbol{k} = \frac{e^2}{h}C \tag{0.50}$$

Thus, coming back to the Dirac Hamiltonian Eq. (0.35), it is clear that electrons in the conduction and valence bands contribute with opposite Hall conductivities given that their associated curvatures and Chern numbers are opposite. Therefore, in this two-level system, if the Fermi level lies inside the band gap, we will observe a quantized Hall conductivity $(e^2/h)C^-$ which will decrease if the Fermi level goes into the bands or we have temperatures with thermal energy k_BT similar to the band gap of the system $|2M|$ [70].

Within this formalism, it can also be demonstrated that the change in the electric polarization $\Delta\boldsymbol{P}$ is also related to the Berry phase dynamics [45, 82, 99, 100]

$$\Delta P_j = \frac{1}{(2\pi)^2}\int_0^T dt \int v_j d\boldsymbol{S} \tag{0.51}$$

using the continuity equation $\partial_t\rho = -\boldsymbol{\nabla}\cdot\boldsymbol{J}$ in absence of electric field $\boldsymbol{\nabla}\cdot\boldsymbol{P} = \rho$ where ρ is the density of charge [1]. Writting generally for a time-dependent adiabatic perturbation the velocity as $v_j^n = \Omega_{k_j,t}^n$ from Eq. (0.48), it is straightforward to show that actually in a complete cycle $\Delta P_j \propto e\nu$ where ν is a topological invariant defined by the Berry phase.

0.5 Helical edge states

A reasonable question within the context of classical solid state physics is that if the bulk system is an insulator, and we observe quantized conductivities when the Fermi level is allocated within the gap, who is responsible for the electronic transport? Or more precisely, where it takes place? This question, which is now obvious, can be addressed by analyzing the bound states of the Dirac Hamiltonian at the interface of the system [19, 101, 102]. Thus, besides demonstrating their existence at the edge, it was also disclosed their helical nature whereby opposite spin particles move in opposite directions in a spin-momentum locking configuration [103].

Roughly speaking, edge states will be guaranteed whenever the topological constraint for the Chern number is fulfilled, which for the particular case of a Dirac Hamiltonian as Eq. (0.35) is given by a band inversion. However, before delving into this assertion time-reversal symmetry should be introduced. That is because systems with a 2x2 Dirac Hamiltonian such as Eq. (0.35) can only present one edge state while TIs have a pair of helical edge states in their boundary [103]. Therefore, the complete spectrum of TIs should take into account these states as it can be observed experimentally through ARPES (angle-resolved photoemission spectroscopy) measurements [24, 104–106].

0.6 Time-reversal symmetry

We have studied how a 2x2 Dirac Hamiltonian can host a topological non-trivial phase defined by a non-zero integer Chern number where the effective transport is associated to a helical edge state. However, TIs have time-reversal symmetry $\hat{T}$ while Eq. (0.35) is non-$\hat{T}$ symmetric. This can be easily understood by noticing that our description through a 2x2 Dirac Hamiltonian is incomplete, at least in the sense that we are selecting only one spin species for each band and hence the inversion of time $t \to -t$, which implies momentum inversion $\boldsymbol{p} \to -\boldsymbol{p}$ and spin inversion $\boldsymbol{s} \to -\boldsymbol{s}$, is not considered by our system since these states have different energy. Mathematically, this is shown by considering the time-reversal symmetry operator for half-integer spin particles

$$\hat{T} = -i\sigma_y \hat{K} \tag{0.52}$$

which is an anti-unitary operator $T^2 = -1$ whose inverse $\hat{T}^{-1} = -\hat{T}$ and where $\hat{K}$ stands for the complex conjugate operator [3]. This will be explained with more detail in Chapter 1. Nevertheless, just taking its definition, it can be checked the previous relations for the particle momentum $\hat{T}\boldsymbol{p}\hat{T}^{-1} = -\boldsymbol{p}$ and spin $\hat{T}\boldsymbol{s}\hat{T}^{-1} = -\boldsymbol{s}$ ($\boldsymbol{s} = \frac{\hbar}{2}\boldsymbol{\sigma}$) implying that the Halmiltonian $H_{2x2}(k) = M(k)\sigma_z + v_F(\boldsymbol{\sigma}\cdot\boldsymbol{p})$ does not commute with $\hat{T}$

$$\hat{T}H_{2x2}\hat{T}^{-1} = -M(k)\sigma_z + v_F(\boldsymbol{\sigma}\cdot\boldsymbol{p}) = -H_{2x2}(-k) \neq H(k) \tag{0.53}$$

being the diagonal term $M(k)\sigma_z$ responsible for this fact. Nevertheless, the combination of these two 2x2 Dirac Hamiltonian in a non-interacting situation does present this symmetry

$$H(k) = \begin{bmatrix} H_{2x2}(k) & 0 \\ 0 & -H_{2x2}(-k) \end{bmatrix} = \begin{bmatrix} M(k) & \hbar v_F k_- & 0 & 0 \\ \hbar v_F k_+ & -M(k) & 0 & 0 \\ 0 & 0 & -M(k) & \hbar v_F k_- \\ 0 & 0 & \hbar v_F k_+ & M(k) \end{bmatrix} \tag{0.54}$$

having each of these Hamiltonians opposite configurations for the Chern number ($M(k) \to -M(k)$), transverse conductivities and spin. Here we have defined $k_\pm = k_x \pm ik_y$. Thus, by simple applying $\hat{T}$ to one of these Hamiltonians, we will describe the physics of the other. Or in other words, we have a spin degeneracy for each band having a definite spin-momentum relation which allows time inversion in the full Hamiltonian $H(k)$. In general notation, if $|n_1(k,\sigma)\rangle$ is an eigenstate of the system $H|n_1(k,\sigma)\rangle = \xi_1|n_1(k,\sigma)\rangle$, being H time-reversal symmetric, by applying $\hat{T}$ to the previous equation we can see that $|n_2(-k,-\sigma)\rangle = \hat{T}|n_1\rangle$ will be also an eigenstate sharing the same energy as $|n_1\rangle$ but with an opposite momentum and spin. That is what we know as Kramers pairs.

By performing a dimensional reduction, i.e., considering semi-infinite boundary conditions in one direction, it is possible to see how each Hamiltonian forming $H(k)$ will

contribute with an edge state resulting together in a pair of non-interacting states with linear dispersion and opposite helicity [103]. That is, we have a quantum spin Hall system in which the spin transport substitutes the charge transport taking place in a quantum Hall system. Thus, although the net transverse electric current in the bulk is zero, several experimental setups can be designed to measure the quantized conductance $G = 2e^2/h$ associated with both edge states and the spin Hall conductance $G_S = e/(4\pi)$ following Landauer-Büttiker formalism [19, 47, 107, 108]. Finally, note that the non-interaction condition between the two Chern species forming $H(k)$ will be flexible to preserve edge states as long as the new terms introduced respect time-reversal symmetry. Topological insulators accept a wide variety of terms in their Hamiltonian which lead to some exotic effects. Examples are the introduction of Rashba spin-orbit coupling, structure inversion asymmetry, proximity effects with a superconductor and even special electron-phonon couplings as we are going to see in Chapter 2 [19, 38, 53, 109]. However, the presence of interactions between both 2x2 Hamiltonians will couple the counter-propagating edge states and hence the conductance will be no longer quantized [19].

0.7 Topological Insulators in two and three spatial dimensions

Although the first QSH system predicted was based on graphene, its low spin-orbit coupling prevented this effect from being carried out in the experimental field using this material. Nevertheless, its physical model was subsequently extended to other 2D materials which also share a honeycomb lattice and could overcome this issue [110–113]. In spite of this, the first experimental realization of a TI was in HgTe/CdTe QWs [47] a year after its theoretical prediction through the effective Dirac Hamiltonian obtained by Bernevig, Hughes and Zhang [23].

$$H_{BHZ} = \begin{bmatrix} H(k) & 0 \\ 0 & H(-k) \end{bmatrix} \tag{0.55}$$

where $H(k) = \epsilon(k)\sigma_0 + H_{2x2}(k)$ has the same form of Eq. (0.35) plus a term $\epsilon(k)\sigma_0$, where σ_0 is the 2x2 identity matrix, playing the role of a kind of k-dependent Fermi level modifying the energy $\xi^{\pm} = \epsilon(k) \pm \sqrt{(M - Bk^2)^2 + \hbar^2 v_F^2 k^2}$. For our purposes, ϵ_k can be set to zero given that it does not play any role in the calculation of the Berry curvature, potential and Chern number [70]. If one performs a unitary transformation [23]

$$U = \begin{bmatrix} \sigma_0 & 0 \\ 0 & -\sigma_z \end{bmatrix} \tag{0.56}$$

which does not affect the spin z-component, it can be demonstrated that the resulting Hamiltonian

$$U^{\dagger}H_{BHZ}U = \begin{bmatrix} H(k) & 0 \\ 0 & H^{*}(k) \end{bmatrix} \tag{0.57}$$

is equivalent to the time-reversal invariant Hamiltonian Eq. (0.54) after rearranging their basis and also to the 2D Dirac Hamiltonian

$$H_D = \begin{bmatrix} M(k) & 0 & 0 & \hbar v_F k_- \\ 0 & M(k) & \hbar v_F k_+ & 0 \\ 0 & \hbar v_F k_- & -M(k) & 0 \\ \hbar v_F k_+ & 0 & 0 & -M(k) \end{bmatrix} = M(k)\beta + v_F(\boldsymbol{\alpha}\cdot\boldsymbol{p}) \tag{0.58}$$

where

$$\alpha_i = \begin{bmatrix} 0 & \sigma_i \\ \sigma_i & 0 \end{bmatrix} \qquad \beta = \begin{bmatrix} \sigma_0 & 0 \\ 0 & -\sigma_0 \end{bmatrix} \tag{0.59}$$

are the Dirac matrices. So, it seems clear that both non-interacting Hamiltonian are still two Chern species related by time-reversal symmetry with opposite Chern numbers. For the particular case of HgTe/CdTe QWs the non-trivial topological regime is achieved for well thicknesses $d > 6.3$ nm [47]. However, it did not take long until these advances were extended to three-dimensions for the family of stoichiometric crystals Bi_2Se_3, Bi_2Te_3 and Sb_2Te_3 [24, 104, 106, 114, 115]. In this case, without using heterostructures, we have the first intrinsic topological insulators. 3DTIs have also an insulating bulk but with 2D metallic surface states instead of metallic edge states according to the dimensionality change in their boundaries. This fact should not be ignored given that the physics will be very sensitive to the system dimensionality as we will see later [49]. Their low-energy effective Hamiltonian, using $k\cdot p$ theory, can be found to be [24]

$$H_{3DTI} = \epsilon(k)\mathbb{1}_{4x4} + \begin{bmatrix} M_2(k) & \hbar v_\perp k_z & 0 & \hbar v_\parallel k_- \\ \hbar v_\perp k_z & -M_2(k) & \hbar v_\parallel k_- & 0 \\ 0 & \hbar v_\parallel k_+ & M_2(k) & -\hbar v_\perp k_z \\ \hbar v_\parallel k_+ & 0 & -\hbar v_\perp k_z & -M_2(k) \end{bmatrix} \tag{0.60}$$

consisting in a 3D Dirac Hamiltonian that can be obtained intuitively by rearranging Eq. (0.58) after including the z-component of the momentum p_z through the Dirac matrix α_z. In this case, we have that $M_2(k) = M_2 - \mathcal{B}_2k^2 - \mathcal{B}_1k_z^2$ also depends on k_z while the term $\epsilon(k) = \mathcal{C} - D_2k^2 - D_1k_z^2$ is not taken as zero for the moment. There exist extended versions of this effective Hamiltonian including k^3 terms, but for general purposes, we will limit to work with Eq. (0.60) unless we need to explicitly address non-linear effects [116–119].

0.7.1 Surface states analysis

Surface states can be represented through the effective Hamiltonian Eq. (0.60) under appropriate boundary conditions. In this section we will reexamine this fact to see how edge states distribute along the material and see the principles to derive the effective 2D model from Eq. (0.60) such as in refs. [53, 70]. One can figure out that in their two-dimensional limit 3DTIs will feature a QSHE. This dimensional reduction can be extended for any given dimension [49, 103].

To get an image of the edge states one can consider finite boundary conditions in an arbitrary direction, z for simplicity ($\Psi(z = \pm L/2) = 0$). Therefore, to calculate the wave functions of Eq. (0.60) it is useful to divide it into two parts, one dependent on k_z and the other part treated as a perturbation that will include the information of k_x and k_y. This is done because one only needs the information of the surface states near $k = 0$ and this approximation will simplify greatly the calculation of the wave functions. In this sense, k_x and k_y are still good quantum numbers of the system while $k_z = -i\partial_z$. Thus, from Eq. (0.60) we have

$$H_{3DTI} = H_0(k_z) + \Delta H(k_x, k_y) \tag{0.61}$$

where

$$H_0 = \begin{bmatrix} h(A_1) & 0 \\ 0 & h(-A_1) \end{bmatrix}; \qquad h(A_1) = \begin{bmatrix} \mathcal{C} + M_2 - D_-\partial_z^2 & -iA_1\partial_z \\ -iA_1\partial_z & \mathcal{C} - M_2 - D_+\partial_z^2 \end{bmatrix} \tag{0.62}$$

and $D_\pm = D_1 \pm \mathcal{B}_1$, $A_1 = \hbar v_\perp$, $A_2 = \hbar v_\parallel$. I have adopted the notation used in ref. [53] in order to make it easier for the reader the procedure. As it can be observed, H_0 is diagonal so one can solve each part separately. However, this is not necessary at all since both are related by time-reversal symmetry and therefore, one only needs to calculate the eigenfunctions belonging to $h(A_1)$ and then, we will apply $\hat{T}$ to get their time-reversal counterparts without solving $h(-A_1)$. Taking a trial wave function $\Psi = \Psi_\lambda e^{\lambda z}$ it can be found four different eigenvalues for $h(A_1)$

$$\beta\lambda_{\alpha=1,2} = \pm\lambda_\alpha = \left[\frac{-F + (-1)^{\alpha-1}\sqrt{R}}{2D_+D_-}\right]^{\frac{1}{2}} \tag{0.63}$$

that can be obtained from solving the Schrödinger equation $h(A_1)\Psi = E\Psi$ and where coefficients $R = F^2 - 4D_+D_-(E - l_1)(E - l_2)$, $F = A_1^2 + D_+(E - l_1) + D_-(E - l_2)$, $l_1 = \mathcal{C} + M_2$ and $l_2 = \mathcal{C} - M_2$ satisfy the previous relations. The total wave function Ψ must be a linear combination of these solutions

$$\Psi = c_1 \begin{bmatrix} \Gamma_1 \\ -iA_1\lambda_1 \end{bmatrix} e^{\lambda_1 z} + c_2 \begin{bmatrix} \Gamma_2 \\ -iA_1\lambda_2 \end{bmatrix} e^{\lambda_2 z} + c_3 \begin{bmatrix} \Gamma_1 \\ iA_1\lambda_1 \end{bmatrix} e^{-\lambda_1 z} + c_4 \begin{bmatrix} \Gamma_2 \\ iA_1\lambda_2 \end{bmatrix} e^{-\lambda_2 z} \tag{0.64}$$

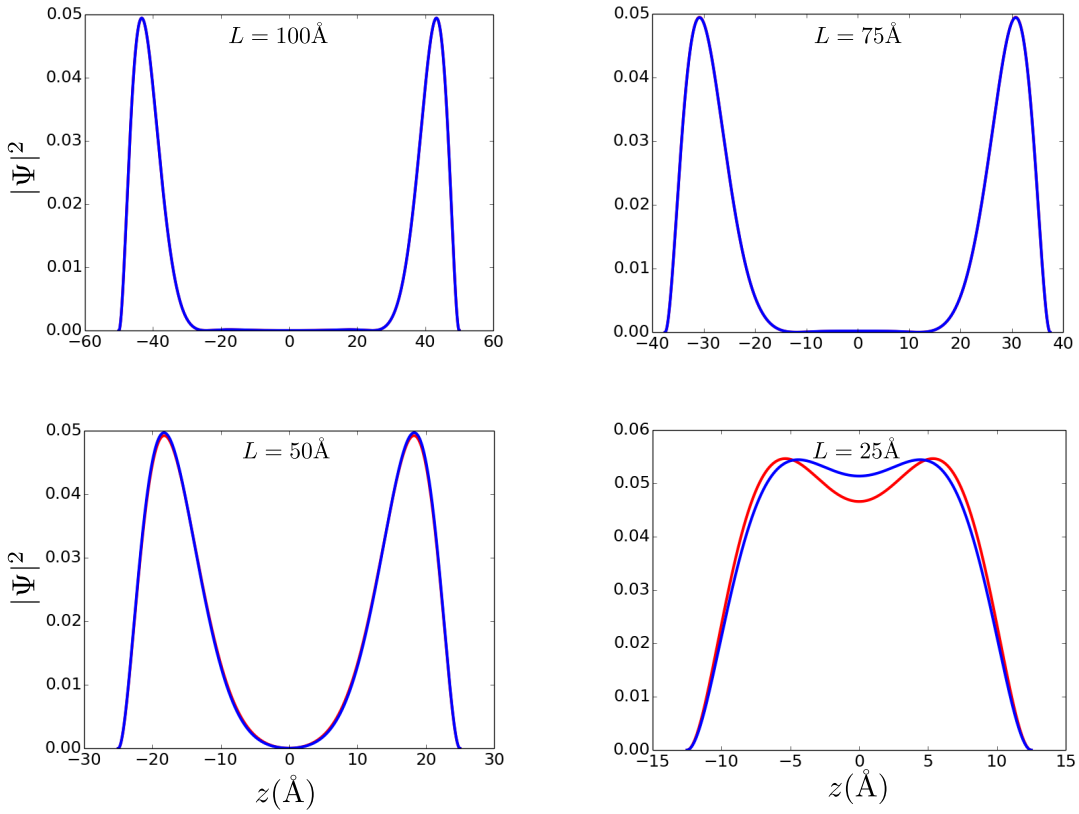

Figure 0.3: Probability density distribution of the electrons associated with the functions Ψ^+ (red line) and Ψ^- (blue line) for different thicknesses L. Plot parameters $M = 0.28$ eV, $\mathcal{B}_1 = 10.0$ eVÅ^2, $\mathcal{C} = -0.0068$ eV, $D_1 = 1.3$ eVÅ^2, $A_1 = 2.2$ eVÅ were taken from ref. [24].

satisfying the boundary conditions and where we have defined $\Gamma_i = \mathcal{C} - M_2 - E - D_+\lambda_i^2$. It can be checked that there are two wave functions satisfying $\Psi(z = \pm L/2) = 0$, one associated with the condition $c_1 = -c_2 = -c_3 = c_4$ and other with $c_1 = -c_2 = c_3 = -c_4$ which define two different energies $E^\pm$ through the relations

$$\frac{\Gamma_1\lambda_2}{\Gamma_2\lambda_1} = \frac{\tanh\left(\frac{\lambda_2 L}{2}\right)}{\tanh\left(\frac{\lambda_1 L}{2}\right)} \qquad \frac{\Gamma_1\lambda_2}{\Gamma_2\lambda_1} = \frac{\tanh\left(\frac{\lambda_1 L}{2}\right)}{\tanh\left(\frac{\lambda_2 L}{2}\right)} \tag{0.65}$$

These energies E^+ and E^-, which can be found numerically, will define the two wave functions of $h(A_1)$

$$\Psi_\uparrow^+ = c_+ \begin{bmatrix} \Gamma_2^+ \sinh\left(\lambda_2^+\right) f_-^+ \\ -iA_1 \cosh\left(\lambda_2^+\right) f_+^+ \end{bmatrix} \tag{0.66}$$

$$\Psi_{\uparrow}^{-} = c_{-} \begin{bmatrix} \Gamma_2^{-} \cosh\left(\lambda_2^{-}\right) f_{+}^{-} \\ -iA_1 \sinh\left(\lambda_2^{-}\right) f_{-}^{-} \end{bmatrix} \tag{0.67}$$

which for the particular case of the family of TIs Bi_2Se_3 represent spin-up electrons due to the configuration of their basis [24]. Here, c_+ and c_- correspond to the normalization factors while superscripts stand for E^+ and E^- and subscripts for the parity of the functions that are defined below

$$f_{+}^{\pm} = \frac{\cosh(\lambda_1 z)}{\cosh\left(\frac{\lambda_1 L}{2}\right)} - \frac{\cosh(\lambda_2 z)}{\cosh\left(\frac{\lambda_2 L}{2}\right)}\bigg|_{E=E_{\pm}} \tag{0.68}$$

$$f_{-}^{\pm} = \frac{\sinh(\lambda_1 z)}{\sinh\left(\frac{\lambda_1 L}{2}\right)} - \frac{\sinh(\lambda_2 z)}{\sinh\left(\frac{\lambda_2 L}{2}\right)}\bigg|_{E=E_{\pm}} \tag{0.69}$$

A representation of the probability density $\left|\Psi_{\uparrow}^{\pm}\right|^2$ of both positive and negative solutions can be found in Fig. 0.3. It can be demonstrated that for large thicknesses (L) both states are well confined near the boundary, sharing the same energy having a similar probability distribution while for thin-films, top and bottom surface states overlap opening a gap between both solutions. The effective 2D model for the surface states can be obtained immediately from the functions $\Psi_{\uparrow}^{+}$, $\Psi_{\uparrow}^{-}$ and their time-reversal counterparts which are taken as unperturbed states. Hence, it can be demonstrated that the 2D effective Hamiltonian which arises

$$H_{2D} = \begin{bmatrix} h_+ & 0 \\ 0 & h_- \end{bmatrix} \tag{0.70}$$

has the form of a 4x4 Dirac Hamiltonian similar to the one derived for HgTe/CdTe QWs and being their parameters dependent on L [70]. It can be shown, as one can deduce from Fig. 0.3, that for large L the parameter M tends to zero having both solutions $E^{\pm}$ the same energy and describing a Dirac cone at low energy [53]. In contrast, for small thicknesses ($\sim 30 - 50$Å), the overlap between top and bottom surfaces states opens a gap $2M$ which describes a pair of Dirac hyperbolae with $M\mathcal{B} > 0$ in their non-trivial topological regime, i.e., a QSH system. This fact is very significant given that it enables us to play with the parameters of the Dirac Hamiltonian which could be potentially useful when studying some transport magnitudes in 2D. In Chapters 2 and 3 we will explore with more detail the role of the parameter $\mathcal{B}$ when deriving an expression for the effective field b and unveil the differences between the orbital magnetic response of a topologically trivial insulator and a non-trivial one. Moreover, this will allow us to take realistic values for the Hamiltonian parameters that will be used throughout the next chapters. Finally, note that for $L \to 0$ a transition to the topologically trivial regime is also predicted [70]. The point at which this transition might occur will depend on the material and the parameters of its 3D effective Hamiltonian.

0.8 Topological insulators in higher dimensions

While in (2+1) space-time dimensions the transport equations ($j^\mu = \delta \mathcal{S}_{eff}/\delta A_\mu$) can be derived from the topological Chern-Simons action [49],

$$\mathcal{S}_{2D} = \frac{C}{4\pi} \int dt \int d^2x A_\mu \varepsilon^{\mu\nu\rho} \partial_\nu A_\rho \tag{0.71}$$

being $d^2x = dx_1 dx_2$, $\mu, \nu, \rho = 0, 1, 2$ the temporal and spatial index, $\varepsilon^{\mu\nu\rho}$ the Levi-Civita tensor and C the first Chern number previously defined, their generalization to higher dimensional systems addressing (4+1)D does not employ the same topological invariant following Chern-Simons theory [49, 120]

$$\mathcal{S}_{4D} = \frac{C_2}{24\pi^2} \int dt \int d^4x \varepsilon^{\mu\nu\rho\sigma\tau} A_\mu \partial_\nu A_\rho \partial_\sigma A_\tau \tag{0.72}$$

and we need to introduce the second Chern number

$$C_2 = \frac{1}{32\pi^2} \int d^4k \varepsilon^{ijmn} tr(f_{ij} f_{mn}) \tag{0.73}$$

defined on the momentum space which works with non-Abelian curvatures

$$f_{ij}^{\alpha\beta} = \partial_i a_j^{\alpha\beta} - \partial_j a_i^{\alpha\beta} + i[a_i, a_j]^{\alpha\beta} \tag{0.74}$$

and potentials

$$a_j^{\alpha\beta}(k) = i \langle \alpha(\mathbf{k}) | \partial_{k_j} | \beta(\mathbf{k}) \rangle \tag{0.75}$$

instead of the Abelian ones. Here, $i, j, l, m = 1, 2, 3, 4$ runs over the momentum coordinates while α stands for the occupied bands in a multi-band model. Physically, we have that the electron dynamics strongly depends on the surface dimensions whose response is given in this case by

$$j_{4D}^\mu = \frac{C_2}{8\pi^2} \partial_\nu A_\rho \partial_\sigma A_\tau \tag{0.76}$$

Therefore, considering for example a constant magnetic and electric field externally applied in the z-direction we obtain $j_{4D} = \frac{C_2}{4\pi^2} B_z E_z$. By applying a dimensional reduction, it is demonstrated that this theory has a direct application to 3DTIs where one can give an expression for the effective action in three spatial dimensions [49]

$$\mathcal{S}_{3D} = \frac{1}{4\pi} \int dt \int d^3x \varepsilon^{\mu\nu\rho\sigma} P_3(x,t) \partial_\mu A_\nu \partial_\rho A_\sigma \tag{0.77}$$

where $P_3(x,t)$ is a pseudo-scalar quantity that can be directly related to the axion field $\theta(x,t)$ in axion electrodynamics [52, 121, 122]. However, this correspondence needs to be treated carefully since both magnitudes have a different physical origin. That is, one is obtained from a topological Chern-Simons action and takes a value $P_3 = n + 1/2$ as can be deduced by the response equation

$$j^{\mu}_{3D} = \frac{1}{2\pi}\varepsilon^{\mu\nu\rho\sigma}\partial_{\nu}P_3\partial_{\rho}A_{\sigma} \tag{0.78}$$

considering $P_3 = P_3(z)$, which describes a quantum Hall effect in the plane xy [49], while $\theta(x,t)$ is a scalar field intended to address the coupling between photons and virtual particles, named axions, in different physical systems [123–125] and that needs to take a value π in the surface of a TI to preserve time-reversal symmetry.

0.9 Conclusions

In this chapter, we have tried to make a didactic introduction of the Dirac Hamiltonian and its connection with the topology in different dimensions. These are the basic elements needed for a comprehension of the theoretical advances included in the following chapters and in their respective publications. The study of the thermoelectricity, which employs Chern-Simons theory, the topological intrinsic field, which makes use of the field interpretation of the Berry curvature, the Dirac oscillator as key to the introduction of relativistic oscillations in TIs preserving time-reversal symmetry, the orbital dynamics as well as the study of the pressure associated with axions within TIs are pieces of the same theoretical background described in this introduction. Moreover, we have gathered some of the elements and skills obtained in a first formative stage which can also be applied to the study of other topological materials.

1 Thermoelectricity in TIs

In this chapter, we describe the theoretical aspects used to give an expression for the Seebeck coefficient and dimensionless figure of merit in topological insulators. The motivation is clear, TIs are currently the best thermoelectric materials. However, its physics involves more than solid state and electronic structure. Through a formalism that employs concepts in algebraic topology and thermal quantum field theory, we determine a topological contribution to the thermoelectric effect. That is, directly from the Chern-Simons actions associated with these systems, we find the electric potential V generated by a temperature gradient in a topological insulator. The Seebeck coefficient which arises contains two terms, one associated directly to the electronic diffusion in a topological band, and other giving an anomalous contribution that we associate to the creation of electron-hole Schwinger's pairs. Once obtained these elements, we can give an expression for the dimensionless figure of merit ZT in the surface of a TI neglecting contributions from the lattice thermal conductivity. Besides that, using the Riemann-Hurwitz formula, we show that the compatibility of the torus symmetry of the Brillouin zones and the Kramers degeneracy for the currents, obliges to use non-Abelian Berry curvatures. That is to say, the $U(1)$ gauge symmetry, which glues Quantum Mechanics and Electrodynamics, must be enlarged to at least the $SU(2)$ carrying us to topological massive Chern-Simmons terms that we directly relate with new thermal excitations.

1.1 Introduction

It is evident that the high efficient thermoelectric performance of TIs should be associated with their singular physics and transport properties [59–61]. They are the best thermoelectric (TE) compounds at room temperature, specially if we are able to reduce their lattice thermal conductivity [43, 65, 126, 127]. A good example is bismuth telluride [128], Bi_2Te_3, which has a small band gap giving a good number of carriers at room temperature (300K) and reaching 2.4 for its dimensionless figure of merit ZT for p-type using alternating layers in a superlattice with Sb_2Te_3 [63]. This is the highest value of thermoelectricity observed so far at room temperature. Even though the electronic struc-

ture of these materials was exhaustively studied in relation to their thermoelectricity, there is still lacking in the literature a physical model able to explicitly take into account their common topological and physical features [51, 129–131]. Semiclassical Boltzmann theory applied in a Landauer approximation gives accurate results for some properties using the ballistic nature of their conducting channels [43, 64–68]. However, they do not take into account directly the non-trivial topology of these systems whose physics links different scientific branches which were developed independently: particle physics, statistical mechanics, condensed matter and algebraic topology. This is a characteristic of materials that exhibit linear dispersion laws instead of quadratic ones, allowing a quantum field interpretation where the spinors play a fundamental role substituting the usual non-relativistic wave function.

From solid state physics, we need obviously the concept of symmetry and periodicity. Thus, in a crystal with translational symmetry, we can use Bloch theorem to reduce the analysis of the different physical properties to the first Brillouin zone (BZ). These are necessary elements to determine the wave functions and eigenstates in a solid. In this sense, parity $\hat{P}$ or space inversion is straightforward followed while time-reversal symmetry $\hat{T}$ is not always fulfilled. For example, the Schrödinger equation

$$i\hbar\frac{\partial}{\partial t}\psi(t) = H\psi(t) \tag{1.1}$$

under time inversion gives $-i\hbar\frac{\partial}{\partial t}\psi(-t) = H\psi(-t)$, where classically $H = \frac{p^2}{2m} + V(x,t)$ is periodic in x and t and hence $\psi(-t)$ is not a solution. This can be solved if the $\hat{T}$ operator has also associated a complex conjugation $\hat{K}$ operator. In fact, we must define $\hat{T} = U\hat{K}$ for spinless states where U is a unitary operator [3]. In the case of having half-integer spin particles, the unitary operator can be written in function of the σ_y Pauli matrix as $U = exp(-i\frac{\pi}{2}\sigma_y)$. This, given that $\sigma_y^2 = 1$, allow us to write the time-reversal operator as

$$\hat{T} = -i\sigma_y\hat{K} \tag{1.2}$$

which acting on the multiparticle state gives $T^2 = 1$ for an even number of fermions or $T^2 = -1$ when the number is odd. Generally written, T^2 has eigenvalue $(-1)^{2s}$ for a particle of spin s, and if $|n\rangle$ is an energy eigenstate, then $T|n\rangle$ is also an eigenstate of the system, sharing the same energy and being orthogonal to each other. Thus, if there is an odd number of electrons there must be (at least) a twofold degeneracy; known as Kramers degeneracy. This is Kramers theorem, which when it is completed with the previous Bloch theorem for the bands, should provide us with the first tools to examine topologically the first Brillouin Zone (BZ) of a TI [25].

1.2 Singularities and translational symmetry

We can represent schematically how the 2D BZ evolves under different translation operations transforming the square BZ into two equivalent cylinders S_1 (Fig.1.1). Consequently, it is easy to see that combining the two lattice periodicities available in two dimensions, a 2D torus $S^1 \times S^1$ arises. That is, the existence of translation symmetry allows us to transform a topologically trivial square into a non-trivial torus with genus $g \neq 0$. Given that all crystals are able to develop these fundamental properties, non-trivial topology is not enough when we study TIs and the presence of singularities which are usually counted on the band structure are needed. Obviously, without extra information, these singularities break the translation symmetry or the periodicity of the Bloch states [17, 18].

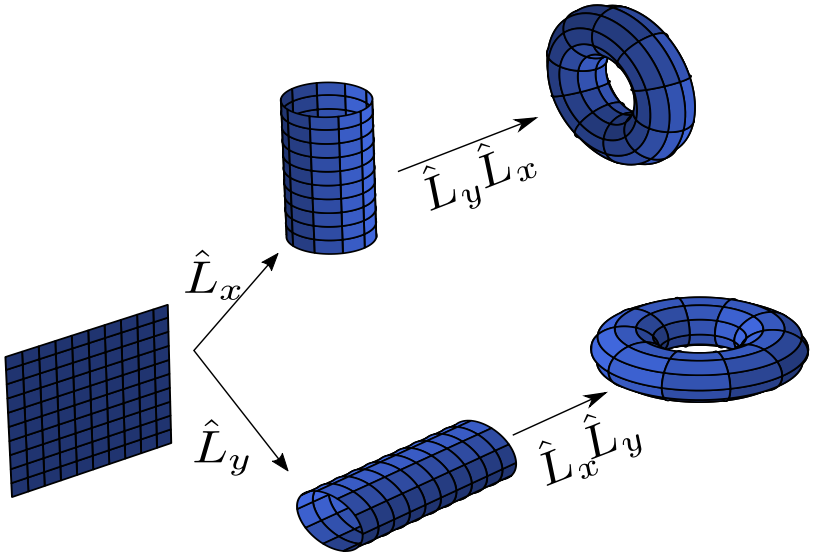

Figure 1.1: Evolution of the $2-D$ Brillouin Zone with trivial topology under different translation symmetries. Applying individual translation symmetries, two cylinders equivalent topologically to two S^1 circles arise. Combining the two translations symmetries we obtain two equivalent torus $T^2 = S^1 \times S^1$.

Analyzing in more detail the possibility of these translation symmetry breaking, we know that infinitesimal translations are generated by the linear momentum operator $\hat{L}(dx) = \hat{1} - \frac{i}{\hbar}\hat{p}(dx)$, where $[\hat{x}, \hat{p}] = i\hbar\hat{1}$ follows the Heisenberg's principle of uncertainty. By extending this operation over the whole crystal one gets the finite translation operator $\hat{L} = \lim_{N\to\infty}[\hat{1} - \frac{i}{\hbar}\hat{p}(\frac{a}{N})]^N = \exp\left(-\frac{i}{\hbar}\hat{p}a\right)$. Taking into account the periodicity of the crystal potential $V(x) = V(x+a)$, which involves the periodicity of the states, we can write

$$L_a \left|\psi(x)\right\rangle = \left|\psi(x-a)\right\rangle = \exp(ika)\left|\psi(x)\right\rangle \tag{1.3}$$

where k is the wavelength number associated to the momentum $p = \hbar k$. On the contrary, the presence of singularities makes that

$$|\psi(x-a)\rangle = \exp(ika)\exp(i\gamma)\,|\psi(x)\rangle \tag{1.4}$$

being γ the Berry phase which gives to electrons an anomalous phase factor during a complete cycle in the parameter space. Thus, in order to maintain the periodicity of the Bloch states, preserving the non-trivial topology that results from having a torus, singularities must take place on the edges of the crystal, where translation symmetry is no longer satisfied. Since singularities manifest in energy bands by means of Fermi points, bands are good hosts for feeding the non-trivial topology of a material whose electronic structure is appropriate and whose surface shows the breaking of translation symmetry. In this way, the Berry phase joints the non-trivial topology of the crystal employing its curvature and connection on the bands [132].

1.3 Riemann-Hurwitz formula and its application to topological insulators

The topological elements of the TI have been found, but now it remains to see how they work together employing their associated invariants. The Riemann-Hurwitz formula, which generalizes the Euler topological invariant, enable us to construct an equation relating the genus g and g' of two compact surfaces, i.e., whose boundary is zero [133]. Actually, this formula establishes the conditions for a map $f : T \to S$ being surjective and holomorphic, reducing the several topological invariants introducing the genus of T, the genus of S, N the degree of the map f and the number of ramifications $e_f(k)$. Riemann used the mentioned formula in the case that the genus of S were zero, i.e., spheres. Much later the general proofs were obtained by Zeuthen and Hurwitz. The formula is

$$2(g_T - 1) = 2N(g_S - 1) + \sum_{k \in T}(e_f(k) - 1) \tag{1.5}$$

In our case we have a 2D torus T^2 with genus $g_T = 1$ mapped in a S^3 sphere with genus $g_S = 0$ and the degree of the map $N = 2$ due to the Kramers double degeneracy, see Fig. 1.2. Hence we obtain five ramifications branches, i.e., $e_f(k) = 5$. This result can be directly related to the second Chern number as discussed below, playing a fundamental role in the transformation of heat in electricity. The number of ramification branches diminishes to three when there are no Kramers pairs, that is, $N = 1$ with $e_f(k) = 3$. But it is very remarkable to observe that this formula does not depend on the dimensions of the involved sphere or torus, which justifies us to work with a T^2 torus instead of a T^3 or T^4 without being worry about new results.

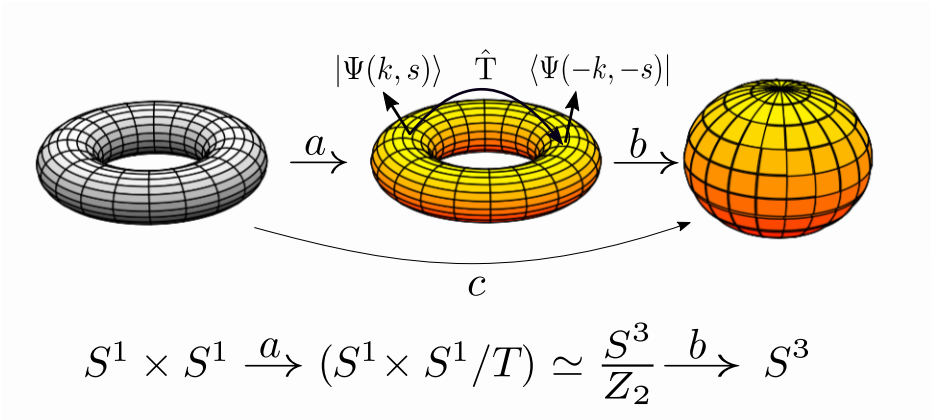

Figure 1.2: Schematic illustration of the projection of a torus into a sphere. The first torus is mapped by a on the second torus, which is equivalent to one sphere since it includes Kramers pairs with the same energy and orthonormal. The map b carries points of the previous torus on a real sphere. It is immediate to see that the map $c = b \cdot a$ is commutative.

In the presence of singularities in the band structure, the map c of Fig. 1.2 can be interpreted as the d_a map within the Hamiltonian H introduced to study TI in (4+1)-D [49],

$$H = \sum_k \psi_k^+ d_a(k) \Gamma^a \psi_k \tag{1.6}$$

being $d_a(k) = (m + p\sum_i \cos k_i, \sin k_x, \sin k_y, \sin k_z, \sin k_w)$ and $\Gamma' s$ the Clifford matrices $\{\Gamma^\mu, \Gamma^\nu\} = 2g^{\mu\nu}\mathbb{1}_{5\times5}$. Then, we can calculate the second Chern number C_2 associated to this Hamiltonian

$$C_2 = \frac{3}{8\pi^2}\epsilon^{abcde}\int dk^4 \hat{d}_a(k)\frac{\partial \hat{d}_b(k)}{\partial k_x}\frac{\partial \hat{d}_c(k)}{\partial k_y}\frac{\partial \hat{d}_d(k)}{\partial k_z}\frac{\partial \hat{d}_e(k)}{\partial k_w} \tag{1.7}$$

which is no more than the winding number resulting from the map $d_a\hat{(k)} \equiv \frac{d_a(k)}{|d(k)|}$ of a four-dimensional torus T^4 to a sphere S^4, having the mass m associated to the spinor's $\Gamma' s$ five critical values given by the condition $\sum_{k,\mu} d_a^2 = 0$, that allows us to identify, in the same way as the Riemann-Hurwitz theorem, five different branches for the second Chern number

$$C_2 \equiv \mu = \begin{cases} 0, m \notin (-4p, 4p) \\ +1, m \in (-4p, -2p) \\ -3, m \in (-2p, 0) \\ +3, m \in (0, 2p) \\ -1, m \in (2p, 4p) \end{cases} \tag{1.8}$$

where p is taken as a mass parameter which must be equal to the background kinetic energy of the particles $2k_BT/v_F^2$ for keeping its physical meaning. In this way, p is mainly associated with the quantization of the temperature [134]. It is easy to see that for non-$\hat{T}$ symmetric Hamiltonians there are only three ramifications available for the second Chern number. As we saw, this can be interpreted, in one straightforward form, into the Riemann-Hurwitz formalism as two different maps, where we change the degree of the map N from 2 to 1.

1.4 Topological Seebeck coefficient

Physically the non-Abelian Berry phase takes into account the allowed bulk degenerate states which are directly related with the change of temperature, as we shall see soon. First, we take the definition of the non-Abelian Berry connection

$$a_j^{\alpha\beta}(k) = i \langle \alpha, \mathbf{k} | \partial/\partial k_j | \beta, \mathbf{k} \rangle \tag{1.9}$$

and the associated field (or curvature)

$$f_{ij}^{\alpha\beta} = \partial_i a_j^{\alpha\beta} - \partial_j a_i^{\alpha\beta} + i[a_i, a_j]^{\alpha\beta} \tag{1.10}$$

and second Chern number

$$C_2 = \frac{1}{32\pi^2} \int d^4k \epsilon^{ijmn} tr(f_{ij} f_{mn}) \tag{1.11}$$

where the indixes of the Levi-Civita tensor stand by $i, j, m, n = 1, 2, 3, 4$ and α refers to the occupied bands. This can be written within a pure gauge Yang-Mills formalism, where their solutions transform in general by $a_\mu = T^i a_\mu^i$ and $f_{\alpha\beta} = T^i f_{\alpha\beta}^i$ being the T^i's the generators of the inner symmetry group, which in our case will be $SU(2)$ [2]. For a $U \in SU(2)$ being position dependent, we have the gauge transformations for the potentials

$$a_\alpha \to a_\alpha^U = U^{-1} a_\alpha U + U^{-1} \partial_\alpha U \tag{1.12}$$

and fields

$$f_{\alpha\beta}\rightarrow f^{U}_{\alpha\beta} = U^{-1} f_{\alpha\beta} U \tag{1.13}$$

It is immediate to observe that the non-Abelian fields are not gauge invariant, unlike what happens with the Abelian ones, which tell us that the curvature depends of the group representation but not the topological numbers. Thus, given that $tr(\epsilon^{ijmn} f_{ij} f_{mn}) = 4\epsilon^{ijmn}\partial_i[tr(a_j\partial_m a_n - \frac{2}{3}a_j a_m a_n)]$, we can define the Chern-Simons term [120]

$$W(a) = -\frac{\mu}{8\pi^2}\int d^3x \epsilon^{ijm} tr(a_i\partial_j a_m - \frac{2}{3}a_i a_j a_m) \tag{1.14}$$

where μ is a topological mass and which is not gauge invariant under gauge transformations

$$\begin{aligned} W(a^U)\rightarrow W(a) - \frac{\mu}{8\pi^2}\int d^3x [\epsilon^{ijm}\partial_i tr(\partial_j U U^{-1} a_m) \\ + \frac{\mu}{24\pi^2}\int d^3x \epsilon^{ijm} tr(U^{-1}\partial_i U U^{-1}\partial_j U U^{-1}\partial_m U)] \end{aligned} \tag{1.15}$$

The first term of the integral is a total derivative that can be made zero in a manifold without boundary, while the second, is an integral written in short as $w(U)$, which provide us topological information of the manifold as a winding number. This integral is actually an integer number coming from the homotopy group $\pi_3(S^3)$ for the $SU(2)$ group and we can take the Abelian Chern-Simons gauge symmetry associated to the background electrodynamics, i.e., the U(1) as a subgroup of transformations close to the surface. In this case, we can rewrite the Chern-Simons transformation for both fields. Hence, the transformation of the Chern-Simons can be rewritten as

$$W(a)\rightarrow W(a) + \frac{\mu}{12\pi}24\pi^2 w(U) = W(U) + 2\pi\mu w(U) \tag{1.16}$$

But as the path integral $e^{i\frac{W}{\hbar}}$ must be invariant, hence it means that μ is an integer. These are going to be the dynamic fields meanwhile the electromagnetic gauge potential A_α will appear as a background gauge field.

Let us go now to the thermodynamic part of the topological thermoelectricity applying the instanton solution associated with the second Chern number developed above. Within this mathematical context, it is possible to make a direct relationship between thermodynamics and quantum formalism. Feynman path integrals give us an expression for the amplitude of probability to evolve a particle from the coordinate $x_i(0)$ to $x_f(t)$ a time later by

$$\langle x_f|\, e^{-iHt}\, |x_i\rangle = \int_{x_i}^{x_f} Dx e^{-i\mathcal{S}} \tag{1.17}$$

where $\mathcal{S}$ is the classical action, which could be obtained by $\mathcal{S} = \int_0^t dt'[\frac{p^2}{2m} - V(x)]$. On the other hand, in Statistical Mechanics the partition function is defined in quite a similar form by $Z(\beta) = tr\left(e^{-\beta H}\right)$ where $\beta \equiv \frac{1}{k_B T}$. There is a way to change from one to the other using the Wick trick, i.e., doing the time a pure complex variable and transforming the Minkowskian space-time in a Euclidean one. Thus, we have $-i\mathcal{S} = \int_0^{-i\tau} d\tau'[\frac{p^2}{2m} - V(x)] = \mathcal{S}_E$ where $\mathcal{S}_E$ is the new Euclidean action. This fixes the concept of temperature relating it directly with the time by $\tau = \hbar\beta$ making

$$tr\left(e^{-\beta H}\right) = \int dx_i \langle x_i|\, e^{-\beta H}\, |x_i\rangle = \int dx_i \int_{x(0)=x_i}^{x(\beta)=x_i} Dx e^{-\mathcal{S}_E} \tag{1.18}$$

where we have assumed a cyclic motion $x(0) = x(\beta)$, i.e, the particle must come back where it started after Euclidean time $\tau = \hbar\beta$ [135, 136]. This is exactly how Berry phase works and justify partially its introduction as a gauge field.

Remember that the Berry phase is directly related with the electric polarization P [58, 100],

$$\Delta P = \frac{e}{2\pi} \int_0^{\tau} dt \int_{\frac{-\pi}{a}}^{\frac{\pi}{a}} dk \sum_{n \in occu} f_n(k) \tag{1.19}$$

being

$$f_n(k) = i\left[\frac{\partial}{\partial k}\langle \psi_n k(t)|\, \frac{\partial}{\partial t}\, |\psi_n k(t)\rangle - \frac{\partial}{\partial t}\langle \psi_n k(t)|\, \frac{\partial}{\partial k}\, |\psi_n k(t)\rangle\right] \tag{1.20}$$

the Abelian Berry curvature. Under a gauge transformation of the electromagnetic potentials $A_\mu \to A'_\mu = A_\mu + \partial_\mu \Lambda(x,t)$ the electron wave function transforms $\psi \to \psi = \psi e^{ie\frac{\Lambda}{\hbar}}$. The above exponential function needs to be single valued while the $\Lambda(x,t)$ doesn't. Thus, we can write it as $\Lambda(x,t) = \frac{2\pi\mu\hbar\tau}{e\hbar\beta} = \mu\frac{2\pi\tau}{e\beta}$ where μ is a winding number quantizing the temperature. This allows to find the electric potential directly related with the temperature by

$$V \to V' = V + \mu\frac{2\pi}{e} k_B T \tag{1.21}$$

which means that we have transformed the electric potential into another, plus a $\mu\frac{2\pi}{e\beta}$ thermal term. This turns out to be a fundamental result: the thermal energy appears quantized by the winding number being added to one electric potential under a gauge transformation. Notice that a Chern-Simons term was necessary since it is not gauge-invariant and appears as surface actions. This allows to have, in non-Abelian Chern-Simons, the coupling constant g directly associated to the temperature, related to the

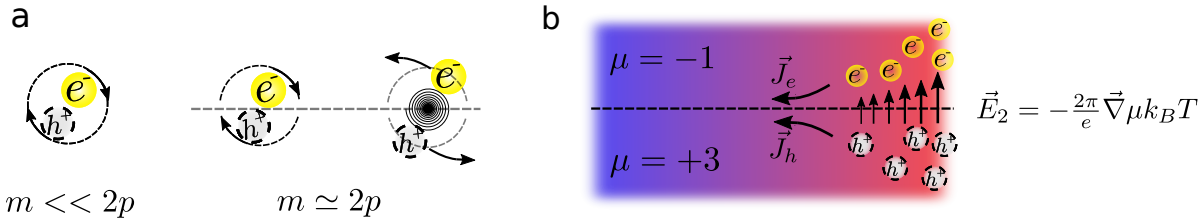

Figure 1.3: (**a**) Schematic illustration of a virtual electron-hole pair when the parameter m is far away from the boundary between two topological branches, that is for example $2p$. When m is close to these value the jump in the topological mass μ generates a potential difference that is able to break the vacuum and to generate a real electron-hole pair representing a new mechanism to transform thermal energy into electric in solid state physics. (**b**) Representation of electron-hole creation at the hot (red) side of the TI where $m \approx 2p$. Electrons and holes take place on different branches, leadind to an electric field $\vec{E}_2$. Due to charge carriers are responsible to thermalize the material, this originates electron J_e and holes J_h currents where each type of carriers have different movilities since they below to diferent branches.

Chern-Simons action transforming $S_{CS} \rightarrow S'_{CS} = S_{CS} + \frac{2\pi\hbar^2\mu}{g^2}$ where μ is the topological mass.

Getting back to the topological electric potential Eq. (1.21), we can easy calculate the Seebeck coefficient

$$S = -\frac{\partial V}{\partial T} = \mu\frac{2\pi}{e}k_B + \frac{2\pi}{e}\frac{\partial \mu}{\partial T}k_B T \tag{1.22}$$

choosing $V' = 0$. We can identify two contributions, the first, that comes purely from the temperature gradient in a topological branch, and the second, which takes into account the contribution due to a change in the topological index μ, i.e, a jump between ramifications. As we will see, the first term is equivalent to that we find when we compute the surface Seebeck coefficient while the second, does not appear since there is only one ramification available on the surface. Once we have seen that the instanton solutions allow us to relate the electric potential V with the temperature T and hence the electric field $\mathbf{E}$ with ∇T, we can give a microscopic picture of how the thermal energy is invested in electricity. Besides determining the electronic diffusion within a topological branch, the main idea is that there is a creation of electron-hole Schwinger's pairs (Fig. 1.3), provided that the electric field is big enough [136–139]. Calculating the critical electric field E_c, following Heisenberg-Euler, we notice that the limit for obtaining a great number of real electron-hole pairs is

$$E_c = \frac{m^2 v_F^3}{e\hbar} \simeq 0.152 V/nm \tag{1.23}$$

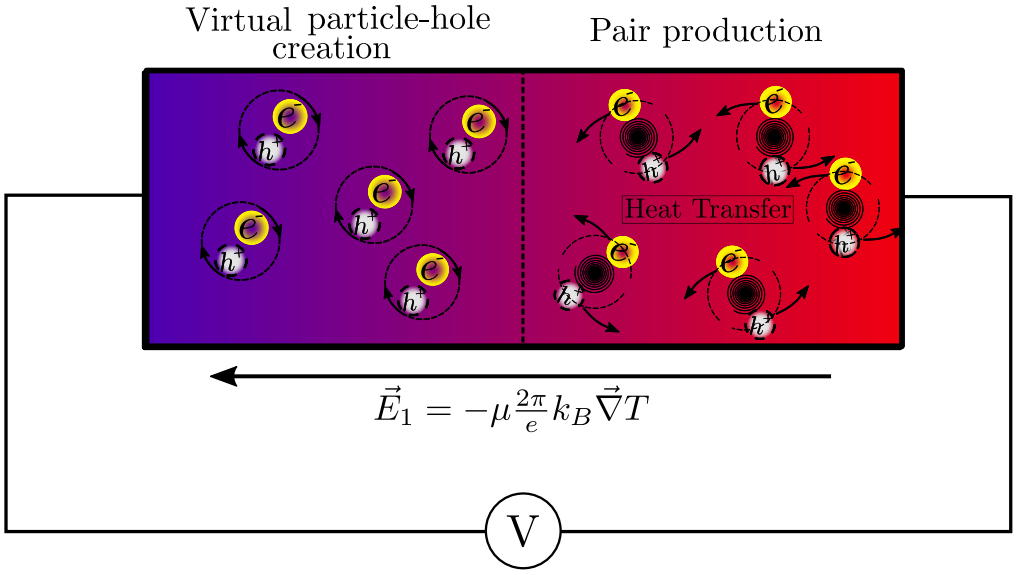

Figure 1.4: Non-Abelian topological contribution to the thermoelectric effect close to the U(1) electromagnetic surface. Charge transport towards the cold (blue) side originates a potential difference V represented by the electric field $\vec{E}_1$. Pair production in the hot side (red) of the material leads to a local heat transfer, increasing the Seebeck coefficient.

where we have considered typical values for the energy gap (≈ 0.21eV) and the Fermi velocity $v_F \simeq 6 \times 10^5$m/s in TIs [24, 140]. This provides a critical electric field of almost ten orders of magnitude lower than the critical electric field in quantum electrodynamics (QED) and with one equivalent temperature of $\zeta = 1.74 \times 10^{-6}$ K nm^{-1}, being these values accessible in these topological materials at so small scales as at hundredths of volt at distances of angstroms. In this way, we can rewrite the second term of the Seebeck coefficient considering that the dependence of μ with the temperature, as we show in Eq. (1.22), is represented by a Heaviside function, leading to the following expression for the Seebeck

$$S = \frac{2\pi}{e} \mu k_B + \frac{2\pi}{e} \delta(\bar{p}) k_B T \tag{1.24}$$

being $\bar{p}$ the different values where μ changes, that is, 0, $\pm m/2$, $\pm m/4$ and where the local increase, represented by the second term, can be interpreted as the contribution originated in the creation of real electron-hole pairs (Fig. 1.4). Eq. (1.24) for the Seebeck coefficient has two terms, the first one quantize S in integers due to the Chern-Simons topological mass, whereas the second corresponds to the variation of this mass respect to the temperature T. The relevant point is that the topological bands allow finding a

new term in the Seebeck coefficient which can increase it depending on the value of the temperature. But what is more important, these strings of singularities separate thermally some regions from other, resulting in a temperature gradient ($\vec{\nabla}T$) which produce an electric field $\vec{E}_2$ capable to create Schwinger's pairs whose electrons and holes have different velocities depending on the level where they are situated respect to the Fermi level (Fig. 1.3). Thus, unlike what happens with metals, the effect of temperature on electrons and holes can be quite different without cancelling each other, leading to a Seebeck coefficient that would be also higher than in a semimetal. It is fundamental to observe that without the topological ramifications we would have a homogeneous crystal without thermoelectricity.

1.5 Surface figure of merit ZT in TIs

Finally, let's calculate the topological contribution to the surface figure of merit in TIs, limiting our calculations to $(2+1)$ dimensions, where the topology is determined through the first Chern number $\bar{n}$ and the winding number n. We start considering that, in a given direction x or y, exists a temperature gradient in our TI in such a way that eigenstates evolve adiabatically. We can define then the Seebeck coefficient through the entropy as $\mathtt{S} = \frac{k_B}{e}\left(ln|\frac{\psi_b}{\psi_t}| + in\theta\right)$ where ψ_b and ψ_t are the final an initial states, θ is the angle between the states and n is the winding number which can only take odd integers values, otherwise the topological Seebeck coefficient would give zero. In fact, we are representing the entropy of a Riemann surface. Notice that although the von Neumann entropy would give zero considering pure states, this is not true considering that these states are in entanglement due to their global topological properties [69]. Actually there are many local Wannier bands, i.e., $\Psi(k,t) = \frac{1}{\sqrt{N}}\sum_i \psi_i(k_i,t)$, providing separate electrons which move coherently producing what is called Thouless charge pump and relates Berry phase with the electric polarization P [141–143]. In fact, due to the previous definitions, it is easy to see that $ln|\frac{\psi_b}{\psi_t}| = 0$ and we can simplify the expression of the Seebeck coefficient for the TI as

$$S = \frac{k_B}{e} in\theta = n\frac{k_B}{e}\int_C i\,\langle\psi(\mathbf{r})|\,\nabla_r\,|\psi(\mathbf{r})\rangle\,d(\mathbf{r}) = \frac{\pi}{e} n\bar{n}k_B \approx 270\mu V/K \tag{1.25}$$

being θ the angle directly associated to the Berry phase on the closed curve C. This leads to an expression very similar to that obtained before, first term of Eq.(1.22), where the product $\mu w(U)$ has been transformed into $n\bar{n}$, where π is the Berry phase of a non-trivial material, n counts the number of times we complete a cycle and $\bar{n}$ is the first Chern number which takes into account the whole topology on the Brillouin zone for our TI.

In order to complete the calculation of the surface figure of merit, we need to know the electronic thermal conductivity and the electric conductivity. For the electronic thermal conductivity, we consider the 2D density of states in the semimetal region as

$$D(\xi) = 2\frac{1}{(2\pi)^2}\int \delta(\xi - \hbar v_F k)2\pi k dk = \frac{1}{\pi\hbar^2 v_F^2}\xi \tag{1.26}$$

where the factor 2 comes from the spin degeneracy. If the system has also valley degeneracy, such as graphene, we need to consider an additional factor 2 [144]. This allows us to obtain the electronic thermal conductivity κ_e as

$$\kappa_e = \frac{1}{2}\frac{\partial}{\partial T}\int d\xi D(\xi)\xi f(\xi) v_F l = \frac{3\zeta(3)}{h}k_B^2 T \tag{1.27}$$

by means of the density of internal energy $u = \int \xi D(\xi) f(\xi) d\xi$, where $f(\xi)$ is the Fermi-Dirac distribution function, $\zeta(3)$ the Riemann zeta function of dimension three (Apery's constant) and where we have supposed a temperature dependent mean free path $l = \hbar v_F / k_B T$. On the other hand, given that we have a ballistic regime for electronic transport, its conductivity σ_e appears given by the simple expression $\sigma_e = \bar{n}\frac{e^2}{h}$ [47, 145]. Therefore, despite using so different expressions than the ones of the metals, where a quadratic dispersion equation is employed instead of the linear one of the semimetal, we obtain a good Wiedemann-Franz law yielded by

$$\frac{\kappa_e}{\sigma_e} = \frac{3\zeta(3)}{\bar{n}}\left(\frac{k_B}{e}\right)^2 T = LT \tag{1.28}$$

where the Lorenz number $L = 3\zeta(3)/\bar{n}\,(k_B/e)^2$ is one constant, as it ought to be, but divided by a Chern number $\bar{n}$ which tell us that this expression is only valid within the context of the non-trivial topological materials that we have considered. Finally, we can calculate the figure of merit Z for these topological insulators

$$Z = \frac{\sigma_e S^2}{\kappa_e} = \frac{S^2}{LT} \tag{1.29}$$

where we are not considering the phononic part of the thermal conductivity [146, 147]. In this way, the dimensionless figure of merit turns out to be a simple expression

$$ZT = n^2\bar{n}^3\frac{\pi^2}{3\zeta(3)} \tag{1.30}$$

This is the extra pure topological figure of merit for the edge states, which is zero in the case of trivial topological materials. Although these conditions are quite ideal and transport constraints can diminish its efficiency under real physical features of each material, this result opens a great hope because it tells us how to improve highly the thermoelectricity associated to the topological materials. In the case of Bi_2Te_3, for the quantum numbers equal to one we obtain a value $ZT = 2.737$ close its present maximum [63]. Additional estimations of the electronic thermal conductivity in ballistic channels can be

found in refs. [148, 149]. They give a value $k_e = \frac{\pi^2}{3}\frac{k_B^2 T}{h}$ which is numerically close to $\frac{3\zeta(3)}{h}k_B^2 T$. Noticeably, this expression leads to the usual Wiedemann-Franz law and a dimensionless figure of merit $ZT = n^2\bar{n}^2 3$ which grows in multiples of 3 in absence of lattice contributions.

1.6 Conclusions

In summary, we have shown the relationship between topological insulators, such as the family Bi_2Te_3, as well as other topological related materials without time inversion protection as the $Pb_{1-x}Sn_xTe$, and their associated thermoelectricity [150]. We have also seen that the second Chern number obtained for the non-Abelian $SU(2)$ field leads to a thermal topological mass on a Chern-Simons action. This is equivalent to have a quantized temperature working in a kind of topological bands that we define as the ramification branches using the Riemann-Hurwitz formula on a Euclidean spacetime where instanton solutions substitute the Bloch oscillating states. Physically what we have is a pumped charge between bands connected by the non-Abelian Berry phase within the insulator bulk at low temperature with an electromagnetic background field on the surface. Therefore, close to the surface we have only an Abelian $U(1)$ Chern-Simons term providing us with one transformation between electric and thermal energy because we have only one kind of states. Moreover, we show that the Schwinger's electron-hole pairs, close to the topological bands, produce an increase of the Seebeck coefficient contributing to the transformation of thermal into electric energy which is one of the key points of the model that we present in this paper. Finally, we calculate a general expression to the dimensionless figure of merit in terms of the Chern number and winding number, getting a value that coincides quite well with the one experimentally measure for the Bi_2Te_3, doing zero its phononic thermal contribution. It is open for future a new class of topological materials using topological indices higher than one which can cross what is considered nowadays the efficient critical value for the ZT figure of merit changing the physical conditions suggested in the presented model [151].

2 Emergent topological fields, electron-phonon coupling and thermal excitations in TIs

Here we develop the idea of the topological intrinsic field b deduced from the Abelian Berry curvature belonging to the surface Hamiltonian of 2DTI and 3DTIs thin films. Besides putting it within the context of the special electrodynamics of these systems, the theoretical model developed through the field b allow us to treat and interpret relativistic oscillations within the Dirac Hamiltonian of these systems. This describes an special mechanism in which electron-phonon coupling allows the transformation between heat from the lattice into electricity. In the same way, we find a new path to introduce thermal excitations in the system obtaining an equivalent result to that found from the Chern-Simons action in the previous chapter. This describes an scenario in which oscillations and thermal excitations can couple to the topological electrons, without changing the entropy of the system and hence contributing to the high efficient thermoelectric performance of TIs.

2.1 Introduction

As we shown in the previous chapter, decreasing the thermal conductivity as much as possible and take advance of the highly conducting edge channels present in TIs seems essential to provide a high efficient thermoelectric response [23, 71]. Besides the experimental difficulties to obtain high-quality thin-films, eliminate bulk carrier transport or adjust the Fermi level to lie in the small topological gap there is not a physical model to guide us towards a new generation of thermoelectric devices by treating phonons or oscillations produced by temperature in the topological context. The problem is that physics is fundamentally local and topology must enter through those tools. With this purpose, we need to connect topology and electrodynamics to introduce phonons and thermal excitations together with the topological electrons at the surface. The scenario which arises after this study, supported on an obtained expression for the topological intrinsic field,

solves most of the difficulties involved in the topological thermoelectricity and allows to find experimental work to confirm it.

The global characteristics of TIs are printed on their band structure within their first Brillouin zone (BZ), concretely through their curvatures and Berry phases. These materials are both insulators in the bulk and semimetals on their surface where they contain Dirac points on account of the band crossings. But the bands are not the unique factor to take into account to determine the topology. One fundamental ingredient is the dimensions of the spacetime where the Hamiltonian is defined. That is why generally, for a given Hamiltonian $H(k)$ following Schrödinger equation, we are able to define a map from the BZ to the manifold of their symmetries $X(k) : BZ \longmapsto \frac{U(n)}{U(n-i)\times U(i)}$ by means of a unitary matrix $U(n)$ which diagonalizes the Hamiltonian for n states (Bloch bands) being i the occupied ones and $n-i$ the unoccupied with respect to the Fermi level. This allows calculating the number of maps $X(k)$ which cannot be deformed continuously each other using the homotopy group obtaining $\pi_1[X(k)] = \pi_3[X(k)] = 0$ and $\pi_2[X(k)] = \mathbb{Z}$, being $\mathbb{Z}$ an integer and each subindex the dimension of the spacetime [2]. That means that there is only one non-trivial topology associated with the direct relabeling of the bands in two dimensions. Or in other words, band insulators with different integers cannot be continuously deformed into each other without crossing a quantum phase transition. This is what happens, for instance, in the Integer Quantum Hall Effect, where the number of chiral edge states are the integers associated to the above homotopy group [18, 54, 152, 153]. But in one or three dimensions we need to introduce more symmetries of the Hamiltonian if we want to take into account their non-trivial topology. In TIs this symmetry is the time-reversal symmetry $\hat{T}$ which induces a Kramers degeneracy [19, 154], such that the square of $\hat{T}$ operator is equal to -1 for half-spin electrons (fermions), acting on the map previously defined as $\hat{T}X(k)\hat{T}^{-1} = X(-k)$. This enables us to define a new topological number by the discrete cyclic group of two elements Z_2 called spin-Chern number [19, 20]. The form to do it is somewhat subtle dividing the Hilbert space into two parts, one for each kind of Kramers states, and calculating the Chern number on them for extending the definition of the topological index [49, 59].

Once we know how the non-trivial topology can be determined on the bands, we need to figure up how the electromagnetic fields and heat exchange behaves physically under such non-trivial topologies. For such aim, we need to employ the axion electrodynamics which enlarges the Maxwell's action using the two Lorentz invariants associated to the fields. That is to say, to add the pseudo scalar quantity $\frac{1}{2}\epsilon_{\mu\nu\alpha\beta}F^{\mu\nu}F^{\alpha\beta}$, besides the usual scalar $F_{\alpha\beta}F^{\alpha\beta}$ which is enough to provide Maxwell electrodynamics in the trivial topological vacuum. Then, we have the axion action

$$\mathcal{S} = \int dx^4 \left(\frac{1}{4\mu_0 c} F_{\alpha\beta}F^{\alpha\beta} - \frac{e^2}{32\pi^2\hbar}\theta(r,t)\epsilon_{\mu\nu\alpha\beta}F^{\mu\nu}F^{\alpha\beta} + \frac{1}{c}A_\mu J^\mu \right) \tag{2.1}$$

which leads directly to the equivalent Maxwell equations in TIs,

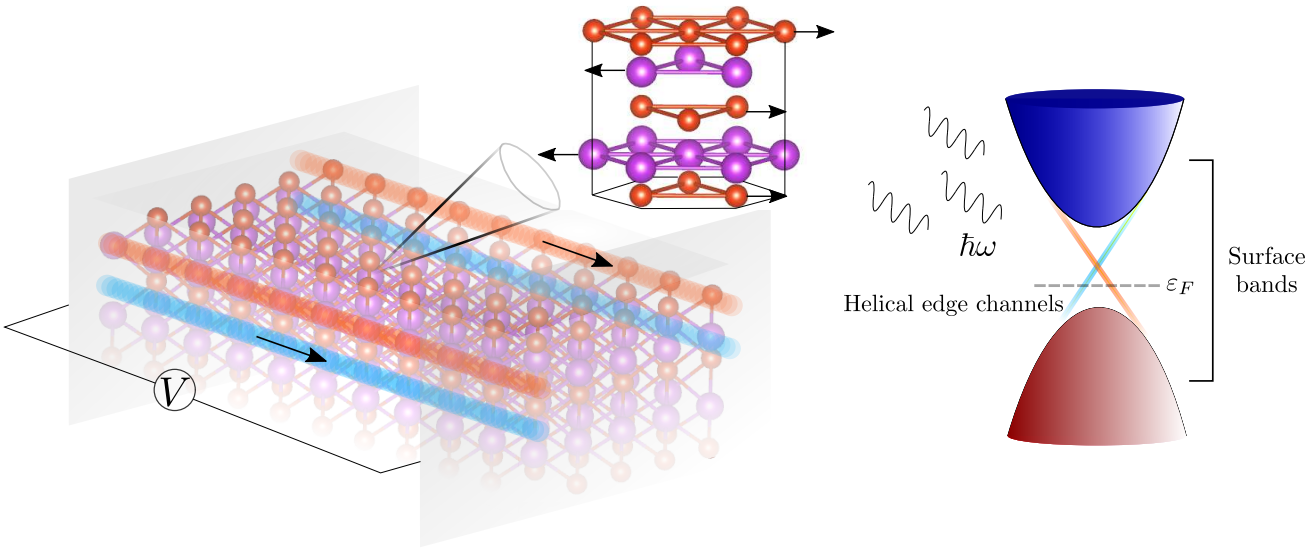

Figure 2.1: Lattice oscillations in the topological electronic transport. Schematic illustration of helical edge states and surface of a 3DTI in thin-film conditions. The energy spectrum is displayed on the right side of the panel. The quintuple layer describes the addition of in-plane lattice oscillations, in this case represented by a polar phonon mode, to the topological electronic transport.

$$\boldsymbol{\nabla} \cdot \left(\boldsymbol{E} + 2\alpha c \left(\frac{\theta}{2\pi} \right) \boldsymbol{B} \right) = \frac{\rho}{\epsilon_0} \tag{2.2}$$

substituting the Gauss law and

$$\boldsymbol{\nabla} \times \boldsymbol{B} = \mu_0 \boldsymbol{J} + \frac{1}{c^2} \frac{\partial \boldsymbol{E}}{\partial t} + \frac{2\alpha}{c} \left[\boldsymbol{B} \frac{\partial}{\partial t} \left(\frac{\theta}{2\pi} \right) + \boldsymbol{\nabla} \left(\frac{\theta}{2\pi} \right) \times \boldsymbol{E} \right] \tag{2.3}$$

instead of the Maxwell-Ampere one, being $\alpha = \frac{e^2}{4\pi\epsilon_0 \hbar c}$ the dimensionless fine structure constant. The other two equations, Faraday and non-existence of isolated magnetic poles, maintain the same form [52, 155, 156]. In particular for the TIs, $\theta = \pi$ and we can choose a gauge function $\Lambda(r,t) = \frac{\hbar 2\pi r}{ea}$ associated to the degree of freedom of the electromagnetic potentials where a is a lattice constant and $|r|$ the modulus of the distance given in the electromagnetic fields. By constraining these fields on a torus, these ingredients are enough to connect θ with the non-trivial topologies of the lattice using Gauss-Bonnet, however, not with the bands through the Chern number. To reach such result we are going to translate the topological information into a physical field named as b. This will be done through the Berry curvature $\Omega_{k_x,k_y} = -2Im\left\langle \partial_{k_x} n \middle| \partial_{k_y} n \right\rangle$ defined on the non-trivial bands of a 2D Dirac Hamiltonian which behaves as a spin-dependent magnetic field in the k-space and whose integral determines the Chern number C.

Supported by this topological field, which is intrinsic to these materials and consistent with their special electromagnetic background, we are able to introduce and interpret the thermodynamic part associated to the phonons in TIs (Fig. 2.1). This is done by including oscillations in the Dirac Hamiltonian, i.e., relativistic phonons associated to the Dirac oscillator [157]. By means of the adiabatic mechanism, we are going to establish an equivalence between the phonon field $\boldsymbol{\omega}$ of the Dirac oscillator and the field $\boldsymbol{b}$ containing the information of the dynamic and the robustness of the topological regime. This is a crucial result for the topological formalism of the thermoelectricity. On the one hand, we demonstrate in a direct way how relativistic phonons enters into the topological context, modifying the Berry curvature and allowing heat-electricity transformation. On the other hand, we give an explanation of why topology is preserved at high temperatures in most of the compounds which exhibit it. The previously mentioned relationship between the field $\boldsymbol{b}$, which can reach values in the order of Teslas for each spin subsystem with the typical parameters in 3DTI thin films, and ω defines a limit (>THz) for the frequencies tolerated by the system without involving entropy change. Under these conditions, we would find a temperature regime in which such excitations would not break the quantum coherence necessary for the conservation of the topological signatures allowing the observation of the high figures of merit associated to the topological states around room temperature.

2.2 The effective topological field b

The family of 3DTIs Bi_2Se_3, Bi_2Te_3, Sb_2Te_3 has a special interest by the fact of being topological besides including on their members the most efficient thermoelectric material up to now. The highly conducting edge states, provided by the topology, are predicted to be responsible for their high figure of merit in low thermal conductivity conditions [64, 71]. However, this must not be the unique ingredient to explain the thermoelectricity in these materials where the coexistence of time-reversal symmetry and non-zero temperatures, which usually involves entropy change, might cause a conflict. Given that, our starting point must be a 2D effective Dirac Hamiltonian used to describe the physics inside 2DTIs as well as in 3DTIs thin films, i.e. when the thickness of a 3DTI is enough small to overlap its top and bottom surface states forcing them to be placed at the edge [70, 103, 158].

$$H_{2D}(\mathbf{k}) = \begin{bmatrix} H_+ & 0 \\ 0 & H_- \end{bmatrix}, \qquad H_\pm = \begin{pmatrix} \pm M(\mathbf{k}) & \hbar v_F k_- \\ \hbar v_F k_+ & \mp M(\mathbf{k}) \end{pmatrix} \tag{2.4}$$

Here $k_\pm = k_x \pm i k_y$, $M(\mathbf{k}) = M - \mathcal{B}k^2$ is the effective mass in the solid, $k^2 = k_x^2 + k_y^2$, v_F is the Fermi velocity, $\hbar$ is the Planck's bar constant and the basis has been rearranged to be $[\psi_{1\uparrow}, \psi_{2\downarrow}, \psi_{2\uparrow}, \psi_{1\downarrow}]$, allowing the separation of the Hamiltonian into two non-interacting time-reversal counterparts $H_\pm$ which can be treated independently [70, 159]. The energy spectrum of Eq. (2.4) define two non-interacting Dirac hyperbolas centered at the Γ point for which conduction and valence bands for H_+ have an associated Berry curvature

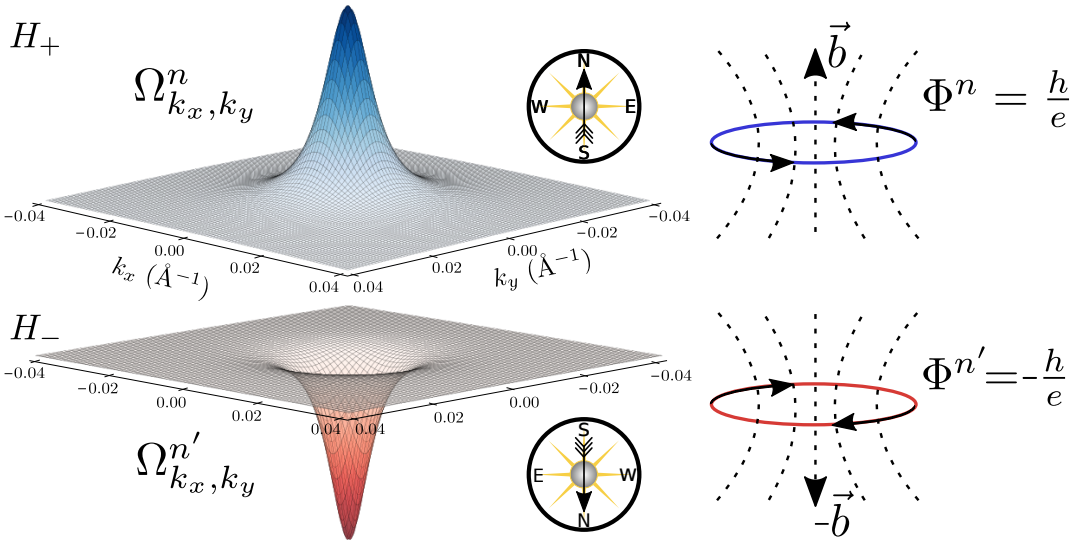

Figure 2.2: Non-trivial Berry curvature and effective flux quantization in TIs. Non-trivial ($M < 0$, $B < 0$) Berry curvature $\boldsymbol{\Omega}_{k_x,k_y}$ for the positive energy eigenstates of $H_\pm$ labelled as $|n\rangle$ and $|n'\rangle$ respectively. The compass indicates the orientation of the field felt by the electrons on each band. In the bulk of a TI, this curvature allows considering the existence of helical orbits with an associated flux $\Phi = \hbar/e\ C$, being $C = \pm 1$ the Chern number associated to the conduction bands of $H_\pm$.

$$\boldsymbol{\Omega}^c_{k_x k_y} = -\boldsymbol{\Omega}^v_{k_x k_y} = -\frac{\hbar^2 v_F^2 (M + \mathcal{B}k^2)}{2[(M - \mathcal{B}k^2)^2 + \hbar^2 v_F^2 k^2]^{3/2}} \hat{\boldsymbol{z}} \tag{2.5}$$

which is spin and band dependent, resulting in the opposite sign for H_- ($M \to -M$). This Berry curvature defines the Chern number $C = 1/(2\pi) \int \boldsymbol{\Omega} d\boldsymbol{k}$ which in the non-trivial regime of H_{2D}, given by the condition $M\mathcal{B} > 0$, is an integer equal to ± 1 which also shares the same dependence of $\boldsymbol{\Omega}$ and its responsible of transport quantization [70]. Thus, for instance, for the conduction band of H_+ we have

$$C = \frac{1}{2}\int_0^\infty \Omega^c dk^2 = \frac{1}{2}\int_0^\infty \frac{\partial}{\partial k^2}\left(\frac{M - \mathcal{B}k^2}{\xi}\right) dk^2 = -\frac{1}{2}\left(sgn(M) + sgn(\mathcal{B})\right) \tag{2.6}$$

where $d^2k = 2\pi k dk$ and $\xi = \sqrt{(M - \mathcal{B}k^2)^2 + \hbar^2 v_F^2 k^2}$ is the positive energy solution. Essentially, the Berry curvature plays the role of a magnetic field in the k-space obtained through the rotational of the Berry potential $\boldsymbol{\mathcal{A}}$ [3]. This allows us to consider in a TI, the presence of a pair spin-momentum locking orbits associated to the topology, which present a quantized flux ($C\ h/e$) in terms of the Chern number C and whose sum obviously gives zero due to $\hat{T}$ symmetry (Fig. 2.2). Of course, this is consistent with the fact of why in the presence of an in-plane electric field we can talk about opposite transverse spin currents

which in the edge produce a quantized electrical conductance $G = (C_+ - C_-)e^2/h$, being $C_\pm$ the Chern numbers associated with the branches $H_\pm$ [15, 47]. The idea to understand and address effects associated with thermal fields and phonons or external fields is to link the topological information into a physical field consistent with their phenomenology. But, how can it be done? The answer lies in the translation of the Berry curvature into the real space. This can be done by noticing that under small gap conditions, as it happens for 3DTIs in the thin-film limit, the non-trivial Berry curvature $\boldsymbol{\Omega}_{k_x,k_y}$ associated to the states of Eq. (2.4) has the form of a single peak Gaussian-like function centered at the Γ point [70], which has characteristic length small enough to consider an equivalent magnetic field $\boldsymbol{b}$ constant along the bulk crystal and whose magnitude must be determined by the constraint that its flux is quantized and equal to $h/e\ C$, i.e., $\hbar/e \int \boldsymbol{\Omega}_{k_x,k_y} d\boldsymbol{k} = \int \boldsymbol{b} d\boldsymbol{S}$.

Given that b can be extracted from the integral, we need now to estimate the area defined by the topological electrons on their motion. This surface element $\Delta \boldsymbol{S}$ can be obtained in an original way by applying Heisenberg's uncertainty principle matching the quantum conductance (e^2/h) with the conductivity $\sigma = \Delta S^{-1} \frac{e^2\tau}{m_e}$ in the Heisenberg limit $(\tau = \hbar/\Delta\varepsilon)$ being e the elementary charge, τ the scattering time and $\Delta\varepsilon = 2\xi$ the energy uncertainty which can be considered to be in the order of the energy of the particle ξ due to the low energy of the topological electrons and that we take equal to 2ξ, i.e., the energy difference between the two eigenstates [160]. In this way, we obtain the following expression for the field $\boldsymbol{b}$

$$\mathbf{b} = \frac{2m_e\xi}{\hbar e} C\ \hat{\mathbf{z}} \approx \frac{2m_e^2 v_F^2}{\hbar e} C\ \hat{\mathbf{z}} \tag{2.7}$$

which can be approximated by setting $\xi \approx m_e v_F^2$ taking into account of the small momentum of the particles and where the electron effective mass can be considered as $m_e = \hbar^2(\frac{\partial^2\xi}{\partial k^2})^{-1} = M/v_F^2$ neglecting any contribution from the Hamiltonian parameter $\mathcal{B}$, that gives us the information about the localization or delocalization of the bands in the space, and limiting to materials that present $v_F^2 >> 2M\mathcal{B}/\hbar^2$. This approximation, easily fulfilled thanks to the small gap and high Fermi velocity that typically characterizes 3DTI thin films ($M \approx -25$ meV, $v_F = 6.17\ 10^5$m/s), determines an equivalent field for electrons on the surface $|b| \approx 5$T for these values consistent with the robustness that characterizes topological surface states and whose sign, determined by the Chern number, keeps time-reversal symmetry intact [70]. This expression for b is not far from the one obtained directly by transforming a narrow Gaussian function from the momentum space to the real space where its value is determined by the inverse of the maximum of the source function. In this way, the large magnitude of b is uniquely due to the size of Berry curvature which is associated to the band singularities. Note that in Eq. (2.7) m_e must not change its sign when we pass from H_+ to H_- $(C \to -C)$ given that its inversion has already been considered in the conductivity change $e^2/h \to -e^2/h$. Thus, our formalism defines an effective area $\Delta S = h\hbar/(2m_e\xi)$ for the electrons inside TIs, which corresponds with the inverse of the 2D density of states, and a magnetic field b with opposite sign for

each band and branch $H_{\pm}$, which attending to the full Hamiltonian, results in a special spin-dependent interaction consistent with the singular dynamic of the topological regime and the band inversion. The obtained expression for the field b also shares a direct correspondence with the critical magnetic field $B_c = m^2c^2/(\hbar e)$ necessary for two photons to create Schwinger pairs in the vacuum, adapted to the particular context of the TIs due to the small gap and the substitution of c by v_F, making this quantity experimentally accessible [138]. Additionally, it can be checked that indeed Eq. (2.7) matches with the critical value of the external magnetic field B making zero the density of states and Fermi sea volume in non-zero Berry curvature systems at $k = 0$, being these quantities proportional to the factor $(1 + \frac{e\boldsymbol{B}\cdot\boldsymbol{\Omega}}{\hbar})$ [73, 161]. Along this chapter and the following, we are going to test this result demonstrating that the field interpretation of the Berry curvature through b is consistent and accurate within the electrodynamics and directly introducing a magnetic field in the Dirac Hamiltonian of TIs.

2.3 The Dirac oscillator

From the historical point of view, the introduction of mechanical oscillations in a relativistic context was first analyzed by M. Moshisnky and A. Szczepaniak [157] incorporating a linear term in r to the Dirac equation. The origin of this term lies in the introduction of an harmonic oscillator potential into the Klein-Gordon equation, leading to the well-known Dirac oscillator

$$i\hbar(\partial\psi/\partial t) = [v_F\boldsymbol{\alpha}(\boldsymbol{p} - im\boldsymbol{r}\omega\beta) + mv_F^2\beta]\psi \tag{2.8}$$

where

$$\alpha_i = \begin{bmatrix} 0 & \sigma_i \\ \sigma_i & 0 \end{bmatrix} \qquad \beta = \begin{bmatrix} \sigma_0 & 0 \\ 0 & -\sigma_0 \end{bmatrix} \tag{2.9}$$

are the Dirac matrices, σ_i the Pauli matrices, m the mass of the particle, r the position and where we have substituted the original speed of light c by the Fermi velocity v_F in order to adapt equation Eq. (2.8) into the context of TIs. Afterwards, the equation was further analyzed, always in the context of Quantum Field Theory (QFT) [162, 163], where working with phonons it is always convenient to employ operators defined on a Fock space and Eq. (2.8) can be rewritten in function of the right and left chiral annihilation and creation operators

$$a_r = \frac{1}{\sqrt{2}}(a_x - ia_y) \qquad a_r^\dagger = \frac{1}{\sqrt{2}}(a_x^\dagger + ia_y^\dagger)$$

$$a_l = \frac{1}{\sqrt{2}}(a_x + ia_y) \qquad a_l^\dagger = \frac{1}{\sqrt{2}}(a_x^\dagger - ia_y^\dagger)$$

being $a_x, a_y, a_x^\dagger$ and $a_y^\dagger$ the usual annihilation and creation operators of the harmonic oscillator. There are two Pauli spinor eigenstates which present entanglement between the spin and orbital degrees of freedom.

$$|\psi_1\rangle = i\frac{2mv_F^2\sqrt{\epsilon}}{E - mv_F^2}a_l^\dagger |\psi_2\rangle \qquad |\psi_2\rangle = -i\frac{2mv_F^2\sqrt{\epsilon}}{E + mv_F^2}a_l^\dagger |\psi_1\rangle \tag{2.10}$$

being $|\psi_1\rangle$ and $|\psi_2\rangle$ the two components of the spinor $|\psi\rangle$, $\epsilon = \frac{\hbar\omega}{mv_F^2}$ takes into account the non-relativistic limit and $|n_l\rangle = \frac{1}{\sqrt{n_l!}}(a_l^\dagger)^{n_l}|0\rangle$ the basis in which the Fock space is expanded [162]. The energy spectrum is $E = \pm E_{n_l} = \pm mv_F^2\sqrt{4\epsilon n_l + 1}$, whose eigenstates can be written as Pauli spinors $|\phi_\uparrow\rangle$ and $|\phi_\downarrow\rangle$ components, employing the angular momentum z-component definition given by $L_z = \hbar(a_r^\dagger a_r - a_l^\dagger a_l)$

$$|-E_{n_l}\rangle = \beta_{n_l}|n_l\rangle|\phi_\uparrow\rangle + i\alpha_{n_l}|n_l - 1\rangle|\phi_\downarrow\rangle \tag{2.11}$$

$$|E_{n_l}\rangle = \alpha_{n_l}|n_l\rangle|\phi_\uparrow\rangle - i\beta_{n_l}|n_l - 1\rangle|\phi_\downarrow\rangle \tag{2.12}$$

where $\alpha_{n_l} = \sqrt{\frac{E_{n_l}+mv_F^2}{2E_{n_l}}}$ and $\beta_{n_l} = \sqrt{\frac{E_{n_l}-mv_F^2}{2E_{n_l}}}$. Finally, time dependent state of the spinors excited by the Dirac oscillator is

$$|\psi(t)\rangle = \left(cos\ \omega_{n_l}t + \frac{i}{\sqrt{4\epsilon n_l + 1}}sin\ \omega_{n_l}t\right)|n_l - 1\rangle|\phi_\uparrow\rangle + \left(\sqrt{\frac{4\epsilon_{n_l}}{4\epsilon_{n_l}+1}}sin\ \omega_{n_l}t\right)|n_l\rangle|\phi_\downarrow\rangle \tag{2.13}$$

In this way, we see how there is one oscillation between the spin-orbit states $|n_l - 1\rangle|\phi_\uparrow\rangle$ and $|n_l\rangle|\phi_\downarrow\rangle$, in such a form that the change of spin polarization implies one for the orbital and vice versa. However, these abstracts does not take into account the topology of the system and are not enough to treat relativistic phonons into TIs without losing the notion of the Berry curvature. With this purpose we are going to introduce it into the adiabatic context to see explicitly how they affect to the topological properties and thus to the thermoelectric response in TIs.

2.4 Perturbative analysis

With these remarks, now we are in a position to interpret the role of relativistic oscillations in TIs. In fact, it can be straightforward to figure out that the role of b is closely related to the phenomenology of the Dirac oscillator Hamiltonian $i\hbar(\partial\psi/\partial t) = [v_F\boldsymbol{\alpha}(\boldsymbol{p} - im\boldsymbol{r}\omega\beta) + mv_F^2\beta]\psi$, which also preserves time-reversal symmetry and incorporates a linear correction in r to the electron momentum p in the form of a magnetic field $B =$

$2m\omega/e$. Remember that b has been interpreted as a magnetic field deduced from the Berry curvature. So, we have an opposite magnetic field for each Dirac band in H_{2D} and also for each Hamiltonian $H_{\pm}$. In a 2D Hamiltonian as Eq. (2.4) the perturbation introduced in the Dirac oscillator enters in the same way of a magnetic field B in the z-direction with opposite sign for each branch $H_{\pm}$ with the usual substitution $2\omega = eB/m$. The factor 2 comes from the non-minimal coupling present in the Dirac oscillator equation to guarantee of having a harmonic oscillator in its non-relativistic limit [157, 164]. Precisely in this limit, is where a spin-orbit coupling of strength $2\omega/\hbar$ arises motivated by the spin-dependent magnetic interaction introduced in the system. As we saw, the Dirac oscillator has been analyzed in different studies [157, 162–164], however, it has not been treated into the adiabatic formalism. Only then, we are going to be capable of visualizing the role of phonons inside the topological context. Given that the Hilbert space was divided into two time-reversal counterparts, we are able to work in only one of the subsystems $H_{\pm}$ where the adiabatic correction to the energy eigenstates can be calculated [1, 5].

$$|n\rangle \to |n\rangle - i\hbar\frac{\partial k_x}{\partial t}\frac{\langle m|\partial_{k_x} n\rangle}{2\xi}|m\rangle - i\hbar\frac{\partial k_y}{\partial t}\frac{\langle m|\partial_{k_y} n\rangle}{2\xi}|m\rangle \tag{2.14}$$

being $|n\rangle$ and $|m\rangle$ the unperturbed eigenstates of H_+ associated respectively with the positive and negative energy solutions $\xi = \pm\sqrt{M^2(k) + \hbar^2 v_F^2 k^2}$.

$$|n\rangle = \frac{1}{\sqrt{2}}\begin{bmatrix} \sqrt{1+\frac{M(k)}{\xi}} \\ e^{i\phi}\sqrt{1-\frac{M(k)}{\xi}} \end{bmatrix} \qquad |m\rangle = \frac{1}{\sqrt{2}}\begin{bmatrix} \sqrt{1-\frac{M(k)}{\xi}} \\ -e^{i\phi}\sqrt{1+\frac{M(k)}{\xi}} \end{bmatrix} \tag{2.15}$$

Rigurously, Eq. (2.14) must have a summation over every state $|m\rangle$ different from $|n\rangle$ but this does not apply to the two-level system considered. Coming back to Eq. (2.14), we know that the Lorentz force provided by $\boldsymbol{\omega}$ increases or decreases (depending on its sign) the electron momentum in the direction i proportionally to their perpendicular components. In that way, as a first approximation to the problem we can formulate the temporal variation of the momentum as $\partial k_i/\partial t = \epsilon_{ijk}k_j\omega_k$ and, regrouping terms, write the correction to the eigenstates given by the Dirac oscillator

$$|n\rangle \to |n\rangle + \frac{\hbar\omega}{4\xi^2}\hbar v_F k\,|m\rangle \tag{2.16}$$

This can be done taking the previously defined derivatives for the eigenstates

$$|\partial_{k_x} n\rangle = \frac{1}{\sqrt{2}}\begin{bmatrix} \frac{\Gamma_{kx}}{2\sqrt{1+\frac{M(k)}{\xi}}} \\ \frac{-ik_y}{k^2}e^{i\phi}\sqrt{1-\frac{M(k)}{\xi}} - \frac{\Gamma_{kx}e^{i\phi}}{2\sqrt{1-\frac{M(k)}{\xi}}} \end{bmatrix} \tag{2.17}$$

$$\left|\partial_{k_y} n\right\rangle = \frac{1}{\sqrt{2}} \begin{bmatrix} \frac{\Gamma_{ky}}{2\sqrt{1+\frac{M(k)}{\xi}}} \\ \frac{ik_x}{k^2} e^{i\phi} \sqrt{1-\frac{M(k)}{\xi}} - \frac{\Gamma_{ky} e^{i\phi}}{2\sqrt{1-\frac{M(k)}{\xi}}} \end{bmatrix} \tag{2.18}$$

as well as the ones corresponding to the negative eigenstates $|m\rangle$. Here, $\Gamma_{k_i} = -\frac{\hbar^2 v_F^2 (M+Bk^2)}{\xi^3} k_i$. Then, it is straightforward to reach the following identities

$$\Omega^c_{k_x,k_y} = i\left(\left\langle \partial_{k_x} n \middle| \partial_{k_y} n \right\rangle - \left\langle \partial_{k_y} n \middle| \partial_{k_x} n \right\rangle\right) = \frac{1}{2}\left(\frac{\Gamma_{k_x} k_x}{k^2} + \frac{\Gamma_{k_y} k_y}{k^2}\right) \tag{2.19}$$

$$-i\left(k_y \left\langle m|\partial_{k_x} n\right\rangle - k_x \left\langle m \middle| \partial_{k_y} n\right\rangle\right) = \left(\frac{k_y^2}{2k^2}\frac{\hbar v_F k}{\xi} + \frac{k_x^2}{2k^2}\frac{\hbar v_F k}{\xi}\right) = \frac{\hbar v_F k}{2\xi} \tag{2.20}$$

From Eq. (2.14) we can compute after some tedious algebra the corrections to the Berry curvature of the bands $\Omega^i_{k_x k_y} = -2Im\left\langle \partial_{k_x} i \middle| \partial_{k_y} i \right\rangle$. Two cases were analyzed, both sharing an ability to modulate the Berry curvature. The first one, considering a purely uniform ω, represents phonons or oscillations with a constant energy dispersion and their corrections have the form of a function similar to the Berry curvature which changes its sign at some point k. Besides being quite restrictive, these modes might not be suitable to introduce in the thermoelectric mechanism. The second case considers an explicit energy dependence on the phonon frequency, i.e. $\hbar\omega = \lambda\xi$, which not only could maximize the coupling with the topological electrons given its linear energy dispersion but at the same time is consistent with its apparent relation with the intrinsic topological field $b = 2m\omega/e$, with no more ingredients than substituting Eq. (2.7) into the previous relation. True to the Dirac oscillator, as well as to test b, we are going to consider $\mathcal{B} = 0$.

2.4.1 Constant ω

The first case corresponds to a purely constant ω, i.e, the phonon frequency does not incorporate any dependence on the position r, the energy or the temperature. In that situation, the correction to the Berry curvature of the conduction band of H_+ results (Fig. 2.3)

$$\Omega^n_{k_x,k_y} \to \Omega^n_{k_x,k_y} - \frac{\hbar\omega}{2\xi}\frac{M}{\xi}\Omega^n_{k_x,k_y} + \frac{\hbar\omega}{2\xi}\frac{\hbar^2 v_F^2}{2\xi^2} - \frac{\hbar\omega}{2\xi}\frac{\hbar^2 v_F^2}{\xi^2}\left(1 - \frac{M^2}{\xi^2}\right) \tag{2.21}$$

which can be written in a more compact form

$$\Omega^n_{k_x,k_y} \to \Omega^n_{k_x,k_y} - \Omega^n_{k_x,k_y}\frac{\hbar\omega}{\xi}\frac{M}{\xi}\left(1 - \frac{1}{2}\frac{\hbar^2 v_F^2 k^2}{M^2}\right) \tag{2.22}$$

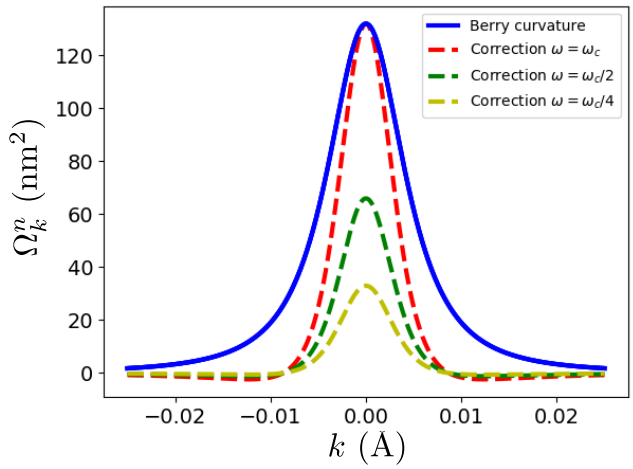

Figure 2.3: Unperturbed Berry curvature (blue solid line) of the conduction band of a Dirac Hamiltonian H_+ and first-order correction to it (dashed lines) for different constant frequencies below the critical value $\omega_c = eb/2m$. The parameters used are $M = -0.025$ eV, $\mathcal{B} = 0$ and $v_F = 6.17\ 10^5$m/s.

using that $\Omega^n_{k_x,k_y} = -\frac{\hbar^2 v_F^2 M}{2\xi^3}$ when $\mathcal{B} = 0$. The perturbation introduced produces a correction to the Berry curvature whose direction will depend on the sign of ω. At critical frequencies $\omega_c = eb/2m$, the magnitude of the perturbation has the value of the unperturbed Berry curvature at $k = 0$ evidencing the good interpretation of our approximation for the topological intrinsic field $b \approx 2M^2/\hbar e v_F^2$ as a measure of the robustness of the topological regime. The behaviour of the corrections is what one can expect from a constant perturbation into the real space and its homologous field into the k-space. This case might be enough to introduce certain phonons in topological insulators, however, it can not be applied generally given that thermal excitations and the majority of the phonons have an energy/momentum dependent nature.

2.4.2 Energy dependent ω

Given the physical equivalence between the frequency ω given by the Dirac oscillator Hamiltonian and the field $b = 2m\xi/\hbar e$ we are going to suppose the phonon frequency to have an energy dependence of the type $\omega = eb/2m = \xi/\hbar$. This dispersion is typical for acoustic phonon modes as well as certain type of polar optical modes in Bi_2Te_3 and Bi_2Se_3 [165, 166]. In this way, we can explore the interpretation of b and demonstrate how oscillation, at least below this limit, can modulate the Berry curvature of the bands. If our interpretation of the field b as a translation of the Berry curvature into the real space is correct, then its corrections should result in a function of the type of the unperturbed Berry curvature. In this case, the corrections to the positive an negative eigenstates read

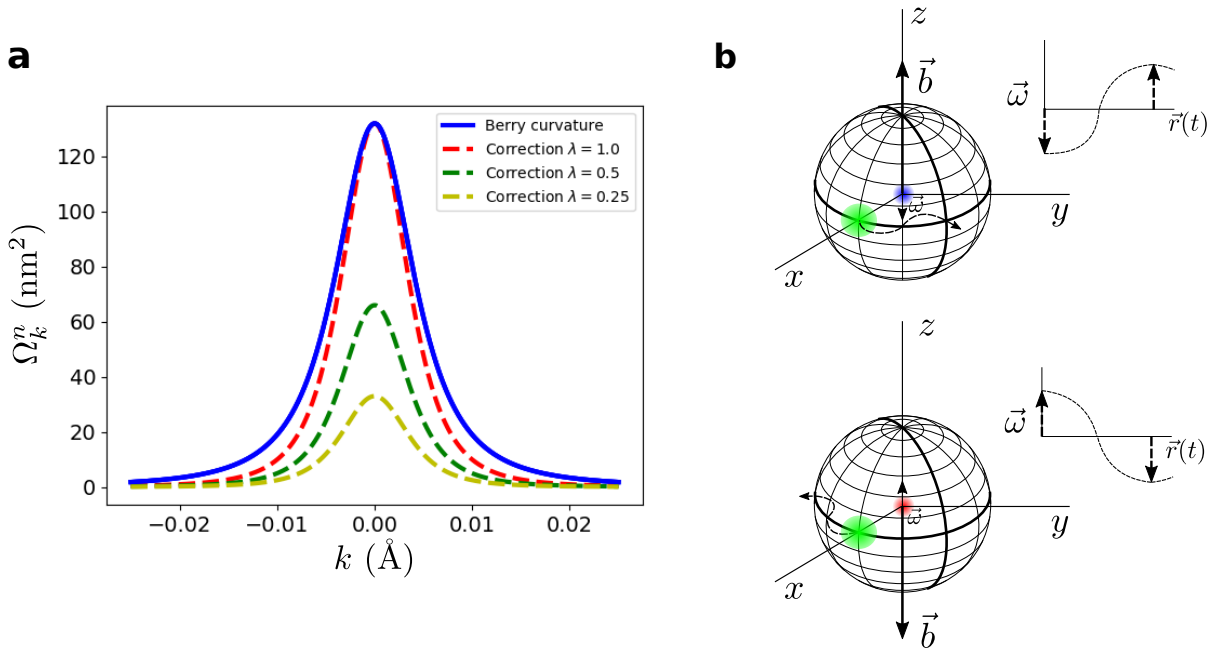

Figure 2.4: (**a**) Unperturbed Berry curvature (blue solid line) of the conduction band (H_+) of a topological insulator ($M < 0$) and first-order correction to it (dashed lines) for different energy dependent frequencies below the critical frequency $\omega_c = eb/2m$. The parameters used are $M = -0.025$ eV, $\mathcal{B} = 0$ and $v_F = 6.17\ 10^5$m/s. (**b**) Schematic illustration of the Berry curvature modulation from the electronic point of view (blue and red points) where in-plane nucleus (green circles) displacements are showed to change the field b defined on each orbital motion. Red and blue points represent electrons with opposite spins for which nucleus move in opposite directions attending to the helical nature of electronic motion in a TI.

$$|n\rangle \to |n\rangle + \frac{\lambda}{2}\frac{\hbar v_F k}{2\xi}|m\rangle \tag{2.23}$$

and the correction to the Berry curvature is slightly different from the previous situation

$$\Omega^n_{k_x,k_y} \to \Omega^n_{k_x,k_y} + \lambda\frac{1}{2}\left(-\frac{\hbar^2 v_F^2}{2\xi^2} + \frac{\hbar^2 v_F^2}{2\xi^2}\frac{\hbar^2 v_F^2 k^2}{\xi^2} - \frac{M}{\xi}\Omega^n\right) = \Omega^n - \lambda\frac{M}{\xi}\Omega^n \tag{2.24}$$

where λ ($\in [0,1]$) is a dimensionless parameter measuring the relative strength of ω with respect to b. The obtained results, plotted in Fig. 2.4, demonstrates how phonons and oscillations can be introduced into the context of TIs modulating the Berry curvature and hence the field b even when the perturbation is not small compared with the energy of the system but whose variation can be adiabatic. Again, for the limit case $\lambda = 1$,

i.e. $\omega = eb/2m$, the obtained first-order correction have the same height at $\Gamma = 0$ than the unperturbed Berry curvature. This confirms the correctness of the expression for the field b and its interpretation as a measure of the topological robustness and as a critical value for the strength of in-plane oscillations and external forces (strain, spin-orbit) supported by the surface states. Beyond this limit, the Berry curvature might change its sign. Of course, these effects are not produced by every phonon mode presented in the crystal but some specific phonons for which the concept helicity must be involved in order to couple topological electrons and capable to cause a correction to the momentum of $\partial k_i/\partial t = \epsilon_{ijk} k_j \omega_k$, i.e., relativistic. This constraint, that will need a suitable phonon dispersion, has been shown to be on the energy range needed for polar optical modes in Bi_2Te_3 and Bi_2Se_3 [166]. The expressions derived above are also extensible to the case of taking into account the dependence of the mass term $M(k) = M - \mathcal{B}k^2$ on the Hamiltonian parameter $\mathcal{B}$ [109]. Finally, it should be noted that the curvature corrections displayed in Eq. (2.24) are valid for quantitative purposes and no for a faithful determination of the Chern number by means of their integral. A pure perturvative calculus of these corrections implies that the temporal variation of the particle momentum must be written in terms of the velocity operator and no with the momentum [73]. This will be explored in the next chapter. However, the approximation used is suitable as an estimation of the effects produced by the perturbations simplifying the calculations and avoiding to deal with gauge dependent corrections.

2.5 Electrodynamics and band topology

Both, electrodynamics and bands, have a common degree of freedom given by the gauge transformations within the Abelian group U(1). Mathematically they also share non-trivial topological features where the homotopy group $\pi_1(U(1))$ is equivalent to the integer numbers: the bands through the Berry curvature and the electrodynamics through torus constraints with genus equal one. Let us to develop it deeper from the physical consequences. Using the periodicity of the Brillouin zones, we can define the function $\Lambda(r,t) = \frac{\hbar 2\pi r}{ea}$, where a is the lattice constant, which allows a transformation of the potentials such that $A_\mu \longrightarrow A'_\mu = A_\mu + \partial_\mu \Lambda(r,t)$. This makes the space-time to be on a torus of four dimensions $T^4 = T^2 \times T^2$ for the electromagnetic fields and taking π degrees between E and B, i.e. sharing a spatial direction. This leads to a quantized electric and magnetic fields,

$$B = n\frac{h}{ea^2} \qquad E = n'\frac{hc}{ea^2} \tag{2.25}$$

where $n, n' \in \mathcal{N}$ are natural numbers which determine the topological sector. Coming back to the EB term of the action we can see how this part of the action is quantized making θ belong to the interval $[0, 2\pi)$ and therefore obtaining a topological vacuum angle that usually is written as $|\theta\rangle = \sum_\nu exp(i\nu\theta)\,|\nu\rangle$, being ν the winding number [156]. The

defined electromagnetic background can be now easily connected with the topology of the bands through the intrinsic topological field b, substituting the area a^2 by the one $\Delta S = h\hbar/(2m_e\xi)$ obtained for the electrons in a TI, resulting that

$$B = \frac{2m_e\xi}{\hbar e}\, C \equiv b \tag{2.26}$$

where n is now interpreted as the Chern number C. Notice that b is associated to the curvature of the bands, while B is a pure magnetic field of axion electrodynamics carrying information of the non-trivial topology on the spacetime. Both things are conceptually very different, one worked with Chern numbers and the other with genus using Gauss-Bonnet theorem; but physically they are connected linking the singularities of the bands and the real spacetime. Consistently, by making the same substitution we also find an expression for the electric field $E = 2m_e^2 v_F^3 n'/\hbar e$ inside TIs, obtaining a value that determines the field needed to force a topological phase transition and which is again related with the corresponding critical field E_c in the vacuum needed to create electron-hole pairs [71, 140, 167]. This is all that we can have for the electromagnetic fields within the TI with constant θ, they are fixed and hence can not intervene in the dynamics, but we can overcome this difficulty just introducing phonons that move the different topological sectors. In this case the lattice constant depends of time and also the above electric and magnetic fields. Berry curvature also do it, as we have shown, keeping gauge invariant the bands with respect to the electromagnetic potentials.

2.6 Phonons and thermal excitations

Now, we can tackle the phenomena of topological thermoelectricity by means of the uncertainty principle, equivalently to a treatment through the instanton solutions of the Chern-Simons action [71], with an effective field b that varies due to the effects of phonons or thermal oscillations. In that case, the role of temperature into the topological transport was addressed by introducing it in the electromagnetic potentials through the gauge transformation $\Lambda(\bar{\tau}) = \frac{2\pi n\bar{\tau}}{e\beta}$ being $\bar{\tau} = \hbar\beta = \hbar/k_B T$ the Euclidean time, but now can be joined up directly by assigning to the energy $\Delta\varepsilon$ an adiabatic temperature dependence $k_B T$. Note that there is an infinite number of orbits for which the relation between b and ΔS defines a quantized flux h/e. Thus, when a phonon or a thermal excitation couples to a topological electron, the electron must move towards another orbit consistent with its new b, curvature and energy in order to maintain the quantum flux $h/e\, C$ constant. In this way, given that all these states share the same electrical conductance $G = \Delta I/\Delta V = e^2/h$ in presence of an external electric field, we can directly find the contribution to the electric potential $\Delta V = \Delta I\, h/e^2$ generated by a thermal gradient, and vice versa, substituting the electric current $\Delta I = e/\tau$ with the scattering time $\tau = \hbar/\Delta\varepsilon = \hbar/k_B T$ defined in Eq. (2.7). Thus, we can obtain the change in the electric potential due to thermal effects

$$V = V' + \frac{2\pi}{e} C k_B T \tag{2.27}$$

and also its associated electric field

$$\boldsymbol{E} = -\frac{2\pi}{e} C k_B \boldsymbol{\nabla} T - \frac{2\pi}{e} \frac{\partial C}{\partial r} k_B T \, \hat{\boldsymbol{r}} \tag{2.28}$$

where the Chern number C takes into account the number of channels taking part in the thermalization of the system. The resulting expressions are identical to that obtained in ref. [71] introducing the thermodynamic part in TIs through a Chern Simons action. The second term in Eq. (2.28) makes reference for strong thermal perturbations which are able to change the Chern number, producing an anomalous Seebeck contribution $S = \frac{2\pi}{e} k_B \frac{\partial C}{\partial T}$ associated to the creation of electron-hole Schwinger pairs or to jumps between bands with different Chern numbers. In contrast, the first one take into account the perturbations which can produce changes in the Berry curvature without changing the Chern number. Focusing on this regime, the explanation of why we can observe the high thermoelectric response associated to the topological edge states around room temperature is immediate. Consider for instance a coherent process (Fig. 2.5a), in which a phonon or a thermal excitation couples to a topological electron increasing the field b and producing an electric field $\boldsymbol{E} = -2\pi/e \; C k_B \boldsymbol{\nabla} T$. As it can be easily calculated, the Seebeck coefficient $S = \partial V / \partial T = 2\pi/e \; k_B C$, and hence the entropy of the system, does not depend on temperature. That is, all the possible final states, associated to a small or a large adiabatic perturbation, share the same Seebeck coefficient, keeping the entropy constant, up to the limit in which the second term of Eq. (2.28) must be considered. In this way, the coherence needed to observe quantized topological signatures would still being conserved up to a temperature $T \sim 2mv_F^2/k_B$ proportional to the band gap of the system ($\Delta\varepsilon = k_B T$). Notice that the sum of all the entropy associated with these processes is zero, as the Chern numbers do when there is time-reversal symmetry. The translation of these results to edge physics is clear. The electric field generated due to the temporal variation of their intrinsic b turns into an enhancement (coherent) or reduction (decoherent) of the relative moment between the two helical currents, however, the edge states remain to be ballistic with a quantized conductance $G = e^2/h \; C$ up to the Chern changes to zero or the coherence is lost (Fig. 2.5b). These results stand uniquely for the thermoelectric response of the edge states without considering quantum interference effects between the top and bottom surfaces in the case of 3DTIs thin films and neglecting contributions from the bulk carriers [66]. From here, it can be obtained an expression for the topological figure of merit ZT associated with the edge states [71]. This is done through a topological formalism which gives a Seebeck coefficient, that despite having a different physical origin and interpretation is in the order of the ones resulting in the Landauer transport formalism from optimizing the position of the Fermi level ξ_F in TIs with a large ratio between the edge and bulk scattering times [43].

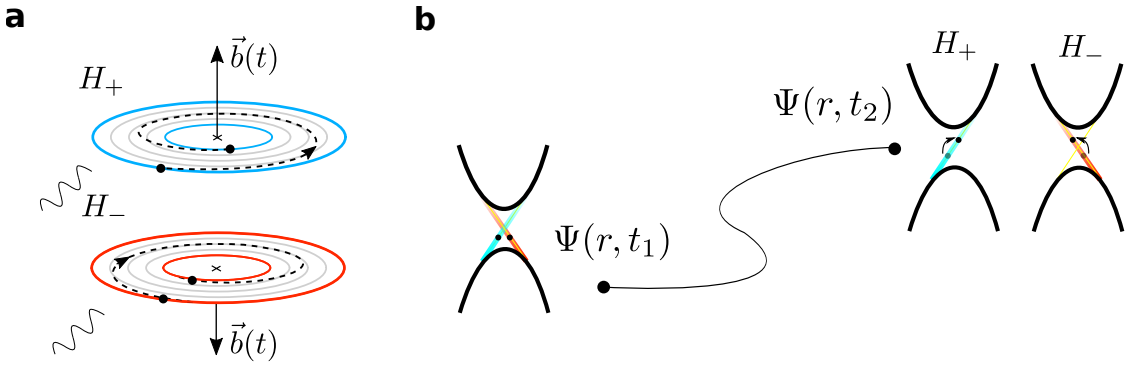

Figure 2.5: Adiabatic coherent process with $\partial C/\partial T = 0$ (**a**) Illustration of an adiabatic coherent process, for which the magnitude of the field b increases. Blue and red circles represent the initial and resulting final states on each branch defined in H_{2D}. (**b**) Adiabatic coherent evolution of electronic wavefuntion $\Psi(r,t)$. Seebeck coefficient and entropy are not modified in this process allowing heat-electricity transformation in a completely reversible process. As a consequence of the enlargement of the b field and the Berry curvature, the moment of the possible final states p_2 are higher than the initial electron moment p_1. Below the critical value, edge states remain to be ballistic with their conductance quantized.

2.7 Conclusions

In summary, we present a formalism based on a purely effective topological intrinsic field b which allows to treat topology in a new way measuring its robustness at the same time it allows to incorporate relativistic phonons and thermal effects into the topological context. Below the limit defined, phonons and thermal excitations could couple to electrons without changing entropy, and hence, the Seebeck coefficient S and maintaining the coherence necessary to keep the quantum conductance $G = e^2/h\ C$ of its highly conducting channels invariant too. This fact is valid for a wide range of values given the magnitude of b, which for the parameters characterising 3DTI thin-films ($M \approx 0.025eV$, $v_F = 6\ 10^5$m/s) defines a field of 5T and a frequency limit above the THz which can be generalizable to any topological insulators in 2D or for 3DTIs in thin film conditions with no more ingredients as their band gap, Fermi velocity and Chern number. This explains exactly how temperature and time-reversal symmetry coexist allowing the observation of the topological signatures and their associated high figure of merit at room temperature [158, 168, 169]. The ingredients provided are basic to derive the expression for the topological figure of merit ZT associated to the Kramers edge states in zero lattice thermal conductivity conditions [71], but additionally, we define in which circumstances the current experimental limit can be overtaken [63].

A new route to find high efficient thermoelectric devices by means of a special coupling between electrons and phonons at the surface is described [170]. In such situation

there should be a depression in the number of phonon modes available in the system to contribute to thermal transport meaning a reduction in the lattice thermal conductivity and a heat-electricity transformation. This can be translated from an enhancement of electron-phonon coupling as it has been observed in 3DTIs Bi_2Se_3 and Bi_2Te_3 where polar optical phonon modes seems to couple strongly with Dirac electrons when the Fermi level lies close to the Dirac point [166]. The map between these results and the model seems immediate since we are considering in-plane oscillations (polar) in our surface Hamiltonian at the same time as the enhancement of electron-phonon coupling takes place for frequencies satisfying the condition $2\omega = eb/m$ previously underlined. This could imply an alternative method to decrease lattice thermal conductivity for certain phonon modes as compared with other techniques (superlattices, impurities, dislocations) for increasing the thermoelectric efficiency or lead to exotic phenomena [63, 171–173]. Additional experimental scenarios can be proposed to support our results. Besides a relativistic electron-phonon coupling and a high thermoelectric response, the study of the topological intrinsic field b can lead to more direct verification. Defined as an outcome of the topological robustness, it enables us to define the critical magnetic and electric fields on each spin subsystem $H_\pm$ that could be measured.

3 Orbital dynamics in 2D materials with non-zero Berry curvature

Motivated by the field interpretation of the Berry curvature we perform a relativistic analysis of the electron dynamics in 2D non-zero Berry curvature systems in presence of an external perpendicular magnetic field. The present formalism allow us to show analytically how the Berry curvature is modulated by a magnetic field whereas their associated topological invariant remains unalterable. This process implies a redefinition of several magnitudes such as the velocity, orbital magnetic moment, energy and density of states which are obtained to address the intrinsic orbital magnetism of non-zero Berry curvature systems. We see that the role of second-order corrections due to the field become important at relatively low values given the small gaps and high Fermi velocities which these systems typically feature. Thus, reaching analytical expressions for all the magnitudes involved, our results unveil new contributions to the orbital magnetization and susceptibility and provide a new path to enhance the intrinsic orbital magnetic response of topological materials. This unveils an anomalous response in the orbital magnetism for topologically non-trivial insulators which is given in terms of the quantum magnetic flux and is explained within the context of the topological intrinsic field b.

3.1 Introduction

One of the most special features of the topological insulators is the presence of protected helical states on their boundaries which are responsible for their singular transport properties [23, 24]. Just as their robustness against non-magnetic impurities or external fields, the quantization of their transport properties also depend directly on the topology by means of a topological invariant which can be defined according to the intrinsic symmetries of the system and its dimensionality [18, 20, 25, 54]. In time-reversal symmetry broken systems as well as in two-dimensional topological insulators this invariant is the first Chern number C obtained throughout the integral of the Berry curvature over the momentum space [26, 49, 70]. Besides the well-known relation between the electric

conductivity and electric polarization vector with the topological invariant [47, 58, 100], great and original advances have been done to address the thermoelectric response of systems with non-zero Berry curvature in presence of electric and magnetic fields [21, 40, 42, 73, 74, 77, 119, 174]. These studies, which not only include the previously mentioned topological materials but also graphene-like systems and Weyl semimetals, take the semi-classical equations of motion for the Bloch electrons or a non-relativistic quantum formalism to derive magnetization and electric and thermal currents for a wide variety of compounds. These are the bases used to study planar Hall and chiral anomaly effects in topological insulators and Weyl semimetals through Boltzmann transport equation with in-plane magnetic fields [175, 176].

Recently, the original studies have been extended by addressing second-order corrections through the Lagrangian formalism [75, 76]. However, determining these quantities in a purely quantum way for these materials, which present a non-zero Berry curvature, involves some difficulties. First, we have to deal with a relativistic system described through a Dirac Hamiltonian [70, 103], where spin and angular momentum are no longer good quantum numbers of the system. Secondly, the evolution of eigenstates needs to be considered adiabatically; i.e., keeping the final and initial states of the system the same along the perturbation to preserve Berry phase effects. In the previous chapter, we made a first approach to the problem by considering directly the Lorentz force produced by the external magnetic field. However, strictly speaking the calculations must be introduced through the velocity operator in a time-independent formalism which allows an accurate calculation of the Chern number. The problem is that this involves dealing with gauge dependent and divergent corrections to the system eigenstates that must be analyzed in detail to get the usual equations of motion for non-zero Berry curvature systems in an adequate relativistic context for these materials at low energies.

Doing that, we give analytical expressions to show how the introduction of a perpendicular magnetic field in 2DTIs and Chern insulators produces a modulation of the Berry curvature, which can affect its shape dramatically, but keeping the Chern number C of the system invariant. Behind these results, we can find the additional contributions to the density of states, orbital magnetic moment and energy corresponding to second-order corrections in perturbation theory. These terms must be taken into account at relatively low external magnetic fields due to the small topological gap characterizing these systems. In particular, we show that for the energy only those terms coming from the modified orbital magnetic moment, which are associated with the correction to the Berry potential, are necessary, while the other obtained with the semi-classical Lagrangian formalism in a relativistic particle-hole symmetric system vanish [75]. Additionally, we observe a modified density of states that is strongly sensitive to the sign of the magnetic field and whose dispersion differs substantially from its first-order expansion [73]. These results can be directly introduced to determine explicitly the thermodynamic grand potential and hence the transport magnitudes in such systems, or in the Dirac oscillator Hamiltonian, as an argument to demonstrate how certain type of chiral photons or phonons can couple to the topological electrons preserving their topology and time-reversal symmetry $\hat{T}$ necessary

for the presence of Kramers pairs [109, 157, 162, 177]. So it turns out that, besides being sensible to include other interactions and effects, the perturbative analysis performed gives non-negligible field corrections to the orbital magnetization and susceptibility while their zero-field expressions are consistent with the different formalism that we complement and help to generalize considering the Berry curvature as a dynamical magnitude [72, 75, 77, 178].

3.2 Orbital dynamics in 2D

Our starting point is again the solid state version of the Dirac Hamiltonian used to describe 2D and 3DTIs [23],

$$H = M(\boldsymbol{k})\beta + v_F(\boldsymbol{\alpha}\cdot\boldsymbol{p}) \tag{3.1}$$

where the Fermi velocity v_F substitutes the speed of light c, β and α_i (σ_i) are the Dirac (Pauli) matrices, $\boldsymbol{p} = \hbar\boldsymbol{k}$ the momentum of the particles and $M(k) = M - \mathcal{B}k^2$ a k-dependent diagonal term where M and $\mathcal{B}$ depend directly on the on-site energies and second-neighbour hopping elements. This effective Hamiltonian allows a simple determination of the system's topology, especially on its two-dimensional version where we can easily differentiate between the topological non-trivial and trivial regimes by looking to the relative sign between the parameters M and $\mathcal{B}$. That is, it reduces to a Bernevig-Hughes-Zhang (BHZ) model with two non-interacting time-reversal copies ($M(k) \to -M(k)$) of a 2D Dirac Hamiltonian $H_{2D} = M(k)\sigma_z + v_F\,\boldsymbol{\sigma}\cdot\boldsymbol{p}$ [23, 70]. Thus, we have $M\mathcal{B} > 0$ for the non-trivial regime and $M\mathcal{B} < 0$ for the trivial one that fixes the integer Chern number C to be 1 or 0 respectively. Remember that $\mathcal{B}$ is usually negative as the energy tends to grow when increasing k and the energy spectrum of Eq. (3.1) is given by $\xi = \pm\sqrt{(M-\mathcal{B}k^2)^2 + \hbar^2 v_F^2 k^2}$. So essentially the topology depends on the sign of M, which for the particular case $M < 0$ (inverted band structure) results non-trivial. A similar Hamiltonian can be obtained from a Kane-Mele model on a honeycomb lattice although with a different topological constraint for the $M\mathcal{B}$ parameters [19]. The introduction of a magnetic field $\boldsymbol{B} = (0,0,B)$ in the z-direction breaks the translational symmetry in x and y directions, which is evident by choosing an axial gauge $\boldsymbol{A} = (-By/2, Bx/2, 0)$ to enter the perturbation in the Hamiltonian through the Peierls substitution $\boldsymbol{p} \to \boldsymbol{p} + e\boldsymbol{A}$, being $-e$ the electron charge. In such situation, the correction to the positive eigenstate by a constant uniform magnetic field has the following form up to first order

$$|+\rangle \to |+\rangle + i\frac{eB}{2}\frac{\langle -|\,\hat{v}_y\,|\partial_{k_x}+\rangle}{2\xi}\,|-\rangle - i\frac{eB}{2}\frac{\langle -|\,\hat{v}_x\,|\partial_{k_y}+\rangle}{2\xi}\,|-\rangle \tag{3.2}$$

being i the imaginary number and $\hat{v}_j = (i/\hbar)[\hat{H}, \hat{r}_j] = \hbar^{-1}\partial_{k_j}H = v_F\sigma_j - 2\hbar^{-1}\mathcal{B}k_j\sigma_z$ the velocity operator in the j direction. In this chapter we labeled again $|+\rangle$ and $|-\rangle$ as the

eigenstates with energy $\xi^{\pm} = \pm\sqrt{M(k)^2 + \hbar^2 v_F^2 k^2}$ of H_{2D}, so that in the denominator it appears a factor $2\xi = \xi^+ - \xi^-$ provided that H is particle-hole symmetric. The system eigenstates, as we saw before, can be found to be

$$|+\rangle = \frac{1}{\sqrt{2}} \begin{bmatrix} \sqrt{1 + \frac{M(k)}{\xi}} \\ e^{i\phi}\sqrt{1 - \frac{M(k)}{\xi}} \end{bmatrix} \qquad |-\rangle = \frac{1}{\sqrt{2}} \begin{bmatrix} \sqrt{1 - \frac{M(k)}{\xi}} \\ -e^{i\phi}\sqrt{1 + \frac{M(k)}{\xi}} \end{bmatrix} \tag{3.3}$$

being $\phi = arctan(k_y/k_x)$.

3.3 Gapped Dirac dispersion

For simplicity, we proceed by setting the Hamiltonian parameter $\mathcal{B}$ as zero. As it seems logical, it is worthy to note that the corrections in Eq. (3.2) are proportional to the product of the magnetic field with the z-component of orbital magnetic moment $\hat{\mathfrak{m}}_z = -e/2(\hat{x}\hat{v}_y - \hat{y}\hat{v}_x)$ of the Bloch electrons [74, 96, 179].

$$|+\rangle \to |+\rangle + \frac{eB}{2}\frac{\langle -|\, \hat{\boldsymbol{r}} \times \hat{\boldsymbol{v}}\, |+\rangle}{2\xi}\, |-\rangle \tag{3.4}$$

However, in order to get a proper definition of the angular momentum and orbital magnetic moment on the band n, the previous expression needs to be corrected by $\mathfrak{m} = -e/2\,(\boldsymbol{r} \times (\boldsymbol{v} - \langle \boldsymbol{v^n} \rangle))$, where $\langle v^n \rangle = \langle n|\, v^n\, |n\rangle = \hbar^{-1}\partial_k \xi^n$ is the average velocity of the electrons in band n. This is equivalent to the addition of the center-of-mass position r_c and its velocity in the Lagrangian formalism [75, 76]. In this way, we can define properly the orbital magnetic moment [42, 73, 74, 179],

$$\mathfrak{m}^n(\boldsymbol{k}) = -i\frac{e}{2\hbar}\,\langle \nabla_{\boldsymbol{k}} n| \times (H - \xi^n)\,|\nabla_{\boldsymbol{k}} n\rangle \tag{3.5}$$

which results

$$\mathfrak{m}_z^n = \frac{e}{\hbar}\xi^n \Omega^n \tag{3.6}$$

for a two-dimensional system as H_{2D} and the first-order corrections to the energy $\xi_1^n = -\mathfrak{m} \cdot \boldsymbol{B}$. While this latter relation is easily obtained through Eq. (3.4), calculating the z-component of the orbital magnetic moment could be not immediate. Thus, despite the second term in Eq. (3.6) $i\frac{e}{2\hbar}\xi^n \langle \nabla_{\boldsymbol{k}} n| \times |\nabla_{\boldsymbol{k}} n\rangle = i\frac{e}{2\hbar}\xi^n(\langle \partial_{k_x} n | \partial_{k_y} n\rangle - \langle \partial_{k_y} n | \partial_{k_x} n\rangle) = \frac{e}{2\hbar}\xi^n\Omega^n$ has not complication given that we have defined previously the Berry curvature $\Omega^n = -2Im\,\langle \partial_{k_x} n | \partial_{k_y} n\rangle$ in a band n. The first term involves a little algebra to achieve it. Thus, for the positive eigenstate we have

$$-i\left\langle \partial_{k_x}+\right| H\left|\partial_{k_y}+\right\rangle = \frac{1}{2}\left[\hbar v_F k\Omega^+\sqrt{\frac{\xi-M(k)}{\xi+M(k)}}+M(k)\Omega^+ + Im(...)\right] = \frac{1}{2}\xi^+\Omega^+ + Im(...)$$

$$+i\left\langle \partial_{k_y}+\right| H\left|\partial_{k_x}+\right\rangle = \frac{1}{2}\left[\hbar v_F k\Omega^+\sqrt{\frac{\xi-M(k)}{\xi+M(k)}}+M(k)\Omega^+ - Im(...)\right] = \frac{1}{2}\xi^+\Omega^+ - Im(...)$$

where the imaginary terms on both expressions cancel after adding both contributions and hence we recover Eq. (3.6). The same result is obtained for the negative solution given that the change $\xi \to -\xi$ maintains it unalterable ($\mathbb{m}_z \propto \xi\Omega \propto 1/\xi^2$). That is, both conduction and valence bands have the same orbital magnetic moment [70]. Nevertheless, the difficulties arise in Eq. (3.2) when one computes the matrix elements

$$\langle -|\begin{pmatrix} 0 & 1 \\ -1 & 0 \end{pmatrix}|\partial_{k_x}+\rangle + \langle -|\begin{pmatrix} 0 & -i \\ -i & 0 \end{pmatrix}\left|\partial_{k_y}+\right\rangle = \frac{1}{2k} \tag{3.7}$$

where it appears a divergence at zero particle momentum after gauge dependent terms have been removed. This behaviour is also present when computing velocity corrections and hence this contribution must be unphysical given that the force exerted by a magnetic field on a particle at rest is zero. We can solve this problem by decoupling the different contributions produced by the perturbation through the other definition of the velocity operator $\hbar^{-1}\partial_k H$. In this way, we can identify the ill-defined terms and properly obtain the corrections for the electron's velocity. Rewriting Eq. (3.2) by using that $\langle m|\,\partial_{k_j} H\,|\partial_{k_l} n\rangle = \partial_{k_j}(H\,|m\rangle)^*\,|\partial_{k_l} n\rangle - \left\langle \partial_{k_j} m\right| H\,|\partial_{k_l} n\rangle$

$$\begin{aligned}|+\rangle \to |+\rangle + i\frac{eB}{4\xi}\Bigg[&\left(\frac{1}{\hbar}\partial_{k_y}\xi^-\langle -|\partial_{k_x}+\rangle - \frac{1}{\hbar}\partial_{k_x}\xi^-\left\langle -\right|\partial_{k_y}+\right\rangle\right)\\ &+\frac{\xi^-}{\hbar}\left(\left\langle \partial_{k_y}-\right|\partial_{k_x}+\right\rangle - \left\langle \partial_{k_x}-\right|\partial_{k_y}+\right\rangle\Big)\\ &-\frac{1}{\hbar}\left(\left\langle \partial_{k_y}-\right| H\,|\partial_{k_x}+\rangle - \langle\partial_{k_x}-|\,H\left|\partial_{k_y}+\right\rangle\right)\Bigg]|-\rangle\end{aligned} \tag{3.8}$$

it can be shown that the third term is purely gauge dependent by rotations $e^{i\phi}$ of the eigenstates, i.e. for $|n'\rangle = e^{-i\phi}|n\rangle$ and $|m'\rangle = e^{-i\phi}|m\rangle$ it changes its sign, and thus we can set one in which this term goes to zero. On the other hand, the first and second terms give a contribution equal to

$$+i\frac{eB}{4\xi}\left(\frac{1}{\hbar}\partial_{k_y}\xi^-\langle -|\partial_{k_x}+\rangle - \frac{1}{\hbar}\partial_{k_x}\xi^-\left\langle -\right|\partial_{k_y}+\right\rangle\right) = -\frac{eB\Omega^+}{4\hbar}\frac{\hbar v_F k}{M} \tag{3.9}$$

$$+i\frac{eB}{4\xi}\left(\frac{\xi^-}{\hbar}\left\langle\partial_{k_y}-\middle|\partial_{k_x}+\right\rangle-\frac{\xi^-}{\hbar}\left\langle\partial_{k_x}-\middle|\partial_{k_y}+\right\rangle\right)=-\frac{eB\Omega^+}{4\hbar}\frac{M}{\hbar v_F k} \tag{3.10}$$

leading their sum to Eq. (3.7) after rearranging terms.

Working with free divergent terms, i.e. the first, which must be considered twice due to the redefinition of the orbital magnetic moment, we can now easily compute velocity corrections in both directions. In fact, it is straightforward to see that corrections due to transverse components disappear and only longitudinal terms remain. Thus, we obtain the following corrections to the velocity which apply to both conduction and valence band by substituting their associated energy and curvature,

$$v_j^n \to \frac{1}{\hbar}\partial_{k_j}\xi^n+\frac{1}{\hbar}\partial_{k_j}\xi^n\frac{e\boldsymbol{B}\cdot\boldsymbol{\Omega^n}}{\hbar}+\mathcal{O}(B^2) \tag{3.11}$$

where $v_j^n=\langle n|\,\hat{v}_j\,|n\rangle$ the average velocity in the band n for the component j and $\mathcal{O}(B^2)=-1/(4\hbar)\,\partial_{k_j}\xi^n\,(eB\Omega/\hbar)^2\hbar^2v_F^2k^2/M^2$ second-order corrections. In a simple way, we are observing the coupling effects between the magnetic field and the Berry curvature, which can be viewed like a magnetic field in the k-space on each band of Hamiltonian (3.1) in two dimensions. Thus, introducing a perpendicular $\boldsymbol{B}$ in these systems enhances or decreases the *field* felt by their electrons depending on the relative sign between $\boldsymbol{B}$ and $\boldsymbol{\Omega}$. For instance, the conduction band of H_{2D} for $M<0$ has a positive Berry curvature in the z direction and therefore an opposite magnetic field will decrease the velocity of their electrons and the Berry curvature even doing it zero or changing its sign. Given that the Lorentz force is radial this process causes an accommodation of the charge without involving any net current, as it can be checked by computing the integral of the previous expression. This is intrinsically related to the renormalization process affecting the phase-space volume and density of states for non-zero Berry curvature systems as we are going to show [42, 73, 76, 161].

Complementing these effects, we can also consider contributions associated with a slow time dependence for B which incorporates a transverse term that can be easily transformed through Faraday's law into the well-known anomalous velocity using that $E_x=\frac{1}{2}\frac{\partial B}{\partial t}y$ and $E_y=-\frac{1}{2}\frac{\partial B}{\partial t}x$. The obtained expression up to first-order

$$v_j^n\to v_j^n\left(1+\frac{e\boldsymbol{B}\cdot\boldsymbol{\Omega}}{\hbar}\right)+\frac{e}{\hbar}(\boldsymbol{E}\times\boldsymbol{\Omega^n})_j \tag{3.12}$$

represents the velocity of the electrons in the band n of a Chern insulator (H_{2D}) or in one of the two branches of a two-dimensional topological insulator in a slowly variant time-dependent magnetic field. In contrast to the first contribution, the second term is associated with the electromotive force $\mathcal{E}$ generated by the variation of B which couples to the Berry curvature to produce a transverse and non-zero electric current.

3.3.1 Berry curvature, Chern number and density of states

Setting aside this latter case, we wondered, as we postulated before if one of the crucial magnitudes for the topology and the transport, the Berry curvature, has experimented changes under this procedure. For the calculation it is convenient to employ an axial gauge $\boldsymbol{A} = (-By/2, Bx/2, 0)$ from which, as we showed, we are able to write the correction to the eigenstates in an easy to handle form

$$|+\rangle \to |+\rangle - \frac{e\boldsymbol{B}\cdot\boldsymbol{\Omega}^{+}}{2\hbar}\frac{\hbar v_F k}{M}|-\rangle \tag{3.13}$$

Once we formulated the correction of the eigenstates the calculation of the Berry curvature corrections for the conduction band can be achieved by applying $-2Im\left\langle \partial_{k_x}+\middle|\partial_{k_y}+\right\rangle$ or $\partial_{k_x}\mathcal{A}_y^{+} - \partial_{k_y}\mathcal{A}_x^{+}$ in Eq. (3.13), being $\mathcal{A}_i^{+} = i\langle +|\partial_{k_i}+\rangle$ the Berry potential and $|+\rangle$ the modified eigenstate. In fact, it is straightforward to show that the obtained corrections to the Berry potential are the same as the theoretically presented in ref. [76] using a Lagrangian formalism. After some algebra, it can be proved that Berry curvature turns out in the following form

$$\Omega^{+} \to \Omega^{+}\left(1 + 2\frac{e\boldsymbol{B}\cdot\boldsymbol{\Omega}^{+}}{\hbar}\right) - 2\Omega^{+}\frac{e\boldsymbol{B}\cdot\boldsymbol{\Omega}^{+}}{\hbar}\frac{\hbar^2 v_F^2 k^2}{M^2} \tag{3.14}$$

demonstrating how a perpendicular magnetic field $\boldsymbol{B}$ modulates the Berry curvature and the field seen by the electrons in these topological systems. Besides the familiar first term in Eq. (3.14) we have obtained a second contribution in the corrections which affects the Berry curvature at k out of $k = 0$. This term is important at intermediate values whereas it falls to zero when $k \to \infty$ and $k = 0$, although it can be shown to be tuned and even to disappear if we consider some energy dependence in the field B.

Since the Berry curvature has been modified, the next step is to compute the first Chern number C given its relation to the transport and hence with different physical observables. With this purpose, we can consider a uniform magnetic field of the form $B \propto m_e^2 v_F^2/(\hbar e)$ just like in the preious chapter and its reference [109], where the translation of the Berry curvature into a real field b was made using the magnetic flux quantization of helical orbits in terms of the Chern. As it has been analyzed, this field is closely related to the critical field B_c needed to create electron-hole Schwinger pairs in the vacuum. However, this consideration is not necessary and one can also proceed equally by extracting B from the integral and computing it numerically (Fig. 3.1a). Choosing the first option, the term $2e\boldsymbol{B}\cdot\boldsymbol{\Omega}/\hbar$ can be written as $-M^3/\xi^3$ given that $M = m_e v_F^2$ and hence

$$C = \frac{1}{2\pi}\int \boldsymbol{\Omega} d\boldsymbol{k} \to \frac{1}{2\pi}\int \boldsymbol{\Omega}\left(1 - 2\frac{M^3}{\xi^3} + \frac{M}{\xi}\right) d\boldsymbol{k} \tag{3.15}$$

where $d\boldsymbol{k} = 2\pi k dk$. By using that $\Omega^{\pm} = \pm\partial/\partial k^2 (M/\xi)$ it is straightforward to see that the sum of second and third terms in the integral cancel

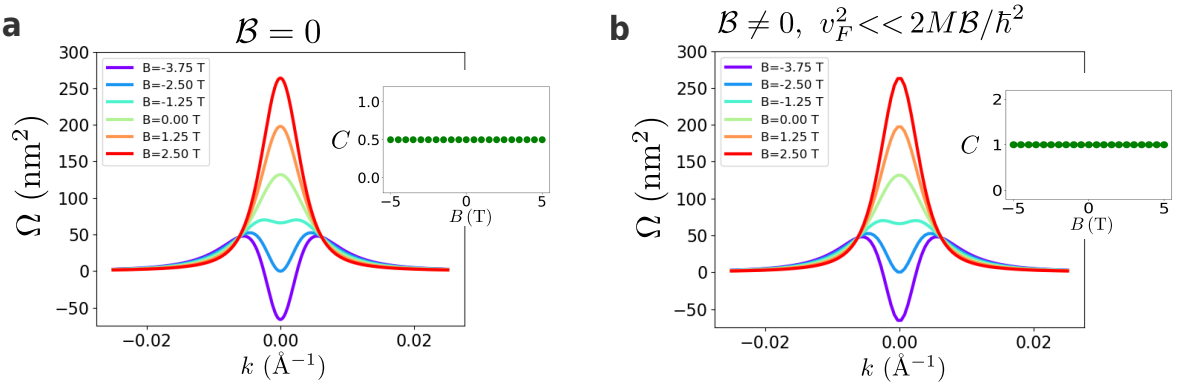

Figure 3.1: Berry curvature corrections for the conduction band of Hamiltonian (2) for different values of $\boldsymbol{B} = (0, 0, B)$. The inset shows the numerical calculations of the Chern number $C = 1/(2\pi)\int \boldsymbol{\Omega} d\boldsymbol{k}$. Plot parameters are (**a**) $M = -0.025$ eV, $v_F = 6.17{\cdot}10^5$m/s, $\mathcal{B} = 0.0$ eVÅ^2 and (**b**) $\mathcal{B} = -5.0$ eVÅ^2

$$\frac{1}{2}\left[\int_0^\infty \frac{1}{2}\frac{\partial}{\partial k^2}\left(\frac{M}{\xi}\right)^2 dk^2 - \int_0^\infty \frac{1}{2}\frac{\partial}{\partial k^2}\left(\frac{M}{\xi}\right)^4 dk^2\right] = \frac{1}{4}\frac{M^2}{\xi^2}\Big|_0^\infty - \frac{1}{4}\frac{M^4}{\xi^4}\Big|_0^\infty = 0 \tag{3.16}$$

As consequence, the Chern number of the band does not change even though the Berry curvature does it. This occurs independently of the magnitude and time dependence of B until Zeeman terms and higher-order effects need to be considered. These calculations can also be derived for non-zero but small $\mathcal{B}$ values ($v_F^2 >> 2\mathcal{B}M/\hbar^2$). In this case, after neglecting terms in the energy derivative $\partial_{k_j}\xi$ in Eq. (3.8), the curvature corrections turn out into a more tedious expression

$$\Omega^+ \to \Omega^+\left(1 + 2\frac{e\boldsymbol{B}\cdot\boldsymbol{\Omega}^+}{\hbar}M\frac{M-\mathcal{B}k^2}{(M+\mathcal{B}k^2)^2}\right) - 2\Omega^+\frac{e\boldsymbol{B}\cdot\boldsymbol{\Omega}^+}{\hbar}\frac{\hbar^2 v_F^2 k^2}{(M+\mathcal{B}k^2)^2}\left(1 - 3\mathcal{B}\frac{M-\mathcal{B}k^2}{\hbar^2 v_F^2}\right) \tag{3.17}$$

but for which the Chern number C is constant and well-defined by an integer value, i.e. ± 1 if $M\mathcal{B} > 0$ and 0 if $M\mathcal{B} < 0$ (Fig. 3.1b). Notice that here $\Omega^+ = -\hbar^2 v_F^2(M + \mathcal{B}k^2)/(2\xi^3)$. In both cases, there is a value ($B \approx -2.5$T for the values of M and v_F taken) for which the Berry curvature falls to 0 at the Γ point. This value is not other than the one delimited by the equation $b = 2m_e^2 v_F^2/(\hbar e)$ in the previous chapter with a difference of a factor $1/2$ which comes from the redefinition of the orbital magnetic moment. This opens the possibility to enter in a regime where electron-hole pair creation might be experimentally accessible for certain k values. In contrast, we find that the case with $eB\Omega/\hbar = -1$ making zero the density of states coefficient $\mathcal{D}$ which arises when considering constant the Berry curvature [73], actually does not take place for $k = 0$ (Fig. 3.2). For these values of

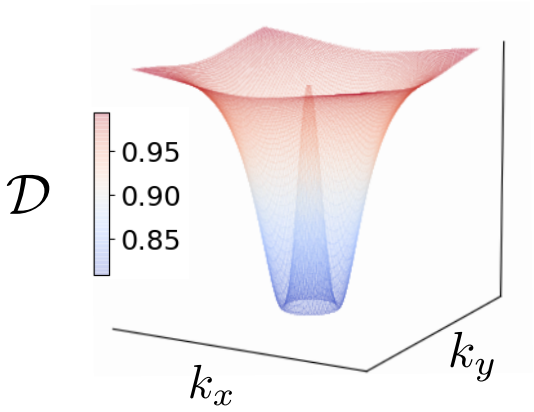

Figure 3.2: Momentum dependence of $\mathcal{D}$ for the critical case $B = -m^2 v_F^2/(e\hbar)$.

B, second-order corrections need to be taken into account and the density of states writes as

$$\mathcal{D} = 1 + \frac{eB\Omega^*}{\hbar} \tag{3.18}$$

with Ω^* the modified Berry curvature displayed in Eq. (3.14) or (3.17) [75, 76]. This function has a minimum at $k \neq 0$ (Fig. 3.3) which can be tuned by B becoming zero for sufficiently high magnetic fields. Nevertheless, the transverse electrical conductivity

$$\sigma_{xy} = -e\left(\partial n_e/\partial \boldsymbol{B}\right)_\mu \tag{3.19}$$

at zero temperature remains to be quantized and equal to $-e^2/\hbar\, C$ being

$$n_e = \int \frac{d\boldsymbol{k}}{(2\pi)^2}\left(1 + \frac{e\boldsymbol{B}\boldsymbol{\Omega}^*}{\hbar}\right) \tag{3.20}$$

the electron density [73].

3.3.2 Energy

We are also in position to write second-order corrections to the energy given that the matrix element $\langle -|\,\Delta H\,|+\rangle = -B\,\langle -|\,\hat{\mathrm{m}}_z\,|+\rangle$ has been computed before. Then, we can directly obtain that

$$\xi \to \xi - \mathbb{m}\cdot\boldsymbol{B} + \frac{1}{2}\frac{(\mathbb{m}\cdot\boldsymbol{B})^2}{\xi}\frac{\hbar^2 v_F^2 k^2}{M^2} \tag{3.21}$$

where $-\mathbb{m}\cdot\boldsymbol{B}$ is the well-known first-order response and the third term comes from

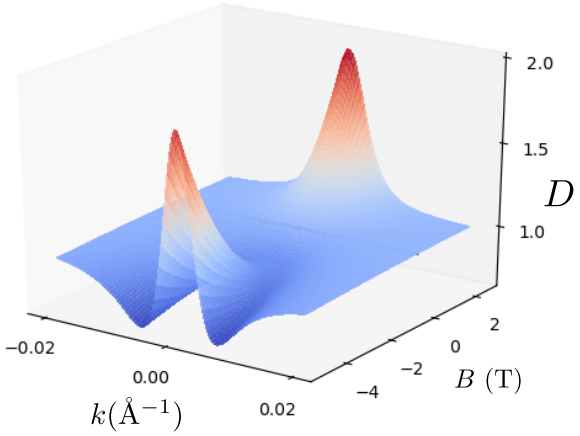

Figure 3.3: Modified density of states of the conduction band as a function of k and B.

second-order effects. This formula seems to enter in conflict with the one obtained from a semi-classical Lagrangian theory [75], in which the energy up to second-order for a relativistic particle-hole symmetric system as Eq. (3.1) is

$$\begin{aligned}\bar{\xi} = \xi_0 - \mathbb{m}\cdot\boldsymbol{B} + \frac{1}{4}\mathbb{m}\cdot\boldsymbol{B}\frac{e\boldsymbol{B}\cdot\boldsymbol{\Omega}}{\hbar} \\ - \frac{1}{8}e^2\epsilon_{sik}\epsilon_{tjl}B_sB_tg_{ij}\alpha_{kl} - eB(\mathcal{A}^*\times v_0)\end{aligned} \tag{3.22}$$

where $g_{ij} = Re\,\langle\partial_i n|\partial_j n\rangle - \langle\partial_i n|n\rangle\langle n|\partial_j n\rangle$ is the quantum metric in the k-space, $\alpha_{kl} = \partial_{kl}\xi_0/\hbar^2$ the inverse of the effective mass tensor, $v_0 = \hbar^{-1}\partial_k\xi$ and $\mathcal{A}^*_j = -\frac{eB\Omega}{\hbar}\frac{\hbar v_F k}{M}i\langle n|\partial_j m\rangle$ is the j component of the modified Berry potential. But by computing g_{ij} and α_{kl} for the positive energy eigenstate we find that

$$g_{xx} = \frac{1}{4}\frac{k_y^2}{k^4}\frac{\hbar^2v_F^2k^2}{\xi^2} + \Omega^2\frac{\xi^2k_x^2}{\hbar^2v_F^2k^2}$$

$$g_{yy} = \frac{1}{4}\frac{k_x^2}{k^4}\frac{\hbar^2v_F^2k^2}{\xi^2} + \Omega^2\frac{\xi^2k_y^2}{\hbar^2v_F^2k^2}$$

$$g_{xy} = g_{yx} = -\frac{1}{4}\frac{k_xk_y}{k^4}\frac{\hbar^2v_F^2k^2}{\xi^2} + \Omega^2\frac{\xi^2k_xk_y}{\hbar^2v_F^2k^2}$$

$$\alpha_{kl} = \delta_{kl}\frac{v_F^2}{\xi} - \frac{\hbar^2v_F^4k_kk_l}{\xi^3}$$

and hence it is worthy to show that actually, the third and fourth terms of Eq. (3.22) cancel and only the one coming from the corrections to the Berry potential holds, recovering the energy dispersion presented in Eq. (3.21).

3.3.3 Orbital magnetization and susceptibility

Given these ingredients, we can reach the grand potential F determining the transport properties of the TIs in presence of perpendicular magnetic fields

$$F = -k_B T \int \frac{d^2k}{(2\pi)^2} \left(1 + \frac{eB\Omega^*}{\hbar}\right) ln(1 + e^{-(\bar{\xi}-\mu)/k_B T}) \tag{3.23}$$

which incorporates the modified density of states and energy obtained with the changes of the Berry curvature and orbital magnetic moment. From here, we can compute the different transport magnitudes and coefficients such as, for instance, the system orbital magnetization $\mathcal{M}$ and susceptibility χ_{orb}. Thus, for zero chemical potential ($\mu = 0$) and zero temperature, it is immediate to obtain the dependency of $\mathcal{M}$ with the external magnetic field B

$$\mathcal{M} = -\frac{e^2 v_F^2}{6\pi|M|}B - \frac{3e^3\hbar v_F^4}{128\pi M^3}B^2 + \frac{e^4\hbar^2 v_F^6}{1260\pi|M|^5}B^3 \tag{3.24}$$

and the orbital magnetic susceptibility $\chi = -(\partial^2 F/\partial B^2)$

$$\chi_{orb} = -\frac{e^2 v_F^2}{6\pi|M|} - \frac{3e^3\hbar v_F^4}{64\pi M^3}B + \frac{e^4\hbar^2 v_F^6}{420\pi|M|^5}B^2 \tag{3.25}$$

with no more ingredients as their band gap $2M$ and Fermi velocity. Remarkably, we find a diamagnetic zero field susceptibility $\chi_0 = -e^2 v_F^2/(6\pi|M|)$ (Fig. 3.4), which is identical to that obtained in ref. [75] ($\chi/\chi_n = -9\pi^2 t/(6\pi|M|)$ with t the first-neighbor hopping parameter), plus additional B-dependent terms which are not negligible for systems with small M. Thus, despite the first and third terms gives always a diamagnetic susceptibility, the second is dependent on the sign of the gap and hence it is expected to show differences between the topological non-trivial and trivial regimes. This stands for individual Chern systems while the linear term in B in the susceptibility cancels for time-reversal symmetric systems as the change $M \to -M$ gives opposite contributions. Finally, notice that for zero gap systems ($M = 0$) these corrections are not well-defined since the Berry curvature vanishes.

3.4 Gapped Dirac dispersion with parabolic dependence

That is all we have for a constant mass term $m_e = Mv_F^2$, as we have in a pure linear dispersion. The external magnetic field modulates the different magnitudes involved in the thermoelectric and magnetoelectric transport. However, 2D and 3D TIs thin-films usually present non-negligible parabolic terms in their spectra [24, 47]. This dependency is introduced in the Dirac Hamiltonian through the k-dependent diagonal term $M - \mathcal{B}k^2$. In this context, we can define properly the Chern number as integer and remove the fermion

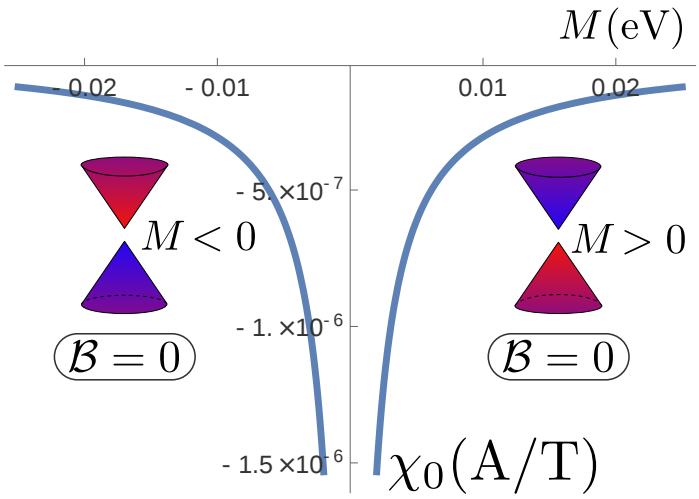

Figure 3.4: Zero-field orbital magnetic susceptibility for $\mathcal{B} = 0$ (gaped Dirac dispersion) as a function of M. The color gradient indicates the z component of the k-dependent spin texture of each regime. For H_{2D}, the red color stands for spin down and blue for spin up.

doubling problem [70, 180–182]. As we saw, introducing a perpendicular magnetic field $\boldsymbol{B} = B\hat{\boldsymbol{z}}$ on H_{2D} causes a correction in the eigenstates of the systems that can be written as [76, 95]

$$|n\rangle \to |n\rangle + \frac{eB}{(\xi^n - \xi^m)} \frac{1}{\hbar} \left(\partial_{k_y} \xi^m \mathcal{A}_x^{mn} - \partial_{k_x} \xi^m \mathcal{A}_y^{mn}\right) |m\rangle \tag{3.26}$$

being $\mathcal{A}_j^{mn} = i \langle m | \partial_{k_j} n \rangle$, $|n\rangle$ and $|m\rangle$ are the eigenstates of the bands n and m with energy ξ^n and ξ^m. These corrections represent the coupling effects between the magnetic field and Berry curvature of the bands which induce second-order corrections to the Berry potential, Berry curvature, particle's velocity, density of states, orbital magnetic moment and energy [95]. Thus, for the Berry potential $\boldsymbol{\mathcal{A}}^n = i \langle n | \partial_{\boldsymbol{k}} n \rangle$ we find from Eq. (3.26) that

$$\mathcal{A}_j^n \to \mathcal{A}_j^n + 2\,\mathrm{Re}\,\mathcal{A}_j^{nm} \frac{\hbar \omega_z^n}{(\xi^n - \xi^m)} \tag{3.27}$$

being $\omega_z^n = \epsilon_{zrs} \frac{eB_z}{\hbar} \frac{1}{\hbar} \partial_{k_r} \xi^m \mathcal{A}_s^{mn}$ as it can be deduced by different formalism [76, 95]. These expressions involve quite tedious calculations especially if we want to take into account the role of the parameter $\mathcal{B}$ in our Hamiltonian or deal with a particle-hole antisymmetric system. We are going to focus on the first case given that as the current literature indicates, there are no differences in the orbital magnetic susceptibility at zero magnetic field $\chi_{orb}(B = 0)$ between the trivial and non-trivial regimes when we consider a gapped Dirac dispersion [72, 75, 77, 95, 178]. This is quite impressive given that both regimes present clear differences in their curvatures and χ_{orb} is directly related with it (Fig. 3.5).

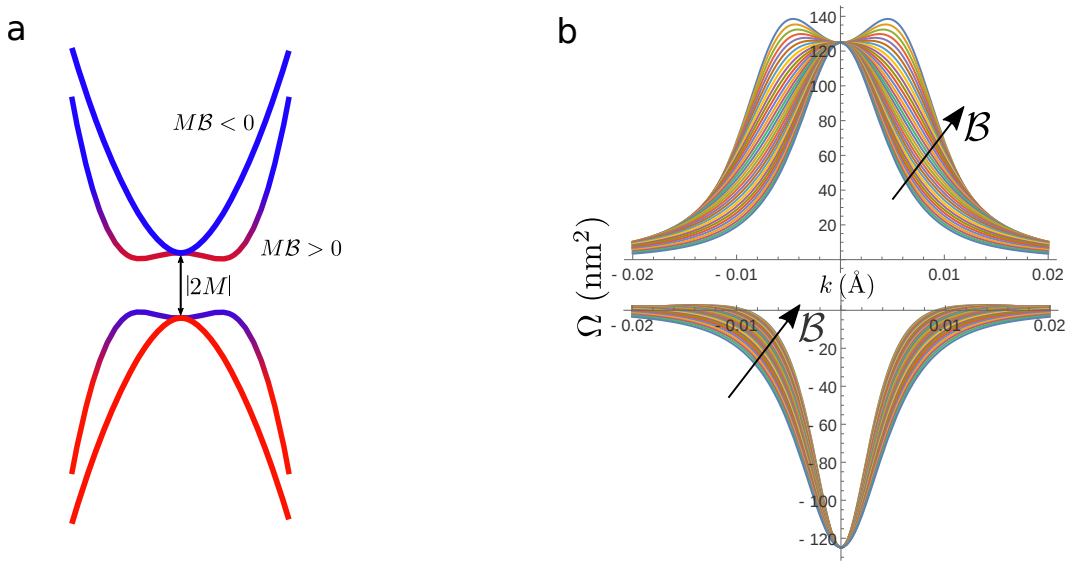

Figure 3.5: (**a**), Energy spectrum of a two-dimensional Dirac Hamiltonian H_{2D} for the trivial ($M > 0, \mathcal{B} < 0$) and non-trivial ($M < 0, \mathcal{B} < 0$) cases. The color gradient indicates the z component of the k-dependent spin texture of each regime. In this configuration, the red color stands for spin down and blue for spin up. (**b**), Berry curvature of the conduction band of H_{2D} for different values of $\mathcal{B}$ ranging from 0 to -300 eVÅ^2 in steps of 10 eVÅ^2. The arrows indicate the change in Ω when increasing $\mathcal{B}$.

Remember that at zero temperature $\chi_{orb} = -\partial^2 E/\partial B^2$ being $E = \int \frac{d\boldsymbol{k}}{(2\pi)^2} D\tilde{\xi}$ the density of energy, $D = 1 + \frac{e\boldsymbol{B}\cdot\tilde{\boldsymbol{\Omega}}}{\hbar}$ the modified density of states, $\tilde{\Omega}$ the modified Berry curvature and $\tilde{\xi} = \xi\left(1 - \frac{e\boldsymbol{B}\cdot\boldsymbol{\Omega}}{\hbar} + \mathcal{O}(B^2)\right)$ the corrected energy resulting from the application of the magnetic field. Then, one would expect to observe some differences although under linear dispersion conditions there are not (Fig. 3.4). Introducing $\mathcal{B}$ and after some algebra, it can be shown that the corrections of the Berry curvature $\Omega^n = -2Im\left\langle \partial_{k_x} n \middle| \partial_{k_y} n \right\rangle = \boldsymbol{\nabla} \times \boldsymbol{\mathcal{A}}^n$, obtained by applying Eq. (3.26) or Eq. (3.27) to the eigenstates of H_{2D}, are given by

$$\tilde{\Omega} = \Omega + 2\frac{eB\Omega}{\hbar}\Omega\left(\frac{M - \mathcal{B}k^2}{(M + \mathcal{B}k^2)^2}F(k^2) - \frac{\hbar^2 v_F^2 k^2}{(M + \mathcal{B}k^2)^2}G(k^2)\right) \tag{3.28}$$

being as usual $\xi = \pm\sqrt{(M - \mathcal{B}k^2)^2 + \hbar^2 v_F^2 k^2}$, $\Omega = -\hbar^2 v^2 (M + \mathcal{B}k^2)/(2\xi^3)$ and

$$F(k^2) = M - \frac{\xi^2 \mathcal{B}}{\hbar^2 v_F^2} - \frac{\mathcal{B}(M - \mathcal{B}k^2)(M + \mathcal{B}k^2)}{\hbar^2 v_F^2}$$

$$G(k^2) = 1 - 6\mathcal{B}\frac{M - \mathcal{B}k^2}{\hbar^2 v_F^2} + 6\mathcal{B}^2\frac{(M - \mathcal{B}k^2)^2}{\hbar^4 v_F^4} - 2\mathcal{B}^2\frac{\xi^2}{\hbar^4 v_F^4}$$

Eq. (3.28) generalizes the results obtained for linear dispersions introducing $\mathcal{B}$ which is essential to define properly the Chern number $C = 1/(2\pi)\int \Omega d\boldsymbol{k}$ as an integer and dis-

tinguish the topological regime from the trivial one [70, 95]. Numerically, it can be tested that the Chern number of the system is fixed for any given value as long as we maintain the sign of $M\mathcal{B}$ invariant.

Having $\tilde{\Omega}$ and hence D, we only need to calculate the second-order corrections for the energy induced by the perpendicular magnetic field B

$$\tilde{\xi} = \xi - \mathrm{m}B + \frac{1}{2}\xi\left(\frac{eB\Omega}{\hbar}\right)^2 \frac{\hbar^2 v_F^2 k^2}{M + \mathcal{B}k^2}\left(1 - 2\mathcal{B}\frac{(M - \mathcal{B}k^2)}{\hbar^2 v^2}\right)^2 \tag{3.29}$$

and then it is straightforward to show how the orbital magnetization at zero-temperature $\mathcal{M}_{orb} = -\partial E/\partial B$ is a function of the magnetic field B given by $\mathcal{M}_{orb} = \mathcal{M}_1 B + \mathcal{M}_2 B^2 + \mathcal{M}_3 B^3$. Or equivalently, we have an orbital magnetic susceptibility $\chi_{orb} = \chi_0 + \chi_1 B + \chi_2 B^2$ where

$$\chi_0 = \frac{e^2 v_F^2(-1 + (1 - 2rs)\beta + 10(1 + rs)\beta^2)}{6\pi(1 - 4\beta)|M|} \tag{3.30}$$

$$\chi_1 = -\frac{3e^3\hbar v_F^4}{64\pi M^3(1 - 4\beta)^{3/2}}\Lambda(\beta) \tag{3.31}$$

$$\chi_2 = \frac{e^4\hbar^2 v_F^6}{420\pi|M|^5(1 - 4\beta)^3}\Theta(\beta) \tag{3.32}$$

We defined $\beta = M\mathcal{B}/\hbar^2 v_F^2$, $s = sgn(M)$ and $r = sgn(\mathcal{B})$. A complete expansion of the functions $\Lambda(\beta)$ and $\Theta(\beta)$ can be found below. Notice that χ_{orb} is given in units of amperes (A) per tesla (T) being typical to represent it as a dimensionless quantity by using a normalization parameter χ_n as the inverse of effective magnetic permeability μ in two-dimensions. That is, $e^2 a v_F/(6\pi^2\hbar)$ for the particular case of a honeycomb lattice with lattice constant a [75, 77]. In Fig. 3.6 we can see that χ_2 is practically paramagnetic for any value of M and $\mathcal{B}$, although a detailed inspection reveals a paramagnetic region defined by the condition $4M\mathcal{B} > \hbar^2 v_F^2$ ($\beta > 1/4$) for the non-trivial topological regime (Fig. 3.8). This term is liable to play an important role only for tiny gaps and/or high magnetic fields where corrections due to Zeeman effects should also be considered. That is, for a typical gap $|2M| = 50\mathrm{meV}$, $v_F = 6 \cdot 10^5$ m/s and a field $B = 1\mathrm{T}$ whose equivalent energy ($\hbar\omega$) does not exceed this gap we have that $|\chi_2/\chi_0| \approx 10^{-3}$ and $|\chi_2/\chi_1| \approx 10^{-2}$. Attending to χ_1, its contribution to the orbital magnetization and susceptibility is opposite for both regimes resulting in paramagnetic for the topological non-trivial and diamagnetic for the normal state when B is positive. Compared to χ_0 the ratio between both is close to 10^{-1} under the same prior conditions and hence become to be non-negligible at relative low-magnetic fields depending on the band gap $2M$ of the system. Its dependence on $\mathcal{B}$ can be explored in more detail in Section 3.4.2. Thus, besides it is evident that χ_2 and χ_1 have a weaker dependence on this parameter compared with M (Fig. 3.6b and c), for a fixed gap both regimes shows a very different response, with a nearly constant

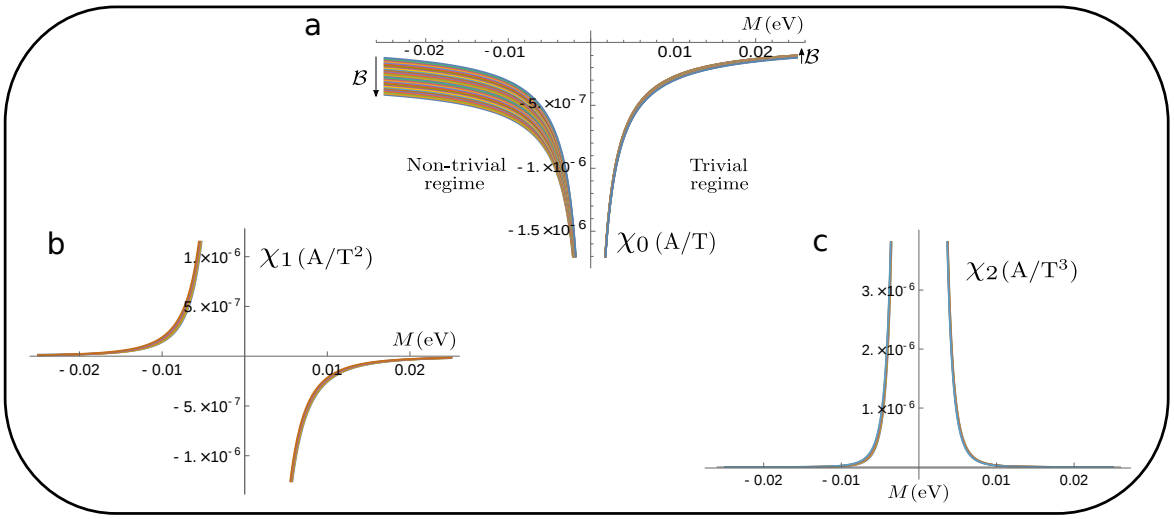

Figure 3.6: (**a**), Zero-field orbital magnetic susceptibility of the trivial and non-trivial topological regimes. $\mathcal{B}$ ranges from 0 to -300 eVÅ^2 and v_F is set to $6 \cdot 10^5$ m/s. In contrast to the current scenario displayed in Fig. 3.4, the introduction of the parabolic dependence at large k given by $\mathcal{B}$ determines a drastic change in the behaviour of both regimes (**b**),(**c**), Linear (χ_1) and quadratic (χ_2) coefficients in the magnetic field of the orbital susceptibility.

dependency for the trivial regime and strong for the topological one (Fig. 3.8). Finally, note that for time-reversal symmetric systems such as Eq. (3.1) the contribution of the two Chern species cancels each other and χ_1 will be zero while the even pairs in the magnetic field for the susceptibility appear with a spin-degeneracy factor $g = 2$.

A significant result is obtained when analyzing the zero-field orbital susceptibility χ_0. A first-look to Fig. 3.6 indicates that there are clear differences with the current scenario in which χ_0 manifest the same behaviour for the non-trivial and trivial cases (Fig. 3.4). However, we can go further by subtracting the common *background* term at zero $\mathcal{B}$ displayed in Fig. 3.4 to Eq. (3.30). This factor is obtained by different methods and it is equal to $\chi_M = -\frac{e^2 v^2}{6\pi|M|}$ [72, 75, 77, 95, 178]. In this way, we find that it appears a continuum spectrum for $\chi_0 - \chi_M$ with a ratio $\frac{5}{6\pi}\frac{e^2}{\hbar^2}$ given in fundamental units when plotted versus $\mathcal{B}$ (Fig. 3.7a). This unexpected behaviour belongs uniquely for the topological regime while for the trivial we have a non-homogeneous dependence on $\mathcal{B}$. In general formulae, we can write the zero-orbital magnetic susceptibility for both topological non-trivial

$$\chi_0 = -\frac{e^2 v^2}{6\pi|M|} + \frac{5e^2}{6\pi\hbar^2}\mathcal{B} \qquad (M < 0, \mathcal{B} < 0) \tag{3.33}$$

and trivial phases

$$\chi_0 = -\frac{e^2 v^2(\hbar^2 v_F^2 - 3M\mathcal{B})}{6\pi|M|(\hbar^2 v_F^2 - 4M\mathcal{B})} \qquad (M > 0, \mathcal{B} < 0) \tag{3.34}$$

by introducing in the same expression the principal parameters M, $\mathcal{B}$ and v_F for the topology and transport which are directly related with the different hopping elements. Thus, roughly speaking for the simplest case of a square lattice with complex spin-dependent first neighbour hopping it_1 and staggered potential for the on-site energies ξ_v and second neighbour hopping t_2 we can reach for the topological regime that

$$\mu\chi_0 \propto -C_1\frac{t_1}{|\xi_v - 4t_2|} - C_2\frac{t_2}{t_1} \tag{3.35}$$

obtaining from the tight-binding that $v_F = 2at_1/\hbar$, $M = \xi_v - 4t_2$, $\mathcal{B} = -2t_2a^2$, $\mu^{-1} \propto e^2 v_F a/\hbar$. Numerical factors accompanying these relations will depend on the crystal structure of the system which determine the coefficients C_1 and C_2.

We can also observe by computing the large $\mathcal{B}$ limit ($M\mathcal{B} >> \hbar^2 v_F^2$) that χ_0 grows linearly for the topological regime while it saturates in a finite value $-\frac{e^2v^2}{8\pi M}$ ($M > 0$) for the trivial insulator with a softer dependence on this parameter (Fig. 3.7b). The role of $\mathcal{B}$ opens a new possibility for tuning the orbital magnetization and susceptibility in topological materials breaking the current scenario in which we need to employ materials with a tiny gap for maximizing the response. This could be experimentally unpleasant given that then you are limited to work with a small frame of temperature and/or magnetic fields. Notice that the orbital susceptibility, also known as geometrical, is dominant only inside the band gap and decays to zero as the Fermi level enters the conduction and valence bands [75]. In other words, a more robust parabolic dependence in the energy spectra causes an enhanced orbital magnetic response in topological materials.

3.4.1 Possible physical interpretation

The present results have another direct experimental consequence. On the one hand, directly from Eq. (3.34) it is straightforward to note that the dependence on $\mathcal{B}$ in the trivial regime seems to be weak, as one can verify it by computing the ratio $(\hbar^2 v_F^2 - 3M\mathcal{B})/(\hbar^2 v_F^2 - 4M\mathcal{B})$ under the high Fermi velocity and small gap conditions that these systems feature. Typically, these are in the range of $10^5 - 10^6$ m/s for the velocity while the gap is in the order of meV [23, 24, 183]. In contrast, a topological non-trivial insulator shows a ratio $\propto \frac{e^2}{\pi\hbar^2}$ independent of such parameters which can be related directly with the quantum magnetic flux $\Phi_0 = h/(2e)$. Thus, varying $\mathcal{B}$ we expect a change in the orbital magnetic susceptibility $\Delta\chi_0 \propto \pi/\Phi_0^2$. This result seems to connect perfectly with the concept of orbit developed in the previous chapter for the topological electrons in 2D and 3DTI thin films by translating the topological information contained in the Berry curvature into a topological effective field b [109]. As we saw, this relies on the concept of orbit for the topological electrons, for which, the topological quantization by means of the

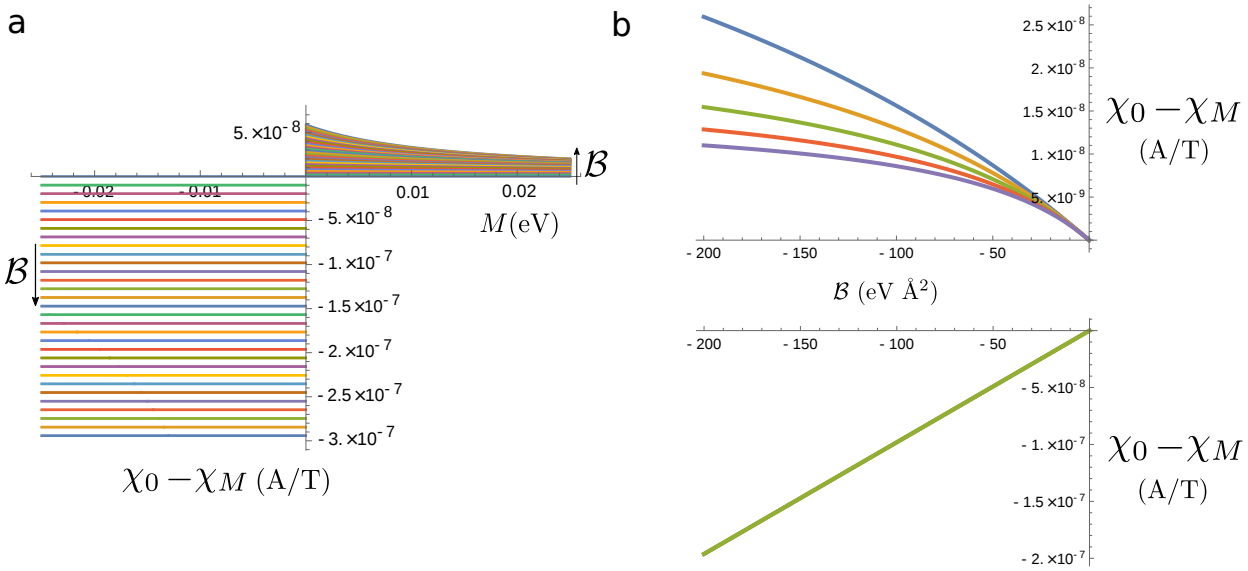

Figure 3.7: Normalized zero-field orbital magnetic susceptibility. **a**, $\chi_0 - \chi_M$ vs M for different $\mathcal{B} \in [-300, 0]$eVÅ^2. **b**, $\chi_0 - \chi_M$ vs $\mathcal{B}$ for different values of M ranging from 10 (blue line) to 50 meV (purple line). The upper panel represents the behaviour of the normalized zero-orbital susceptibility in a trivial insulator $M\mathcal{B} < 0$ whereas the lower panel stands for a topologically non-trivial insulator ($M\mathcal{B} > 0$) . This latter case exhibits no dependence on the gap giving a linear diamagnetic contribution to the zero-orbital susceptibility.

Chern number allows to associate a quantized flux to each orbit and hence an effective magnetic field b and area ΔS to these electrons.

$$b \approx \frac{(2)m^2 v_F^2}{\hbar e} \qquad \Delta S \approx \frac{h\hbar}{(2)m^2 v_F^2} \tag{3.36}$$

Here m is the effective mass and the factor (2) vanishes when redefining the orbital magnetic moment [95]. That is, matching b with the solid-state version of the Schwinger critical field [138]. In summary, it can be defined a magnetic field b from the Berry curvature on each band of a TI or Chern insulator with net value zero in presence of time-reversal symmetry. Mathematically, it is straightforward to connect these results with the orbital magnetic susceptibility given that by its proper definition b and ΔS define a quantized flux $\Phi = h/e$ associated to each band. So, this magnetic flux should be reflected as is in the system's response to an external magnetic field. This must occur when one band is fully filled, i.e., when the Fermi level lies in the band gap and the orbital susceptibility is dominant. Physically, by looking at the energy dispersion it is obvious that varying $\mathcal{B}$ makes it more localized/delocalized in the k-space and modifies

the effective mass of the particles. Given that the topology is the same ($sgn(M\mathcal{B})$) remains invariant), this would change the effective area of the electrons ΔS and also the field b associated to each band to keep its flux invariant inducing a singular magnetic response that needs to be related to this flux.

Further corrections can be taken into account implying that the numerical factor accompanying π/Φ_0^2 in the second term of Eq. (3.33) should experiment changes. Notice that by considering $\mathcal{B}$ in our Hamiltonian we are introducing a k-dependent mass term in our system. So the perpendicular magnetic field should also give a diagonal contribution in the perturbed Hamiltonian that could be introduced in Eq. (3.26). This would lead to more accurate expressions but from the physical point of view, this would also imply the necessity to consider Zeeman corrections. Nevertheless, if one performs the simple calculation associated with first-order corrections of this term to the energy it is easy to show that $\langle n|\,\Delta H_z\,|n\rangle = \frac{eB}{2\hbar}\mathcal{B}$ being $\Delta H_z = \frac{eB}{\hbar}\mathcal{B}\sigma_z(k_x y - k_y x)$. Comparing this factor with the first-order term $-\mathbb{m}\cdot\boldsymbol{B}$ we can verify that at low energy $\frac{eB\mathcal{B}/\hbar}{eB\xi\Omega/\hbar} \approx \frac{M\mathcal{B}}{\hbar^2 v^2}$ is again negligible for a wide range of parameters that typically characterize these materials.

3.4.2 Orbital susceptibility at finite magnetic fields. β dependency

The functions $\Lambda(\beta)$ and $\Theta(\beta)$ associated with the orbital magnetic susceptibility terms at non-zero magnetic fields are

$$\chi_1 = -\frac{3e^3\hbar v_F^4}{64\pi M^3(1-4\beta)^{3/2}}\Bigg[\sqrt{1-4\beta}\,\left(1-6\beta-6\beta^2(-1+2\beta)\right)+ 4\beta^3(-2+3\beta)\Bigg(2\,\mathrm{arctanh}\left(\frac{-1+2\beta}{\sqrt{1-4\beta}}\right) - \ln\left(-\frac{\beta^2}{\sqrt{1-4\beta}}\right) + \ln\left(+\frac{\beta^2}{\sqrt{1-4\beta}}\right)\Bigg)\Bigg]$$

$$\chi_2 = \frac{e^4\hbar^2 v_F^6\,(1-14\beta+68\beta^2-120\beta^3+128(1+rs)\beta^5-512(1+rs)\beta^6+1024(1+rs)\beta^7)}{420\pi|M|^5(1-4\beta)^3}$$

It is important to note that χ_1 is real for any value of β and the imaginary factors arising when $\beta > 1/4$ in both terms of the fraction cancel. A numerical representation of χ_1 vs β can be found in Fig. 3.8. The particular case $\beta = 1/4$ corresponds to the condition $4M\mathcal{B} = \hbar^2 v^2$ which makes the energy dispersion to be fully parabolic $\xi = \pm(M + \mathcal{B}k^2)$. Despite all terms contain a factor $(1-4\beta)$ in their denominators it can be checked that

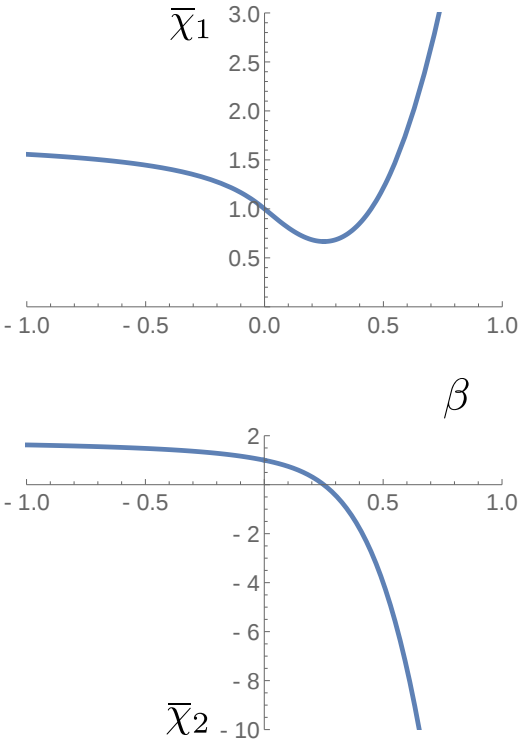

Figure 3.8: $\mathcal{B}$ dependence of the χ_1 and χ_2 coefficients. Normalized coefficients $\bar{\chi}_1 = \chi_1/\chi_1(\mathcal{B}=0)$ and $\bar{\chi}_2 = \chi_2/\chi_2(\mathcal{B}=0)$ vs the dimensionless parameter $\beta = \frac{M\mathcal{B}}{\hbar^2 v_F^2}$. Just as the zero-field term χ_0, χ_1 and χ_2 also show clear differences between the trivial and non-trivial insulating regimes.

no divergences occur since the numerators also have the same root for positive β, i.e., for $M\mathcal{B} > 0$. By computing the previous formulae for χ_1 and χ_2 it can be shown their weak dependence on $\mathcal{B}$ which results negligible for a wide range of values taking into account the different magnitude between these terms and the zero-field term χ_0. This fact is more marked for the trivial regime ($\beta < 1$) in all terms of the orbital magnetic susceptibility and more corrections might be expected to reduce the $\mathcal{B}$ contribution increasing the discrepancies between both topological trivial and non-trivial regimes. Notice that in the chart, the coefficients are normalized by their value at zero $\mathcal{B}$, so they still present a divergent behaviour when closing the band gap.

3.5 Conclusions

All materials respond as paramagnetic or diamagnetic under an applied external magnetic field although their physical origins are very different. For example, diamagnetism depends mainly on the atomic number and the orbital electron radius, while paramagnetism strongly depends on the temperature and magnetic momenta of the ground state

within the first order approach. This last condition can be overcome by introducing higher order perturbative terms as occurs with van Vleck paramagnetism when also considering the magnetization of excited states. However, in 2D materials with non-zero Berry curvature, new orbital magnetizations emerge from this property.

First, we have performed a relativistic quantum formalism for two-dimensional topological systems with non-zero Berry curvature in presence of a perpendicular magnetic field. We have found that the change in the velocity of the electrons due to the coupling of the magnetic field and the Berry curvature involves new corrections in their energy, orbital magnetic moment and density of states which is associated with their relativistic nature. This is accompanied by a modulation of the Berry curvature, suitable to work on the Bloch electron dynamics, that keeps the Chern number of the system invariant opening the door to study higher-order non-trivial magnetic and thermoelectric effects in Chern and topological insulators.

Afterwards, we introduced the natural k dependence in the energy dispersion and mass that the Dirac electrons have in condensed matter. Given the crucial role of this term for a proper definition of the topological invariant Chern number, the analytical expressions which results from this perturbative analysis of the Dirac Hamitonian in presence of a perpendicular magnetic field are able to disentangle the topological orbital effects besides extending the previous results using linear dispersion to a broader variety of compounds. The new scenario which arises involve drastic differences in the orbital magnetic response of the topological trivial and non-trivial regimes. Thus, while a trivial insulator is predicted to have a limited dependence on $\mathcal{B}$ based on the common values that these materials have, its topological counterpart features a unexplored term in the zero-field orbital magnetic susceptibility which is given in fundamental units and is inversely proportional to the square of the quantum magnetic flux. The results obtained go further in the study singular physics of these materials approaching it to the quantum phase transition phenomenology and enables different paths to modulate the orbital magnetization and susceptibility in these materials. As well, they establish the basis to treat directly other non-linear thermoelectric and magnetoelectric properties of non-zero Berry curvature systems.

4 Axion detection in TIs via pressure measurements

In this chapter, we analyze the axion electrodynamics in TIs considering its Lagrangian density in its natural form. That is, taking that the axion field θ is a function of time and space. In this way, $\theta(r,t)$ can be interpreted as a Klein-Gordon field satisfying the boundary conditions of the crystal whose associated density of energy gives an internal pressure quite similar to the Casimir but with a very different origin and magnitude. Since no Casimir effect is expected because of all surfaces being metallic, the results obtained could lead to the experimental verification of axions in TIs via pressure measurements.

4.1 Introduction

The quantum field theory tells us that the vacuum is not empty, but it is formed by virtual particles which are created and destroyed within fluctuating fields having a zero-point energy [184, 185]. One paradigmatic example is given by the vacuum of quantum electrodynamics, where the virtual photons transform into pairs of electron-positron. Those photons have high energy, high frequency, or short wavelength. Thus, two near parallel conductor plates can cut such photons selecting the ones of short wavelength and even creating a region of negative energy in their inner part. This means that it must appear an attractive force between those plates or one equivalent pressure on them, which is known as the Casimir effect [186–189]. That is to say, this assumes that the photons of high frequency go in by the surfaces where there are no conductors, which do not apply to the topological insulators where all its surface is metallic. Later on, this calculation was generalized to dielectrics, showing that the condition of having good metallic boundary conditions for the plates was not necessary for obtaining such effect [190–192]. Although there are differences; for instance, the Casimir employing the van der Waals interaction shows that the pressure depends on the magnitude of the fine structure constant α [193]. This is also a straightforward dependence that is present in this paper for the TIs employing its associated axion electromagnetic fields and without needing to use van der Waals

fluctuations. The special dynamics and features of these materials, which present both conductor and insulating behaviours, made them very interesting for introducing different fields and boundary conditions to measure experimentally singular Casimir effects [194–196].

For taking into account all this physics, we need to enlarge the usual Maxwell electrodynamics action, which only uses the scalar Lorentz invariant associated with the fields for obtaining all Maxwell electrodynamics in the vacuum, because classically the pseudoscalar invariant does not contribute to the motion equations more than with a surface term. In fact, the Lorentz pseudoscalar can only be implemented physically within an action working on a phase of an exponential expression, i.e. in a quantum formalism [134]. Besides that, it is also necessary to introduce a scalar field $\theta(\boldsymbol{r},t)$ field, named axion field to take into account the non-trivial topology. This field might be interpreted as an angle between the electric $\boldsymbol{E}$ and magnetic $\boldsymbol{B}$ fields because it keeps invariant the action under a shift of 2π. In the non-trivial zone of the TIs, i.e. in the surfaces, where the bands are crossed, this field takes a constant value equal to π for conserving the time invariance $\hat{T}$ and having Kramers currents. Hence, the axion electrodynamics employs the two Lorentz invariants associated with the fields and a new scalar field [48, 49, 52, 109, 197].

Furthermore, the non-trivial topology of TIs is simultaneously found within the band structure through their Berry curvature besides in the axion electrodynamics. In one case, the $\boldsymbol{E}$ and $\boldsymbol{B}$ fields can also be determined by constraining it into a Brillouin zone torus $S^1 \times S^1$ employing the Gauss-Bonnet formula, whereas the Chern number is used for the bands through the Berry curvature only [109, 198]. The crossing bands singularities in the $k-$space are in correspondence with the genus of the torus in the Brillouin zone. More accurately, in TIs, where the topology is non-trivial, taking the energy $\xi(\boldsymbol{r_n},\boldsymbol{k}) = \xi(\boldsymbol{k}) + e\boldsymbol{E}\cdot\boldsymbol{r_n} - \mathbb{m}_{\boldsymbol{n}}(\boldsymbol{k})\cdot\boldsymbol{B}$ under electric and magnetic fields, the equations of motion for an electron in a single band n would be [73, 199]

$$\frac{\partial}{\partial t}\boldsymbol{k} = -\frac{1}{\hbar}\nabla_{\boldsymbol{r}}\xi_n - \frac{e}{\hbar}\frac{\partial}{\partial t}\boldsymbol{r_n}\times\boldsymbol{B} \tag{4.1}$$

$$\frac{\partial}{\partial t}\boldsymbol{r_n} = \frac{1}{\hbar}\nabla_{\boldsymbol{k}}\xi_n - \frac{\partial}{\partial t}\boldsymbol{k}\times\boldsymbol{\Omega_n} \tag{4.2}$$

where $\mathbb{m}_{\boldsymbol{n}} = -\frac{e}{2}\langle n|\,\boldsymbol{r}\times(\boldsymbol{v}-\langle\boldsymbol{v}\rangle)\,|n\rangle = \frac{e}{\hbar}\xi_n\boldsymbol{\Omega_n}$ is the orbital magnetic moment of the electrons in the band n, $\langle\boldsymbol{v}\rangle$ their average velocity, Ω_n the Berry curvature, $\hbar$ the Planck bar constant and $-e$ the charge of the electron. This shows clearly a relationship between the transport in the bands or in the lattice, where the electric and magnetic fields produce anomalous contributions to the particle's velocity in presence of non-zero Berry curvatures. Thus, it is straightforward to obtain the quantized electric conductivity $\sigma_{xy} = \frac{e^2}{h}C_n$ for a filled band, being $C_n = \frac{1}{2\pi}\int_{S^1\times S^1} d^2k\,\Omega_n$ the integer Chern number of the n-band, just using $\boldsymbol{j_n} = -\frac{e}{(2\pi)^2}\int_{S^1\times S^1} d^2k\frac{\partial}{\partial t}\boldsymbol{r_n}$ [141]. This is one of the main results for the topological transport, but we are interested to focus on the pressure made by the electromagnetic fields. For such aim, we are going to enlarge the axion electrodynamics action allowing it

to propagate the scalar field $\theta(\boldsymbol{r}, t)$ within the bulk, while in the surface takes the constant value $\theta(\boldsymbol{r}, t) = \pi$.

4.2 Axion electrodynamics and confined electromagnetic fields

The action in the axion electrodynamics contains the two Lorentz invariants associated to the fields. That is to say, it is added the pseudoscalar quantity $\frac{1}{2}\epsilon_{\mu\nu\alpha\beta}F^{\mu\nu}F^{\alpha\beta} = -\frac{4}{c}\boldsymbol{E}\cdot\boldsymbol{B}$, besides the usual scalar $F_{\alpha\beta}F^{\alpha\beta} = -2(E^2/c^2 - B^2)$ which is enough to provide Maxwell electrodynamics in the trivial topological vacuum, without taking into account finite local boundaries for the fields or their global properties. Hence we have the Lagrangian density [52, 200]

$$\mathcal{L} = -\frac{1}{4\mu_0}F_{\alpha\beta}F^{\alpha\beta} - A_\mu J^\mu + \frac{e^2 c}{32\pi^2\hbar}\theta(r,t)\epsilon_{\mu\nu\alpha\beta}F^{\mu\nu}F^{\alpha\beta} \tag{4.3}$$

where the first two terms are associated with the usual Maxwell's electrodynamics and the last term gives the axion electromagnetic contribution through the $\theta(r, t)$ scalar field. This leads directly to the equivalent Maxwell equations in TIs considering the variation of the electromagnetic potential A_μ

$$\boldsymbol{\nabla}\cdot\boldsymbol{D} = \rho_f - \frac{e^2}{4\pi\hbar}\boldsymbol{\nabla}\left(\frac{\theta}{\pi}\right)\cdot\boldsymbol{B} \tag{4.4}$$

$$\boldsymbol{\nabla}\times\boldsymbol{H} = \boldsymbol{J_f} + \frac{\partial\boldsymbol{D}}{\partial t} + \frac{e^2}{4\pi\hbar}\left[\frac{\partial}{\partial t}\left(\frac{\theta}{\pi}\right)\boldsymbol{B} + \boldsymbol{\nabla}\left(\frac{\theta}{\pi}\right)\times\boldsymbol{E}\right] \tag{4.5}$$

The first equation substitutes the Gauss expression, while the second does it for the Ampere-Maxwell. The other two equations, Faraday and non-existence of isolated magnetic poles, maintain the same form allowing to define locally the usual electromagnetic potentials [155, 156]. It is necessary to observe in the previous equations, that $\theta(r, t)$ must be a scalar field of modulo 2π for the action. That is to say, it needs to be a function of the space and time if the new electrodynamics wants to take into account the topological background. In fact, the axions can be thought as excitations of the $\theta(\boldsymbol{r}, t)$ scalar field coupled to the electromagnetic field as the phonons, magnons or plasmons do for obtaining polaritons [122, 201]. Their coupling with the photons is quite weak and we are going to neglect their mass m_θ in this work where these axions are going to play a fundamental role under thermal changes in the TIs.

To have the same non-trivial topology for the bands and for the lattice, in the surface, where $\theta = \pi$ we can determine the magnetic and electric fields living on torus on each

Brillouin zone. This can be done through the magnetic and static electric flux quantization over the torus [71, 109, 202]

$$|\boldsymbol{B_\theta}| = n\frac{h}{ea^2} \tag{4.6}$$

$$|\boldsymbol{E_\theta}| = n'\frac{hv_F}{ea^2} \tag{4.7}$$

Here, $n, n' \in \mathcal{N}$ are natural numbers that determine the topological sector and v_F the Fermi velocity that share the relativistic Dirac electrons and photons due to having both rest mass zero; i.e., the relativistic Minkowski spacetime is taken with v_F instead of c for assuming the diffusion equation $\xi = pv_F$ for low energies. It is worthy to observe that we can choose a common gauge function $\Lambda(x,t) = \frac{xh}{ea}$ for the electromagnetic potential and the Berry connection, being x the position of one point of the torus and a the lattice constant [2]. This means that we can synchronize the change of the phase $\theta(x,t)$ on the Bloch bands and the electromagnetic potential for each topological sector where the function is continuous, keeping control of the gauge freedom parameter. This allows to define simultaneously Eq. (4.1) and Eq. (4.2) on the surface, where the singularities exist, for the electromagnetic fields associated to the axion electrodynamics as pieces of the same topological manifold. Mathematically we are using the common gauge $U(1)$ Abelian group, which is not trivial topologically, for the bands and the lattice symmetries in the case of TIs; i.e. $\pi_1(S^1) = Z$ can have homotopies with values different than zero and define them out of each singularity [2].

It is immediate to find the density of energy of these topological axion electromagnetic fields $\xi_\theta = \frac{1}{2}(\boldsymbol{E_\theta D_\theta} + \boldsymbol{H_\theta B_\theta})$ given by

$$\xi_\theta = \frac{\pi\hbar v_F}{\alpha a^4} \tag{4.8}$$

being α the fine structure constant in this medium with the Fermi velocity v_F instead of c [203, 204]. This term corresponds only to the fields because the density of energy due to the electric polarization $\boldsymbol{P}$ and magnetization $\boldsymbol{M}$ cancel each other. $\boldsymbol{M}$ is negative while $\boldsymbol{P}$ is positive as can be seen from the above generalized Maxwell equations. Explicitly, the values are given by

$$\boldsymbol{M} = -\frac{e^2}{4\pi\hbar}\boldsymbol{E} \qquad \boldsymbol{P} = \frac{e^2}{4\pi\hbar}\boldsymbol{B} \tag{4.9}$$

taking that the fields have π radians between them [49]. Actually, this expression was calculated in a Brillouin zone, but it must be the same in all these zones for the surfaces. Interpreting the energy density as a classical conductor is very easy since $\boldsymbol{E} = \sigma/\epsilon_0\ \hat{\boldsymbol{n}}$,

where σ is the surface density of charge, and the density of energy is $\xi = \sigma^2/(2\epsilon_0)$. Notice that here $\hat{\boldsymbol{n}}$ stands for the unit vector normal to the surface. That is, the energy density in the surface is associated to the square of the charge density and reasoning in parallel, we could also think that we have a growth of the density of charges due to the topological fields that exert an orthogonal force to the metallic surface and outwards in the direction $\hat{\boldsymbol{n}}$. But going to the generalized Gauss equation we obtain that $\rho = \alpha v_F \epsilon B \partial_{\boldsymbol{n}}(\frac{\theta}{\pi})$, where the $\frac{\theta}{\pi}$ is a step Heaviside function, going from 1 to 0 outside the TI, whose derivative gives a Dirac delta function. Thus, the density of charge in the surface gives $\sigma = \alpha \epsilon v_F B$ which grows with these fields.

4.3 Axion pressure vs Casimir pressure

We can observe that the above density of energy, Eq. (4.8), might be interpreted as a pressure and only differs on some constants from the Casimir pressure between two conductor plates placed at a distance d instead of the lattice constant a, nevertheless its source is absolutely different (Fig. 4.1). Remember that the Casimir pressure at $T = 0$ is given by

$$P = -\frac{\pi^2 \hbar c}{240 d^4} \tag{4.10}$$

and its dependence at low temperatures can be written as

$$P = -\frac{\pi^2 \hbar c}{240 d^4} \left[1 + \frac{1}{3} \left(\frac{T}{T_e} \right)^4 \right] \tag{4.11}$$

where $T_e = \frac{\hbar c}{2 d k_B}$ is the effective temperature, whose pressure is important at distances higher than the thermal wavelength $\frac{\hbar c}{k_B T}$ [190, 191, 205]. Unlike what happens for the electric and magnetic fields, the scalar axion field $\theta(\boldsymbol{r}, t)$ is defined in all the material and it can evolve naturally with the temperature changes as we show in what follows.

Following with the TI, in a layer with width d where the x and y lengths are much higher than d, the scalar axion $\theta(\boldsymbol{r}, t)$ field has good Dirichlet conditions in the z-direction orthogonal to the plates. That is to say, we have a normalized field $\bar{\theta} = \theta/\pi$ which satisfies that $\bar{\theta}(z = 0) = \bar{\theta}(z = d) = 1$, knowing that $\theta(\boldsymbol{r}, t) = \pi$ must be the constant values that this field takes on the surface. Hence we have a discrete quantized linear moment $p_z = n_z \hbar \frac{2\pi}{d}$ as the translator generator. In fact, it is a Klein-Gordon field with rest mass zero and Lagrangian density $\mathcal{L} = \frac{1}{2} \partial_\mu \bar{\theta} \partial^\mu \bar{\theta}$ [206], which allows to quantize it via the mode expansion

$$\bar{\theta}(\boldsymbol{r}, t) = \frac{1}{(2\pi)^3} \int \frac{d^3 \boldsymbol{p}}{\sqrt{2 p_0}} [a_{\boldsymbol{p}} exp(-\frac{i}{\hbar} \boldsymbol{p}.\boldsymbol{r}) + a^\dagger_{\boldsymbol{p}} exp(+\frac{i}{\hbar} \boldsymbol{p}.\boldsymbol{r})] \tag{4.12}$$

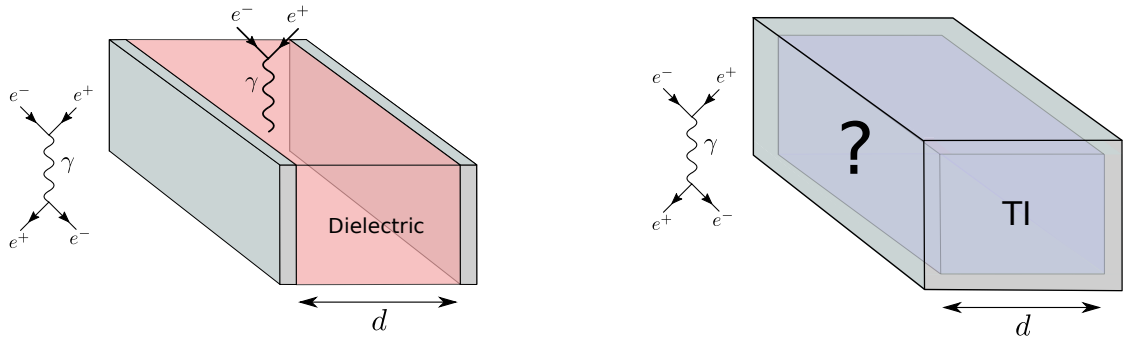

Figure 4.1: Representation of the Casimir effect (left panel) between two conductor plates placed at a distance d and its counterpart effect produced by the axions within the topological insulators (right panel). Due to all the surfaces in the TI are metallic no virtual photons are expected to penetrate leading to a measurable pressure different from the Casimir between opposite plates.

where the Lorentz invariant measure is given by $\int \frac{d^3\boldsymbol{p}}{2p_0}$, being $p_0 = \xi v_F^{-1}$, making to define the creation-annihilation operators by $a_p = \sqrt{\frac{\hbar}{2p_0}} f(p_0, p)$ and $a_p^\dagger = \sqrt{\frac{\hbar}{2p_0}} f(-p_0, -p)$ being $f(p_0, p)$ and $f(-p_0, -p)$ relativistic normalized annihilation and creation operators to obtain the only non vanishing commutators

$$[a_{\boldsymbol{p}}, a_{\boldsymbol{p'}}^\dagger] = (2\pi)^3 2\hbar\omega\delta^3(\boldsymbol{p} - \boldsymbol{p'}) \tag{4.13}$$

which keep the form of the Heisenberg's indeterminacy within the canonical quantization for this real scalar field. Thus, the dispersion energy $\xi_n = v_F\sqrt{p_s^2 + (\hbar\frac{2\pi n}{d})^2}$, where $p_s^2 = p_x^2 + p_y^2$ are the momenta on the surfaces determined by x and y coordinates, allow us to write the density of energy

$$\xi_{0A} = \sum_{n=0}^{\infty} \frac{1}{2\hbar^2(2\pi)^2} \int \xi_n d^2 p_s \tag{4.14}$$

This leads us to an infinite value which needs regularization as usually is made for the Casimir effect with the difference of having one polarization for the axions instead of the two arising for photons [207]. For doing this regularization we use the factor $e^{-\epsilon d\xi_n/2\pi\hbar v_F}$ whose limit is one when ϵ tends to zero. Making this straightforward calculation we have for the integral the result $\frac{4\pi}{v_F^2}(\frac{2\pi\hbar v_F}{\epsilon d})^3 e^{-n\epsilon}(1 + n\epsilon + \frac{n^2\epsilon^2}{2})$. In this way, the sum on n is made by considering it as a geometric progression with ratio $e^{-\epsilon}$

$$\sum_{n=0}^{\infty} e^{-n\epsilon} = \frac{1}{1 - e^{-\epsilon}} \approx \frac{1}{\epsilon} + \frac{1}{2} + \frac{\epsilon}{12} - \frac{e^3}{720} + \frac{\epsilon^5}{30240} + ...$$

$$\sum_{n=0}^{\infty} e^{-n\epsilon} n\epsilon = \frac{\epsilon\, e^{\epsilon}}{(e^{\epsilon}-1)^2} = \frac{1}{\epsilon} - \cancel{\frac{\epsilon}{12}} + \cancel{\frac{e^3}{240}} - \frac{\epsilon^5}{6048} + ...$$

$$\sum_{n=0}^{\infty} e^{-n\epsilon} \frac{n^2\epsilon^2}{2} = \frac{\epsilon^2}{2}\frac{e^{\epsilon}(e^{\epsilon}+1)}{(e^{\epsilon}-1)^3} \approx \frac{1}{\epsilon} - \cancel{\frac{e^3}{240}} + \frac{\epsilon^5}{3024} + ...$$

for obtaining the density of energy

$$\xi_{0A} = \frac{12\pi^2\hbar v_F}{\epsilon^4 d^3} - \frac{\pi^2\hbar v_F}{180 d^3} + \frac{\pi^2\epsilon^2}{1260 d^3} \tag{4.15}$$

where we have developed the approximation till quadratic terms in ϵ and subtracted the zero-point energy $\frac{1}{2}\hbar\omega$ in Eq. (4.14) [186]. In contrast with the third term that tends to zero, the first term diverges as ϵ becomes smaller. Nevertheless, this term is well-known as the one associated with the vacuum contribution in non-periodicity conditions or long distances $\frac{1}{2(2\pi)^2\hbar^2}\int_0^{\infty} dn \int \xi_n\, d^2p_s$ whose contribution, making use of the same regulator, must be subtracted for obtaining the equivalent Casimir pressure

$$P = -\frac{\pi^2\hbar v_F}{60 d^4} \tag{4.16}$$

for the axion field $\theta(\boldsymbol{r}, t)$. This expression differs from the one exerted by the photons in some constants that are associated with the change in the field periodicity, number of wave polarizations and velocity propagation of the fields in the medium. However, its dependence on the distance and sign remain invariant, and hence it tends to decrease the distance between the surfaces giving an attractive force between them, as it happens with the Casimir force.

Furthermore, we can see the dependence on the temperature of the above pressure. Having that the partition function of this gas of bosons is given by

$$Z = \prod_p \left(\sum_{N=0}^{\infty} exp\left[-N\frac{\xi_n - \mu}{k_B T} \right] \right) = \prod_p \frac{1}{1 - exp\left[-\frac{\xi_n - \mu}{k_B T} \right]} \tag{4.17}$$

where the sum was taken as a geometric series with N the number of particles and μ the chemical potential. This is possible if and only if $\xi_n - \mu \geq 0$ or when the chemical potential is negative or zero because we can reach the fundamental state. Notice that this condition cannot be filled by a fermion system where the chemical potential is always positive. From the physical point of view, it seems natural to think that the axions are special photons in the TIs or at least that both are directly related. Now we can calculate the density of free energy F of our system for a finite temperature T

$$F = \frac{k_B T}{(2\pi)^2 \hbar^2} \sum_{n=(0)1}^{\infty} \int d^2 p_s ln \left(1 - exp\left[-\frac{\xi_n - \mu}{k_B T}\right]\right) \tag{4.18}$$

where we used that $ln\, Z = -\sum_p ln[1 - exp(-(\frac{\xi_n - \mu}{k_B T}))]$ and where the sum in n has a factor of $1/2$ for the term $n = 0$ for taking into account properly the zero-energy point energy as before [186]. Setting $\mu = 0$ and making the change of variable $x = \frac{\xi_n}{k_B T}$ with $d^2 p_s = 2\pi (k_B T)^2 v_F^{-2} x dx$, we have

$$F = \frac{(k_B T)^3}{2\pi \hbar^2 v_F^2} \sum_{n=(0)1}^{\infty} \int_{\frac{2\pi n \hbar v_F}{k_B T d}}^{\infty} ln(1 - e^{-x}) x dx \tag{4.19}$$

Thus, for $n = 0$ we can do an integration by parts and employ the result $\frac{1}{(s-1)!} \int \frac{x^{s-1} dx}{e^x - 1} = \zeta(s)$ for obtaining

$$F = -\frac{(k_B T)^3}{4\pi \hbar^2 v_F^2} \zeta(3) + \frac{(k_B T)^3}{2\pi \hbar^2 v_F^2} \sum_{n=1}^{\infty} \int_{\frac{2\pi n \hbar v_F}{k_B T d}}^{\infty} ln(1 - e^{-x}) x dx \tag{4.20}$$

where $\zeta(s)$ is the Riemann zeta function. On the other hand, the second integral has not an analytical expression, but for low temperatures (or distances) with $\frac{2\pi \hbar v_F}{k_B T d}$ much higher than one, the logarithm can be expanded in powers of e^{-x} and the dominant term is for $n = 1$. Thus, we have for this integral term the approximation $-\frac{(k_B T)^3}{2\pi \hbar^2 v_F^2}[1 + \frac{2\pi \hbar v_F}{k_B T d}] exp(-\frac{2\pi \hbar v_F}{k_B T d})$. Therefore, we find the density of free energy of the axions associated with the topological fields at low-temperatures

$$F = -\frac{\pi^2 \hbar v_F}{180 d^3} - \frac{(k_B T)^3}{4\pi \hbar^2 v_F^2} \zeta(3) - \frac{(k_B T)^3}{2\pi \hbar^2 v_F^2} \left[1 + \frac{2\pi \hbar v_F}{k_B T d}\right] exp\left(-\frac{2\pi \hbar v_F}{k_B T d}\right) + \frac{(k_B T)^4 d}{2\pi^2 (\hbar v_F)^3} \zeta(4) \tag{4.21}$$

and the pressure exerted by them on the surfaces

$$P = -\frac{\pi^2 \hbar v_F}{60 d^4} + \frac{2\pi k_B T}{d^3} exp\left(-\frac{2\pi \hbar v_F}{k_B T d}\right) - \frac{(k_B T)^4}{2\pi^2 (\hbar v_F)^3} \zeta(4) \tag{4.22}$$

Again, the last term corresponds to the temperature dependence of the free energy without taking into account the axion field periodicity which is subtracted following the same procedure as before. Notice that for photons this latter factor, known as the black body free energy of a photon gas $2(k_B T)^4 d/(\pi^2 \hbar^3 c^3)\zeta(4)$, is proportional to four times the given value due to the change in the number of possible polarization and periodicity of the fields. It is worthy to observe that for low temperatures or distances the second term in Eq. (4.22) is negligible when compared with the other two. Thus, we can write the force or

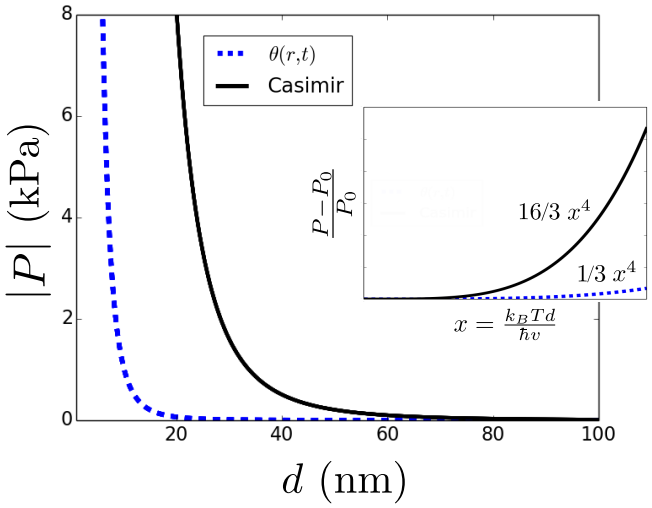

Figure 4.2: Distance dependency of the pressure associated with the axions in a topological insulator (dashed line) compared with the pressure exerted by the photons in the Casimir effect (solid line) taking $T = 10$ K and $v_F = 6\ 10^5$ m/s. The inset shows the normalized pressure with respect to the dimensionless parameter $x \equiv T/T^* = k_B T d/(\hbar v) << 1$ for both cases.

pressure exerted on the surfaces as $P = P_0(1+\frac{1}{3}(\frac{T}{T^*})^4)$. This follows the same dependence as the Casimir force Eq. (4.11) but redefining its principal variables $P_0 = -\frac{\pi^2 \hbar v_F}{60 d^4}$ and the effective temperature $T^* = \hbar v_F/(k_B d)$ (Fig. 4.2). In this context, it seems obvious that is possible to get a technological advantage when making thin-film based devices due to having an effective pressure for the axions substantially smaller than the one of Casimir. This latter fact about its magnitude constitutes a differentiating signature when testing experimentally the physics of the axions in these systems.

4.4 Conclusions

We have examined the topological magneto-electric effect of the TIs and obtained a behaviour quite similar to that of Casimir, although with very different origins. The electric and magnetic fields have a very high density in the surface and inside the TIs it is the axionic scalar field that acts as the temperature-dependent Casimir. Thus, we can obtain a distribution of the topological energy associated to the electric, magnetic and axion fields within the TIs. All these results are suitable for being measured and therefore help to understand both the topological behaviour of the TIs and the electrodynamics of axions.

Conclusion and Outlooks

In this thesis, we have tackled theoretically different aspects related to the transport and physics of topological insulators. Precisely, their singular physics, as well as that of other topological materials, can sometimes make this task a challenge but it also opens the possibility to study special effects and properties as it is described in the introduction or in the current literature. This thesis was born with the aim of giving a microscopic formalism for the thermoelectricity in topological insulators, but delving into this effect has led us to explore and find an interpretation to some fundamental points of the physics of these systems such as the Riemann-Hurwitz formula, the topological contribution to the thermoelectric effect, the field interpretation through b, the intrinsic orbital magnetism, the Berry curvature modulation, the axion electrodynamics and the pressure associated with the scalar field $\theta(r,t)$, etc. All these elements are pieces of the same mechanism that need to be glued by an effective action in which the topology of the system plays a leading role.

We have started with a brief introduction to the physics of the Berry phase and its connection with the Dirac Hamiltonian for different space-time dimensions to revise some of the main concepts which TIs employ and that has been needed in our research. At the same time, I have also gathered some of the concepts and skills obtained in the first formative stage carried out at the beginning of my thesis. Next, I have developed the microscopic formalism obtained for the thermoelectricity in TIs starting directly from the effective Chern-Simons action that these systems employ for the electronic transport and whose necessity has been demonstrated using pure mathematical concepts, summarized in the Riemann-Hurwitz formula. We have given a new formula for the topological Seebeck coefficient, electric field and potential generated by a temperature gradient in these materials and we have calculated the topological contribution to the dimensionless figure of merit in the surface of a TI. Following the same line of reasoning, we have proceeded to address the electronic transport in presence of lattice oscillations through the Dirac oscillator Hamiltonian. This second study reaches a successful field interpretation of the Berry curvature which allows to understand the role of phonons in the relativistic electronic Hamiltonian of these systems at low energy as well as their intrinsic orbital magnetism which arises from their non-trivial Berry curvature. From a fundamental point of view, besides answering why TIs can preserve time-reversal symmetry in presence of temperature gradients and phonons, an efficient route to transform heat from the lattice

into electricity was also described. In our next effort, we have provided a relativistic calculation of the corrections to the Dirac Hamiltonian in presence of magnetic fields which is demonstrated to be consistent with the existing formalisms based on Lagrangian theory, Landau Levels and non-relativistic quantum mechanics. In addition, we have given a physical interpretation for the coupling between the Berry curvature and the magnetic field and we have finally revealed the differences between the orbital magnetic response of both topological non-trivial and trivial regimes. In the final chapter, we have analyzed the TIs from the standpoint of axion electrodynamics to address a fundamental result, their inner pressure. This latter case pretends to establish a path to measure directly the existence of axions via pressure measurements in analogy with the Casimir effect.

The research carried out during these years has answered most of the questions that gave rise to this thesis, but it has also induced new ideas and perspectives that I would like to explore in the future. Moreover, several theoretical findings and predictions such as the field b, the role of phonons, and the axion pressure in TIs have been done and look forward to experimental verification. Probably this is only the beginning. Pending studies could search for materials that exhibit higher topological numbers to enhance their thermoelectric properties and beat the current experimental limit, treat theoretically the lattice contribution to the thermal conductivity in TIs, extend the coupling of the Berry curvature with the external electromagnetic fields to study other transport properties, etc. On the other hand, I do not rule out extending my research to other topological materials or even exploring the fundamental origins of the topological phase transitions. I am confident that someday all the diverse pieces that topological materials comprehend will be connected and that these will be crucial for future technology.

List of Publications

In this appendix I include a detailed description of the articles that I have produce throughout this thesis and of the specific chapters in which they have been addressed. All these articles are open access distributed under the terms of the Creative Commons CC BY license, which permits unrestricted use, distribution, and reproduction, provided the original work is properly cited. Our last contribution to the study of the intrinsic orbital magnetism in non-zero Berry curvature systems has been already submitted to a Journal but it has not been accepted yet. The results contained in this latter work can be found in the final part of Chapter 3 and in ref. [208].

[I] On behind the physics of the thermoelectricity of topological insulators, *Scientific Reports* **9**, 6324 (2019)

Authors
Daniel Baldomir,[*a] Daniel Faílde[a]

[a] Departamento de Física Aplicada, Instituto de Investigacións Tecnolóxicas, Universidade de Santiago de Compostela, E-15782 Campus Sur s/n, Santiago de Compostela, Spain.

PhD student contribution: Contributing author. Active participation in all the calculations presented in the article as well as in the writing and figure creation.

Chapter of the thesis in which it is used: 1

Journal information
Journal Name: Scientific Reports
Publisher: Springer Nature
ISSN: 2045-2322 **DOI:** https://doi.org/10.1038/s41598-019-42744-3
Impact factor in 2020: 4.380 (JRC data) **Quartile in Multidisciplinary Sciences: Q1**

[II] Emergent topological fields and relativistic phonons within the thermoelectricity in topological insulators, *Scientific Reports* **11**, 14335 (2021)

Authors
Daniel Faílde,[*a] Daniel Baldomir[*a]

[a] Departamento de Física Aplicada, Instituto de Investigacións Tecnolóxicas, Universidade de Santiago de Compostela, E-15782 Campus Sur s/n, Santiago de Compostela, Spain.

PhD student contribution: First and corresponding author. Active participation in all the calculations presented in the article as well as in the writing and figure creation.

Chapter of the thesis in which it is used: 2

Journal information
Journal Name: Scientific Reports
Publisher: Springer Nature
ISSN: 2045-2322 **DOI:** https://doi.org/10.1038/s41598-021-93667-x
Impact factor in 2020: 4.380 (JRC data) **Quartile in Multidisciplinary Sciences: Q1**

[III] Orbital dynamics in 2D topological and Chern insulators, *New Journal of Physics* **23**, 113002 (2021)

Authors
Daniel Faílde,[*a] Daniel Baldomir[*a]

[a] Departamento de Física Aplicada, Instituto de Investigacións Tecnolóxicas, Universidade de Santiago de Compostela, E-15782 Campus Sur s/n, Santiago de Compostela, Spain.

PhD student contribution: First author. Active participation in all the calculations presented in the article as well as in the writing and figure creation.

Chapter of the thesis in which it is used: 3

Journal information
Journal Name: New Journal of Physics
Publisher: IOP Science
ISSN: 1367-2630 **DOI:** https://doi.org/10.1088/1367-2630/ac29fc
Impact factor in 2020: 3.732 (JRC data) **Quartile in Physics, Multidisciplinary: Q1**

[IV] On the inner topological pressure within the topological insulators, *Annalen der Physik* 2100313 (2021)

Authors
Daniel Faílde,[a] Daniel Baldomir*[a]

[a] Departamento de Física Aplicada, Instituto de Investigacións Tecnolóxicas, Universidade de Santiago de Compostela, E-15782 Campus Sur s/n, Santiago de Compostela, Spain.

PhD student contribution: First author. Active participation in all the calculations presented in the article as well as in the writing and figure creation.

Chapter of the thesis in which it is used: 4

Journal information
Journal Name: Annalen der Physik
Publisher: Wiley
ISSN: 0003-3804 **DOI:** https://doi.org/10.1002/andp.202100313
Impact factor in 2020: 2.987 (JRC data) **Quartile in Physics, Multidisciplinary: Q1**

Bibliography

[1] S.-Q. Shen, *Topological Insulators: Dirac Equation in Condensed Matter* (Springer, 2018).

[2] M. Nakahara, *Geometry, Topology and Physics* (CRC Press, 2003).

[3] B. A. Bernevig, *Topological Insulators and Topological Superconductors* (Princeton university press, 2013).

[4] G. Tkachov, *Topological Insulators: The Physics of Spin Helicity in Quantum Transport* (CRC Press, 2015).

[5] D. Vanderbilt, *Berry Phases in Electronic Structure Theory: Electric Polarization, Orbital Magnetization and Topological Insulators* (Cambridge University Press, 2018).

[6] K. v. Klitzing, G. Dorda, and M. Pepper, Phys. Rev. Lett. **45**, 494 (1980).

[7] D. C. Tsui, H. L. Stormer, and A. C. Gossard, Phys. Rev. Lett. **48**, 1559 (1982).

[8] E. H. Hall, American Journal of Mathematics **2**, 287 (1879).

[9] R. B. Laughlin, Phys. Rev. B **23**, 5632 (1981).

[10] R. Karplus and J. M. Luttinger, Phys. Rev. **95**, 1154 (1954).

[11] J. E. Hirsch, Phys. Rev. Lett. **83**, 1834 (1999).

[12] M. Dyakonov and V. Perel, Physics Letters A **35**, 459 (1971).

[13] C.-X. Liu, S.-C. Zhang, and X.-L. Qi, Annual Review of Condensed Matter Physics **7**, 301 (2016).

[14] C.-Z. Chang, J. Zhang, X. Feng, J. Shen, Z. Zhang, M. Guo, K. Li, Y. Ou, P. Wei, L.-L. Wang, Z.-Q. Ji, Y. Feng, S. Ji, X. Chen, J. Jia, X. Dai, Z. Fang, S.-C. Zhang, K. He, Y. Wang, L. Lu, X.-C. Ma, and Q.-K. Xue, Science **340**, 167 (2013).

[15] B. A. Bernevig and S.-C. Zhang, Phys. Rev. Lett. **96**, 106802 (2006).

[16] M. V. Berry, Proceedings of the Royal Society of London. A. Mathematical and Physical Sciences **392**, 45 (1984).

[17] F. D. M. Haldane, Phys. Rev. Lett. **61**, 2015 (1988).

[18] C. L. Kane and E. J. Mele, Phys. Rev. Lett. **95**, 146802 (2005).

[19] C. L. Kane and E. J. Mele, Phys. Rev. Lett. **95**, 226801 (2005).

[20] D. N. Sheng, Z. Y. Weng, L. Sheng, and F. D. M. Haldane, Phys. Rev. Lett. **97**, 036808 (2006).

[21] J. Shi, G. Vignale, D. Xiao, and Q. Niu, Phys. Rev. Lett. **99**, 197202 (2007).

[22] J. E. Moore, Nature **464**, 194 (2010).

[23] B. A. Bernevig, T. L. Hughes, and S.-C. Zhang, Science **314**, 1757 (2006).

[24] H. Zhang, C.-X. Liu, X.-L. Qi, X. Dai, Z. Fang, and S.-C. Zhang, Nature Physics **5**, 438 (2009).

[25] L. Fu and C. L. Kane, Phys. Rev. B **76**, 045302 (2007).

[26] T. Thonhauser and D. Vanderbilt, Phys. Rev. B **74**, 235111 (2006).

[27] B. Yan and C. Felser, Annual Review of Condensed Matter Physics **8**, 337 (2017).

[28] P. Li, Y. Wen, X. He, Q. Zhang, C. Xia, Z.-M. Yu, S. A. Yang, Z. Zhu, H. N. Alshareef, and X.-X. Zhang, Nature Communications **8**, 2150 (2017).

[29] B. Q. Lv, H. M. Weng, B. B. Fu, X. P. Wang, H. Miao, J. Ma, P. Richard, X. C. Huang, L. X. Zhao, G. F. Chen, Z. Fang, X. Dai, T. Qian, and H. Ding, Phys. Rev. X **5**, 031013 (2015).

[30] X.-L. Qi, T. L. Hughes, and S.-C. Zhang, Phys. Rev. B **82**, 184516 (2010).

[31] L. Fu and E. Berg, Phys. Rev. Lett. **105**, 097001 (2010).

[32] Y. Tokura, K. Yasuda, and A. Tsukazaki, Nature Reviews Physics **1**, 126 (2019).

[33] J. Li, Y. Li, S. Du, Z. Wang, B.-L. Gu, S.-C. Zhang, K. He, W. Duan, and Y. Xu, Science Advances **5**, 10.1126/sciadv.aaw5685 (2019).

[34] Y. Deng, Y. Yu, M. Z. Shi, Z. Guo, Z. Xu, J. Wang, X. H. Chen, and Y. Zhang, Science **367**, 895 (2020).

[35] A. A. Zyuzin and A. A. Burkov, Phys. Rev. B **86**, 115133 (2012).

[36] X. Huang, L. Zhao, Y. Long, P. Wang, D. Chen, Z. Yang, H. Liang, M. Xue, H. Weng, Z. Fang, X. Dai, and G. Chen, Phys. Rev. X **5**, 031023 (2015).

[37] A. Y. Kitaev, Physics-Uspekhi **44**, 131 (2001).

[38] L. Fu and C. L. Kane, Phys. Rev. Lett. **100**, 096407 (2008).

[39] J. D. Sau, R. M. Lutchyn, S. Tewari, and S. Das Sarma, Phys. Rev. Lett. **104**, 040502 (2010).

[40] L. Zhang, New Journal of Physics **18**, 103039 (2016).

[41] M. Stone, Phys. Rev. B **85**, 184503 (2012).

[42] D. Xiao, Y. Yao, Z. Fang, and Q. Niu, Phys. Rev. Lett. **97**, 026603 (2006).

[43] Y. Xu, Z. Gan, and S.-C. Zhang, Phys. Rev. Lett. **112**, 226801 (2014).

[44] X.-F. Wang, Y. Hu, and H. Guo, Phys. Rev. B **85**, 241402 (2012).

[45] L. Fu and C. L. Kane, Phys. Rev. B **74**, 195312 (2006).

[46] F. Herman, C. D. Kuglin, K. F. Cuff, and R. L. Kortum, Phys. Rev. Lett. **11**, 541 (1963).

[47] M. König, S. Wiedmann, C. Brüne, A. Roth, H. Buhmann, L. W. Molenkamp, X.-L. Qi, and S.-C. Zhang, Science **318**, 766 (2007).

[48] L. Fu, C. L. Kane, and E. J. Mele, Phys. Rev. Lett. **98**, 106803 (2007).

[49] X.-L. Qi, T. L. Hughes, and S.-C. Zhang, Phys. Rev. B **78**, 195424 (2008).

[50] X. Wang, Y. Du, S. Dou, and C. Zhang, Phys. Rev. Lett. **108**, 266806 (2012).

[51] L. Müchler, F. Casper, B. Yan, S. Chadov, and C. Felser, Phys. Status Solidi RRL **7**, 91 (2013).

[52] L. Wu, M. Salehi, N. Koirala, J. Moon, S. Oh, and N. P. Armitage, Science **354**, 1124 (2016).

[53] W.-Y. Shan, H.-Z. Lu, and S.-Q. Shen, New Journal of Physics **12**, 043048 (2010).

[54] A. P. Schnyder, S. Ryu, A. Furusaki, and A. W. W. Ludwig, Phys. Rev. B **78**, 195125 (2008).

[55] J. Xiong, Y. Luo, Y. Khoo, S. Jia, R. J. Cava, and N. P. Ong, Phys. Rev. B **86**, 045314 (2012).

[56] H.-T. He, G. Wang, T. Zhang, I.-K. Sou, G. K. L. Wong, J.-N. Wang, H.-Z. Lu, S.-Q. Shen, and F.-C. Zhang, Phys. Rev. Lett. **106**, 166805 (2011).

[57] A. A. Taskin, H. F. Legg, F. Yang, S. Sasaki, Y. Kanai, K. Matsumoto, A. Rosch, and Y. Ando, Nature Communications **8**, 1340 (2017).

[58] D. Xiao, M.-C. Chang, and Q. Niu, Rev. Mod. Phys. **82**, 1959 (2010).

[59] M. Z. Hasan and C. L. Kane, Rev. Mod. Phys. **82**, 3045 (2010).

[60] Y. V. Ivanov, A. T. Burkov, and D. A. Pshenay-Severin, physica status solidi (b) **255**, 1800020 (2018).

[61] N. Xu, Y. Xu, and J. Zhu, npj Quantum Materials **2**, 51 (2017).

[62] J. P. Heremans, R. J. Cava, and N. Samarth, Nature Reviews Materials **2**, 17049 (2017).

[63] R. Venkatasubramanian, E. Siivola, T. Colpitts, and B. O'Quinn, Nature **413**, 597 (2001).

[64] R. Takahashi and S. Murakami, Phys. Rev. B **81**, 161302 (2010).

[65] R. Takahashi and S. Murakami, Semiconductor Science and Technology **27**, 124005 (2012).

[66] P. Ghaemi, R. S. K. Mong, and J. E. Moore, Phys. Rev. Lett. **105**, 166603 (2010).

[67] J. Liang, L. Cheng, J. Zhang, H. Liu, and Z. Zhang, Nanoscale **8**, 8855–8862 (2016).

[68] H. Osterhage, J. Gooth, B. Hamdou, P. Gwozdz, R. Zierold, and K. Nielsch, Applied Physics Letters **105**, 123117 (2014).

[69] S. Ryu and Y. Hatsugai, Phys. Rev. B **73**, 245115 (2006).

[70] H.-Z. Lu, W.-Y. Shan, W. Yao, Q. Niu, and S.-Q. Shen, Phys. Rev. B **81**, 115407 (2010).

[71] D. Baldomir and D. Faílde, Scientific Reports **9**, 6324 (2019).

[72] M. Koshino and T. Ando, Phys. Rev. B **81**, 195431 (2010).

[73] D. Xiao, J. Shi, and Q. Niu, Phys. Rev. Lett. **95**, 137204 (2005).

[74] T. Thonhauser, D. Ceresoli, D. Vanderbilt, and R. Resta, Phys. Rev. Lett. **95**, 137205 (2005).

[75] Y. Gao, S. A. Yang, and Q. Niu, Phys. Rev. B **91**, 214405 (2015).

[76] Y. Gao, S. A. Yang, and Q. Niu, Phys. Rev. Lett. **112**, 166601 (2014).

[77] S. Ozaki and M. Ogata, Phys. Rev. Research **3**, 013058 (2021).

[78] J. Zak, Phys. Rev. Lett. **62**, 2747 (1989).

[79] P. A. M. Dirac, Proceedings of the Royal Society of London. Series A, Containing Papers of a Mathematical and Physical Character **117**, 610 (1928).

[80] D. J. Griffiths and D. F. Schroeter, *Introduction to Quantum Mechanics* (Cambridge University Press, 2018).

[81] W. P. Su, J. R. Schrieffer, and A. J. Heeger, Phys. Rev. Lett. **42**, 1698 (1979).

[82] M. J. Rice and E. J. Mele, Phys. Rev. Lett. **49**, 1455 (1982).

[83] D. Zheng, G.-M. Zhang, and C. Wu, Phys. Rev. B **84**, 205121 (2011).

[84] S.-Q. Shen, W.-Y. Shan, and H.-Z. Lu, SPIN **01**, 33–44 (2011).

[85] M. Sprinkle, D. Siegel, Y. Hu, J. Hicks, A. Tejeda, A. Taleb-Ibrahimi, P. Le Fèvre, F. Bertran, S. Vizzini, H. Enriquez, S. Chiang, P. Soukiassian, C. Berger, W. A. de Heer, A. Lanzara, and E. H. Conrad, Phys. Rev. Lett. **103**, 226803 (2009).

[86] Z. Zhu, Y. Cheng, and U. Schwingenschlögl, Phys. Rev. B **85**, 235401 (2012).

[87] Z. Zhu, Y. Cheng, and U. Schwingenschlögl, Phys. Rev. Lett. **108**, 266805 (2012).

[88] S.-Y. Xu, C. Liu, N. Alidoust, M. Neupane, D. Qian, I. Belopolski, J. D. Denlinger, Y. J. Wang, H. Lin, L. A. Wray, G. Landolt, B. Slomski, J. H. Dil, A. Marcinkova, E. Morosan, Q. Gibson, R. Sankar, F. C. Chou, R. J. Cava, A. Bansil, and M. Z. Hasan, Nature Communications **3**, 1192 (2012).

[89] X. Su-Yang, X. Y., W. L. A., J. S., M. F., D. J. H., O. J., S. B., B. A., L. H., C. R. J., and H. M. Z., Science **332**, 560 (2011).

[90] T. L. Schmidt, S. Rachel, F. von Oppen, and L. I. Glazman, Phys. Rev. Lett. **108**, 156402 (2012).

[91] C. Liu, T. L. Hughes, X.-L. Qi, K. Wang, and S.-C. Zhang, Phys. Rev. Lett. **100**, 236601 (2008).

[92] S. K. Kim, H. Ochoa, R. Zarzuela, and Y. Tserkovnyak, Phys. Rev. Lett. **117**, 227201 (2016).

[93] M. Hohenadler, Z. Y. Meng, T. C. Lang, S. Wessel, A. Muramatsu, and F. F. Assaad, Phys. Rev. B **85**, 115132 (2012).

[94] M. Hohenadler, F. Parisen Toldin, I. F. Herbut, and F. F. Assaad, Phys. Rev. B **90**, 085146 (2014).

[95] D. Faílde and D. Baldomir, New Journal of Physics **23**, 113002 (2021).

[96] G. Sundaram and Q. Niu, Phys. Rev. B **59**, 14915 (1999).

[97] P Streda, Journal of Physics C: Solid State Physics **15**, L717 (1982).

[98] M.-C. Chang and Q. Niu, Phys. Rev. Lett. **75**, 1348 (1995).

[99] R. Resta, Ferroelectrics **136**, 51 (1992).

[100] R. D. King-Smith and D. Vanderbilt, Phys. Rev. B **47**, 1651 (1993).

[101] R. Jackiw and C. Rebbi, Physical Review D **13**, 3398 (1976).

[102] M. Kohmoto and Y. Hasegawa, Phys. Rev. B **76**, 205402 (2007).

[103] B. Zhou, H.-Z. Lu, R.-L. Chu, S.-Q. Shen, and Q. Niu, Phys. Rev. Lett. **101**, 246807 (2008).

[104] Y. L. Chen, J. G. Analytis, J.-H. Chu, Z. K. Liu, S.-K. Mo, X. L. Qi, H. J. Zhang, D. H. Lu, X. Dai, Z. Fang, S. C. Zhang, I. R. Fisher, Z. Hussain, and Z.-X. Shen, Science **325**, 178 (2009).

[105] F. Yang, L. Miao, Z. F. Wang, M.-Y. Yao, F. Zhu, Y. R. Song, M.-X. Wang, J.-P. Xu, A. V. Fedorov, Z. Sun, G. B. Zhang, C. Liu, F. Liu, D. Qian, C. L. Gao, and J.-F. Jia, Phys. Rev. Lett. **109**, 016801 (2012).

[106] D. Hsieh, D. Qian, L. Wray, Y. Xia, Y. S. Hor, R. J. Cava, and M. Z. Hasan, Nature **452**, 970 (2008).

[107] M. Büttiker, Phys. Rev. B **38**, 9375 (1988).

[108] A. Roth, C. Brüne, H. Buhmann, L. W. Molenkamp, J. Maciejko, X.-L. Qi, and S.-C. Zhang, Science **325**, 294 (2009).

[109] D. Faílde and D. Baldomir, Scientific Reports **11**, 14335 (2021).

[110] J. Kim, S. S. Baik, S. W. Jung, Y. Sohn, S. H. Ryu, H. J. Choi, B.-J. Yang, and K. S. Kim, Phys. Rev. Lett. **119**, 226801 (2017).

[111] Q. Liu, X. Zhang, L. B. Abdalla, A. Fazzio, and A. Zunger, Nano Letters **15**, 1222 (2015).

[112] M. Ezawa, New Journal of Physics **14**, 033003 (2012).

[113] M. Tahir and U. Schwingenschlögl, Scientific Reports **3**, 1075 (2013).

[114] D. Hsieh, Y. Xia, L. Wray, D. Qian, A. Pal, J. H. Dil, J. Osterwalder, F. Meier, G. Bihlmayer, C. L. Kane, Y. S. Hor, R. J. Cava, and M. Z. Hasan, Science **323**, 919 (2009).

[115] Y. Xia, D. Qian, D. Hsieh, L. Wray, A. Pal, H. Lin, A. Bansil, D. Grauer, Y. S. Hor, R. J. Cava, and M. Z. Hasan, Nature Physics **5**, 398 (2009).

[116] C.-X. Liu, X.-L. Qi, H. Zhang, X. Dai, Z. Fang, and S.-C. Zhang, Phys. Rev. B **82**, 045122 (2010).

[117] L. Fu, Phys. Rev. Lett. **103**, 266801 (2009).

[118] T. Misawa, T. Yokoyama, and S. Murakami, Phys. Rev. B **84**, 165407 (2011).

[119] P. Bhalla, Phys. Rev. B **103**, 115304 (2021).

[120] R. Jackiw and R. Young, *Topological Investigations of Quantized Gauge Theories* (North-Holland, Netherlands, 1984).

[121] A. Sekine and K. Nomura, Journal of Applied Physics **129**, 141101 (2021).

[122] R. Li, J. Wang, X.-L. Qi, and S.-C. Zhang, Nature Physics **6**, 284 (2010).

[123] E. Witten, Physics Letters B **86**, 283 (1979).

[124] P. Sikivie, Physics Letters B **137**, 353 (1984).

[125] M. C. Huang and P. Sikivie, Phys. Rev. D **32**, 1560 (1985).

[126] P.-H. Chang, M. S. Bahramy, N. Nagaosa, and B. K. Nikolic, Nano letters **14**, 3779 (2014).

[127] B. Z. Rameshti and R. Asgari, Physical Review B **94**, 205401 (2016).

[128] D. Wright, Nature **181**, 834 (1958).

[129] M. Eschbach, E. Młyńczak, J. Kellner, J. Kampmeier, M. Lanius, E. Neumann, C. Weyrich, M. Gehlmann, P. Gospodarič, S. Döring, et al., Nature communications **6**, 8816 (2015).

[130] J. Lado, V Pardo, and D Baldomir, Physical Review B **88**, 155119 (2013).

[131] U. Aydemir and G. J. Snyder, Journal of Materials Chemistry C **3**, 10332 (2015).

[132] B. Simon, Physical Review Letters **51**, 2167 (1983).

[133] R. Hartshorne, *Algebraic Geometry*, Vol. 52 (Springer Science & Business Media, 2013).

[134] S. Deser, R. Jackiw, and S. Templeton, Phys. Rev. Lett. **48**, 975 (1982).

[135] M. Le Bellac, *Thermal Field Theory* (Cambridge University Press, 2000).

[136] D. Ashok, *Finite Temperature Field Theory* (World scientific, 1997).

[137] C. K. Dumlu and G. V. Dunne, Physical Review D **84**, 125023 (2011).

[138] G. V. Dunne and C. Schubert, Phys. Rev. D **72**, 105004 (2005).

[139] G. V. Dunne, Q.-h. Wang, H. Gies, and C. Schubert, Physical Review D **73**, 065028 (2006).

[140] W. Heisenberg and H. Euler, Zeitschrift für Physik **98**, 714 (1936).

[141] D. Thouless, Physical Review B **27**, 6083 (1983).

[142] R. Resta, Rev. Mod. Phys. **66**, 899 (1994).

[143] M Switkes, C. Marcus, K Campman, and A. Gossard, Science **283**, 1905 (1999).

[144] S. Das Sarma and E. H. Hwang, Phys. Rev. B **87**, 035415 (2013).

[145] R. Landauer, The Philosophical Magazine: A Journal of Theoretical Experimental and Applied Physics **21**, 863 (1970).

[146] O. A. Tretiakov, A. Abanov, and J. Sinova, Applied Physics Letters **99**, 113110 (2011).

[147] B. Peng, H. Zhang, H. Shao, Y. Xu, G. Ni, R. Zhang, and H. Zhu, Physical Review B **94**, 245420 (2016).

[148] C. L. Kane and M. P. A. Fisher, Phys. Rev. B **55**, 15832 (1997).

[149] U. Sivan and Y. Imry, Phys. Rev. B **33**, 551 (1986).

[150] S. Roychowdhury, U Sandhya Shenoy, U. V. Waghmare, and K. Biswas, Applied Physics Letters **108**, 193901 (2016).

[151] W. Liu, Q. Jie, H. S. Kim, and Z. Ren, Acta Materialia **87**, 357 (2015).

[152] R. Roy, Phys. Rev. B **79**, 195322 (2009).

[153] J. E. Avron, R. Seiler, and B. Simon, Phys. Rev. Lett. **51**, 51 (1983).

[154] S. Murakami, Phys. Rev. Lett. **97**, 236805 (2006).

[155] A. M. Essin, J. E. Moore, and D. Vanderbilt, Phys. Rev. Lett. **102**, 146805 (2009).

[156] T. Olsen, M. Taherinejad, D. Vanderbilt, and I. Souza, Phys. Rev. B **95**, 075137 (2017).

[157] M. Moshinsky and A. Szczepaniak, Journal of Physics A: Mathematical and General **22**, L817 (1989).

[158] L. Zhao, H. Deng, I. Korzhovska, Z. Chen, M. Konczykowski, A. Hruban, V. Oganesyan, and L. Krusin-Elbaum, Nature Materials **13**, 580 (2014).

[159] H. Li, L. Sheng, D. N. Sheng, and D. Y. Xing, Phys. Rev. B **82**, 165104 (2010).

[160] I. P. Batra, Solid State Communications **124**, 463 (2002).

[161] C. Duval, Z. Horváth, P. A. Horváthy, L. Martina, and P. C. Stichel, Modern Physics Letters B **20**, 373 (2006).

[162] A. Bermudez, M. A. Martin-Delgado, and E. Solano, Phys. Rev. A **76**, 041801 (2007).

[163] P Rozmej and R Arvieu, Journal of Physics A: Mathematical and General **32**, 5367 (1999).

[164] F. M. Andrade and E. O. Silva, EPL (Europhysics Letters) **108**, 30003 (2014).

[165] N. Ashcroft, A. W, N. Mermin, W. Ashcroft, D. Mermin, N. Mermin, and B. P. Company, *Solid State Physics*, HRW international editions (Holt, Rinehart and Winston, 1976).

[166] R. Heid, I. Y. Sklyadneva, and E. V. Chulkov, Scientific Reports **7**, 1095 (2017).

[167] H. Pan, M. Wu, Y. Liu, and S. A. Yang, Scientific Reports **5**, 14639 (2015).

[168] M. B. Hastings, Phys. Rev. Lett. **107**, 210501 (2011).

[169] B. C. Park, T.-H. Kim, K. I. Sim, B. Kang, J. W. Kim, B. Cho, K.-H. Jeong, M.-H. Cho, and J. H. Kim, Nature Communications **6**, 6552 (2015).

[170] J. Yan, Y. Zhang, P. Kim, and A. Pinczuk, Phys. Rev. Lett. **98**, 166802 (2007).

[171] O. A. Tretiakov, A. Abanov, S. Murakami, and J. Sinova, Applied Physics Letters **97**, 073108 (2010).

[172] P. Chakraborty, L. Cao, and Y. Wang, Scientific Reports **7**, 8134 (2017).

[173] M. U. Muzaffar, S. Zhang, P. Cui, J. He, and Z. Zhang, Advanced Functional Materials **30**, 2003162 (2020).

[174] T. Qin, Q. Niu, and J. Shi, Phys. Rev. Lett. **107**, 236601 (2011).

[175] S. Nandy, A. Taraphder, and S. Tewari, Scientific Reports **8**, 14983 (2018).

[176] S. Nandy, G. Sharma, A. Taraphder, and S. Tewari, Phys. Rev. Lett. **119**, 176804 (2017).

[177] A. Bermudez, M. A. Martin-Delgado, and A. Luis, Phys. Rev. A **77**, 063815 (2008).

[178] H. Fukuyama, Journal of the Physical Society of Japan **76**, 043711 (2007).

[179] M.-C. Chang and Q. Niu, Journal of Physics: Condensed Matter **20**, 193202 (2008).

[180] L. Susskind, Phys. Rev. D **16**, 3031 (1977).

[181] Y.-F. Zhou, H. Jiang, X. C. Xie, and Q.-F. Sun, Phys. Rev. B **95**, 245137 (2017).

[182] K. M. M. Habib, R. N. Sajjad, and A. W. Ghosh, Applied Physics Letters **108**, 113105 (2016).

[183] D. C. Elias, R. V. Gorbachev, A. S. Mayorov, S. V. Morozov, A. A. Zhukov, P. Blake, L. A. Ponomarenko, I. V. Grigorieva, K. S. Novoselov, F. Guinea, and A. K. Geim, Nature Physics **7**, 701 (2011).

[184] P. W.Milonni, *The Quantum Vacuum: An Introduction To Quantum Electrodynamics* (Academic Press, Inc., 1994).

[185] J. C.Itzykson, *Quantum Field Theory* (Dover Books on Physics, 2012).

[186] H. B. G. Casimir, Proc. Kon. Ned. Akad. Wet. **51**, 793 (1948).

[187] H. B. G. Casimir and D. Polder, Phys. Rev. **73**, 360 (1948).

[188] S. K. Lamoreaux, Phys. Rev. Lett. **78**, 5 (1997).

[189] U. Mohideen and A. Roy, Phys. Rev. Lett. **81**, 4549 (1998).

[190] E. Lifshitz, J. Exp. Theor. Phys. **29**, 94 (1955).

[191] J. Schwinger, L. L. DeRaad, and K. A. Milton, Annals of Physics **115**, 1 (1978).

[192] K. A. Milton, L. L. DeRaad, and J. Schwinger, Annals of Physics **115**, 388 (1978).

[193] R. L. Jaffe, Phys. Rev. D **72**, 021301 (2005).

[194] A. G. Grushin and A. Cortijo, Phys. Rev. Lett. **106**, 020403 (2011).

[195] P. Rodriguez-Lopez and A. G. Grushin, Phys. Rev. Lett. **112**, 056804 (2014).

[196] H. B. Chan, V. A. Aksyuk, R. N. Kleiman, D. J. Bishop, and F. Capasso, Science **291**, 1941 (2001).

[197] N. P. Armitage and L. Wu, SciPost Phys. **6**, 46 (2019).

[198] D. J. Thouless, M. Kohmoto, M. P. Nightingale, and M. den Nijs, Phys. Rev. Lett. **49**, 405 (1982).

[199] M.-C. Chang and Q. Niu, Phys. Rev. B **53**, 7010 (1996).

[200] F. Wilczek, Phys. Rev. Lett. **58**, 1799 (1987).

[201] G. D. Mahan, *Many-Particle Physics* (Springer, Boston, MA, 2000).

[202] A. van Oudenaarden, M. H. Devoret, Y. V. Nazarov, and J. E. Mooij, Nature **391**, 768 (1998).

[203] C. Jang, S. Adam, J.-H. Chen, E. D. Williams, S. Das Sarma, and M. S. Fuhrer, Phys. Rev. Lett. **101**, 146805 (2008).

[204] J. P. Reed, B. Uchoa, Y. I. Joe, Y. Gan, D. Casa, E. Fradkin, and P. Abbamonte, Science **330**, 805 (2010).

[205] G. L. Klimchitskaya, International Journal of Modern Physics A **17**, 751–760 (2002).

[206] M. E. Tobar, B. T. McAllister, and M. Goryachev, Physics of the Dark Universe **26**, 100339 (2019).

[207] M. Bordag, G. Klimchitskaya, U. Mohideen, and V. Mostepanenko, *Advances in the Casimir Effect* (Oxford University Press, Oxford, 2009).

[208] D. Faílde and D. Baldomir, *Anomalous response in the orbital magnetic susceptibility of 2D topological systems*, arXiv:2111.05021 [cond-mat.mes-hall] (2021).

The origin of this thesis lies in the study of the thermoelectric properties of topological insulators, currently the best thermoelectric materials. Our perspective was theoretical from the beginning given the lack of a microscopic theory in the literature that answers why these systems have such an efficient thermoelectric response, represented by their well known experimental figure of merit. Coherently, this leads us to explore, throughout the different chapters of this thesis, other effects and interactions such as the electron-phonon coupling, orbital dynamics and axion electrodynamics which are a consequence of the non-trivial topology of these materials.